Euscorpius

Occasional Publications in Scorpiology

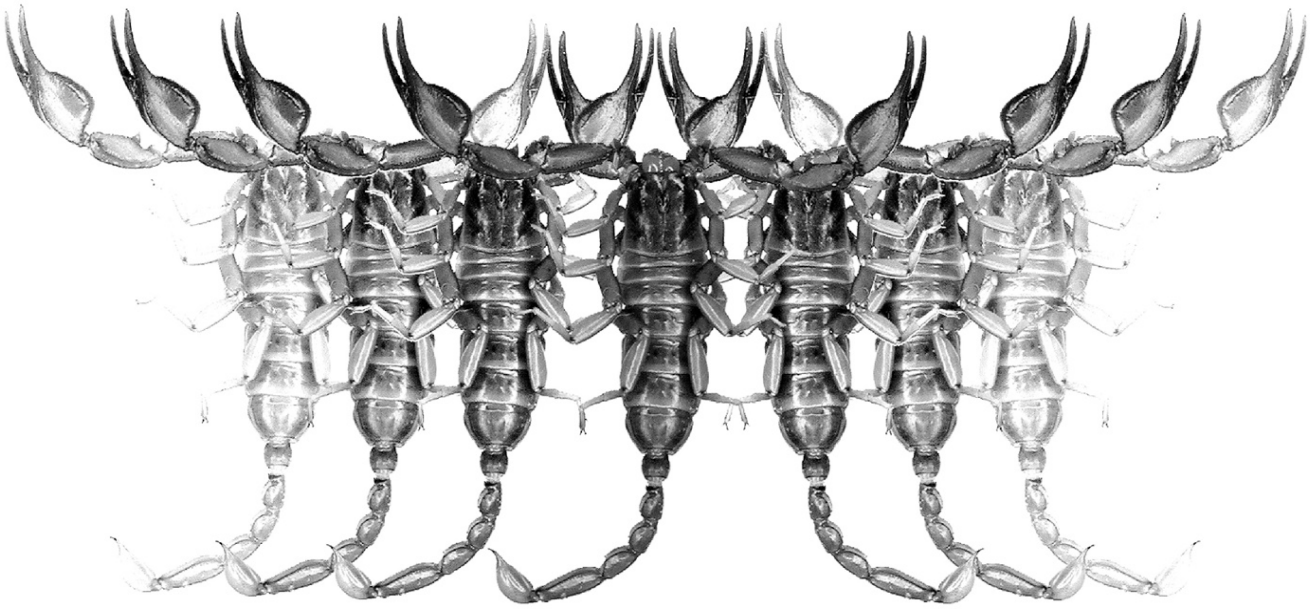

The genus *Androctonus* Ehrenberg, 1828 (Scorpiones: Buthidae) in Oman

Graeme Lowe

September 2025 — No. 424

Euscorpius

Occasional Publications in Scorpiology

EDITOR: **Victor Fet**, Marshall University, **'fet@marshall.edu'**

ASSOCIATE EDITOR: **Michael E. Soleglad, 'msoleglad@gmail.com'**

TECHNICAL EDITOR: **František Kovařík, 'kovarik.scorpio@gmail.com'**

Euscorpius is the first research publication completely devoted to scorpions (Arachnida: Scorpiones). ***Euscorpius*** takes advantage of the rapidly evolving medium of quick online publication, at the same time maintaining high research standards for the burgeoning field of scorpion science (scorpiology). ***Euscorpius*** is an expedient and viable medium for the publication of serious papers in scorpiology, including (but not limited to): systematics, evolution, ecology, biogeography, and general biology of scorpions. Review papers, descriptions of new taxa, faunistic surveys, lists of museum collections, and book reviews are welcome.

Derivatio Nominis

The name ***Euscorpius*** Thorell, 1876 refers to the most common genus of scorpions in the Mediterranean region and southern Europe (family Euscorpiidae).

Euscorpius is located at: https://mds.marshall.edu/euscorpius/
Archive of issues 1-270 see also at: http://www.science.marshall.edu/fet/Euscorpius

(Marshall University, Huntington, West Virginia 25755-2510, USA)

ICZN COMPLIANCE OF ELECTRONIC PUBLICATIONS:

Electronic ("e-only") publications are fully compliant with ICZN (*International Code of Zoological Nomenclature*) (i.e. for the purposes of new names and new nomenclatural acts) when properly archived and registered. All ***Euscorpius*** issues starting from No. 156 (2013) are archived in two electronic archives:

- **Biotaxa,** http://biotaxa.org/Euscorpius (ICZN-approved and ZooBank-enabled)
- **Marshall Digital Scholar**, http://mds.marshall.edu/euscorpius/. (This website also archives all *Euscorpius* issues previously published on CD-ROMs.)

Between 2000 and 2013, ICZN ***did not accept online texts*** as "published work" (Article 9.8). At this time, *Euscorpius* was produced in two ***identical*** versions: online (*ISSN 1536-9307*) and CD-ROM (*ISSN 1536-9293*) (laser disk) in archive-quality, read-only format. Both versions had the identical date of publication, as well as identical page and figure numbers. ***Only copies distributed on a CD-ROM*** from ***Euscorpius*** in 2001-2012 represent published work in compliance with the ICZN, i.e. for the purposes of new names and new nomenclatural acts.

In September 2012, ICZN Article 8. What constitutes published work**,** has been amended and allowed for electronic publications, disallowing publication on optical discs. From January 2013, ***Euscorpius*** discontinued CD-ROM production; only online electronic version (ISSN 1536-9307) is published. For further details on the new ICZN amendment, see http://www.pensoft.net/journals/zookeys/article/3944/.

Publication date: 9 September 2025

http://zoobank.org/urn:lsid:zoobank.org:pub:BA956334-FAFA-47AA-A75A-34B5934584FE

Euscorpius — Occasional Publications in Scorpiology. 2025, No. 424

The genus *Androctonus* Ehrenberg, 1828 (Scorpiones: Buthidae) in Oman

Graeme Lowe

Monell Chemical Senses Center, 3500 Market St, Philadelphia, USA

http://zoobank.org/urn:lsid:zoobank.org:pub:BA956334-FAFA-47AA-A75A-34B5934584FE

Summary

The taxonomic position of *Androctonus* populations in Oman was investigated by analyzing morphological variation in a comprehensive sample representing 150 records gathered from 95 localities spread throughout the country. Two new allopatric species are described, separated by multivariate morphometric analysis and meristic characters: (1) *A. omanensis* **sp. n.**, distributed across most of Oman, is characterized by wider, deeper metasomal segments IV–V, shorter legs, more robust pedipalps, more granules on lateral inframedian carinae of metasoma II–III, and sparser setation on basitarsal spurs; and (2) *A. ammophilus* **sp. n.**, distributed in the dunes of the Rub' al-Khali (Empty Quarter) of northwest Oman, and adjacent Saudi Arabia and United Arab Emirates, is characterized by narrower, shallower metasomal segments IV–V, longer legs, more elongate pedipalps, fewer granules on lateral inframedian carinae of metasoma II–III, and denser setation on basitarsal spurs. The emergence of the Rub' al-Khali sand system during Pleistocene glaciations, and the transition to hyper-arid conditions in the region, are hypothesized to be abiotic factors promoting ecological speciation of *A. ammophilus* **sp. n.**, and vicariant speciation of *A. omanensis* **sp. n.**

Introduction

The genus *Androctonus* is broadly distributed across Palearctic deserts, extending from western North Africa (Kovařík et al., 2025; Lourenço, 2005; Ythier & Lourenço, 2022), to western Asia (Barahoei et al., 2022; Kovařík & Ahmed, 2013; Lourenço, 2005; Pocock, 1897; Tikader & Bastawade, 1983). Of 50 currently recognized species, the majority (29) occur in North Africa, while less than half (15) occur in the Middle East exclusive of Africa, and even fewer in Asia (6). This suggests that the diversity of *Androctonus* in the latter two regions may be underestimated. Large, dark *Androctonus* are common and widespread in the Middle East, where their stings have serious impacts on public health (Amr et al., 2021; Dehghani & Fathi, 2012; Ismail et al., 1994; Ozkan et al., 2006). They were formerly classified under a single species, *A. crassicauda* (Olivier, 1807), but recent taxonomic studies have assigned regional populations to at least eleven different taxa: *A. azerianus* Yağmur & Kovařík, 2025 (Iran), *A. barahoeii* Kovařík & Yağmur, 2025 (Iran), *A. caspius* Kovařík et al., 2025 (Iran), *A. crassicauda* s. str. (Olivier, 1807) (Iran), *A. ishtar* Yağmur et al., 2025 (Iraq), *A. kunti* Yağmur, 2023 (Turkey, Iran), *A. orientalis* (Birula, 1900) (Iran), *A. sumericus* Al-Khazali & Yağmur, 2023 (Iraq), *A. tihamicus* Alqahtani et al., 2023 (Red Sea coast of Saudi Arabia), *A. transcaucasicus* Kovařík et al., 2025 (Armenia, Azerbaijan, Iran), and *A. turkiyensis* Yağmur, 2021 (Turkey) (Al-Khazali & Yağmur, 2023; Alqahtani et al., 2023; Barahoei et al., 2025; Yağmur, 2021, 2023; Yağmur et al., 2025a, 2025b). Analysis of cytochrome oxidase subunit I mitochondrial DNA sequences indicated that other populations of *A.* '*crassicauda*' in the Arabian Peninsula may include at least two lineages in northern and central Saudi Arabia, hypothesized to represent cryptic species (Alqahtani et al., 2022b, 2022c). Recently described members of the *A.* '*crassicauda*' species complex are based on differences in coloration, granulation, trichobothriotaxy, carinal dentition of metasomal segments, and morphometrics. The stability of these characters needs to be further tested by examining variation over wider geographic ranges. In this paper, morphological variation in *A.* '*crassicauda*' populations in Oman is analyzed based on extensive material accumulated over several decades. Substantial variation was found and most samples are herein categorized as a single new species, *A. omanensis* **sp. n.**, distributed across sandy habitats throughout Oman. A second new species, *A. ammophilus* **sp. n.**, is described from aeolian dunes of the Rub' al-Khali (Empty Quarter) on the basis of differences in morphometrics, granulation and setation.

Materials & Methods

Examined material was loaned from museums, collected by the author, or donated by other collectors. Collections were made by day, and by night using ultraviolet (UV) detection. Locality coordinates were recorded by GPS, or extracted from maps. Laboratory methods generally follow Sissom et al. (1990).

Specimens were preserved in 70% ethyl or isopropyl alcohol and examined under a dissecting microscope, viewing either in reflected white light or blue-green fluorescence excited by UV (395 nm) light. Digital imaging methods generally followed Lowe & Fet (2024) and Lowe & Tang (2024). To quantify lightness of pigmentation, specimens were photographed under white light with a Canon EOS 5DsR camera equipped with a Canon 100 mm f/2.8 macro lens (ISO 100, f/13, 2 s). Linear RAW conversion of *.CR2 files yielded grayscale images of luminance encoded in uncompressed 8-bit TIFF format. These were analyzed by the software Image J 1.52a (Schneider et. al., 2012) to obtain measures of local reflected light intensity of the cuticle.

Anatomical terminology generally follows Stahnke (1971) and Kovařík (2009). Terminology of cheliceral dentition follows Vachon (1963), of tarsal segments and setation, Haradon (1984), of hemispermatophores, Kovařík et al. (2018), and of trichobothriotaxy, Vachon (1974, 1975). Terminology of metasomal carination is modified from Francke, 1977 (Figs. 195–196): on segments I–IV are paired carinae: dorsolateral, lateral supramedian, lateral inframedian (when present), ventrolateral and ventrosubmedian; on segment V are paired carinae: dorsolateral, ventrolateral, ventrosubmedian (reduced to granule rows), and an unpaired ventromedian carina. Morphometric measurements are indicated in Figs. 179–196: pedipalp chela width was measured between bounding vertical tangent planes of the manus, orthogonal to the intercondylar axis of the movable finger (Fig. 184); pedipalp chela depth was measured between bounding horizonal tangent planes of the manus, parallel to the intercondylar axis, with the ventral surface of the manus level; pedipalp femur length was measured from the proximal limit of the dorsointernal carina, where it converges with the dorsoexternal carina (Fig. 180); pectine length was measured along its anterior margin (Fig. 191); metasomal segment lengths were measured between the posterior limit of the segment and the anterior limit of the dorsolateral carina (excluding the anterior peduncle which is often partially obscured by the adjacent segment and inaccessible without disarticulating rigid specimens) (Figs. 195–196); telson length was measured between bounding vertical planes orthogonal to the plane tangent to the dorsal surface of the vesicle, with anterior bounding plane at the anterior limit of the vesicle and posterior bounding plane tangent to the aculeus (excluding the anterior peduncle which is often partially obscured by metasoma V and inaccessible without disarticulating rigid specimens) (Fig. 195). Measurements were acquired manually with a Mitutoyo CD-6“ CX digimatic caliper and IT-012U input tool. Measurement errors of variables used in multivariate analyses were estimated from repeated measurements of sclerite dimensions of a typical adult specimen (Tab. 9). Standard deviations exceeded 0.04 mm and the results of single caliper measurements are reported in mm, with a precision of one decimal place (Tabs. 1–3). Summary statistics of variables are given as range = minimum – maximum, and mean ± SD. Software used in data analysis and plotting were: Origin 7.0 (https://www.originlab.com), Microsoft Excel version 2412 (Microsoft Corporation, Washington, USA), and NCSS 2023 version 23.0.1 (NCSS LLC, Utah, USA). PCA was run in Origin 7.0 and NCSS; LDA was run in NCSS; Monte Carlo simulations were run in Origin 7.0.

Abbreviations

General: 3D, 3-dimensional; ANOVA, analysis of variance; CV, coefficient of variation (= SD/ mean); D, depth; ka, thousand years ago; juv., juvenile; L, length; LDA, linear discriminant analysis; Ma, million years ago; MIS, marine isotope stage (nomenclature of Quaternary climatic cycles); N, number of samples analyzed; OTU, operational taxonomic unit; P, probability of rejecting null hypothesis; PCA, principal components analysis; PDO, Petroleum Development of Oman; R, Pearson’s correlation coefficient; SD, standard deviation; UPGMA, unweighted pair-group method with arithmetic mean (in hierarchical cluster analysis); UV, ultraviolet; W, width. *Specimen repositories*: EAD, Environment Agency, Abu Dhabi, United Arab Emirates; FKCP, private collection of Frantisek Kovařík, Prague, Czech Republic; GLPC, private collection of Graeme Lowe, Auckland, New Zealand; MCZ, Museum of Comparative Zoology, Cambridge, Massachusetts, USA; MNHN, Museum National d‘Histoire Naturelle, Paris, France; MZUF, Museo Zoologico "La Specola" dell‘ Università de Firenze, Florence, Italy. NHMB, Naturhistorisches Museum, Basel, Switzerland; ONHM, Oman Natural History Museum, Muscat, Oman; UAE, United Arab Emirates; USNM, Smithsonian National Museum of Natural History (= United States National Museum), Washington D.C., USA.

Systematics

Buthidae C. L. Koch, 1837
Androctonus Ehrenberg, 1828
(Figures 1–208, Tables 1–9)

Androctonus Ehrenberg in Hemprich & Ehrenberg, 1828 (part), pl. II, fig. 1–2, 4–5, 8; Vachon, 1952: 117–121, 402–406; Stahnke, 1972: 32; Levy & Amitai, 1980: 21–22; Tikader & Bastawade, 1983: 242; Sissom, 1990: 100; Fet & Lowe, 2000: 64–65 (complete reference list until 1998); Lourenço, 2005: 146–147; Kovařík, 2009: 24: Barahoei et al., 2022: 198–199; Ythier, 2021: 1–2; Ythier & Lourenço, 2022: 240–241; Kovařík et al., 2025: 4; Yağmur et al., 2025a: 5.

Type species. *Scorpio australis* Linnaeus, 1758.

Diagnosis. Medium to large buthids, adults 50–110 mm. *Carapace*: weakly trapezoidal, subrectangular, granulate, with distinct anterior submedian, superciliary, central median, central lateral and posterior median carinae; median ocular tubercle located in posterior 2/3 of carapace; 5 pairs of

lateral eyes in Type 5 arrangement (Loria & Prendini, 2014). *Mesosoma*: tergites granulate, I–II with 1–3 carinae, III–VI with 3 carinae, VII with 5 carinae; sternites III–VI smooth, posterior margins smooth or micro-granulate; spiracles narrow, elongate; sternite VII with 4 carinae; posterior margins of tergite VII and sternite VII with microsetal fringes. *Metasoma*: segment I with 10, II–IV with 8–10, V with 5 carinae; segments robust, relatively wide and deep, strongly carinate; segments I–IV with dorsolateral carinae moderately to strongly elevated posteriorly, dorsal furrow moderately to deeply excavated; segment V with dorsolateral carinae variably smooth, costate granulate to denticulate, angulate in cross section; posterior margins of segments I–III with microsetal fringes. *Telson*: vesicle pyriform; aculeus stout, as long as or longer than vesicle; subaculear tubercle absent. Chelicerae: fingers with typical buthid dentition (Vachon 1963: 162, fig. 1), fixed finger with 2 denticles on ventral surface. *Pedipalps*: orthobothriotaxic, type Aβ (Vachon 1974, 1975); femur with d_2 on dorsal surface, e_2 distal to d_5; patella with d_3 internal to dorsomedian carina, esb_2 distal to, but near esb_1; chela manus with Eb_2 proximal to Eb_1, V_1-V_2 axis parallel to V1 carina, V_2 in medial position posterior to V_1; *eb* located on proximal fixed finger, *db* in middle third of fixed finger, *db* proximal to, or level with *est*; *dt* and *it* located on distal fixed finger; femur with dense, compact distal external macrosetal cluster (Lowe & Tang, 2024); dentate margins of fixed and movable fingers with 9–16 linear, non-imbricated subrows of median denticles, flanked by single internal and external accessory denticles; movable finger typically with 3 large subdistal denticles; subdistal fingers with 2 pairs of Cruz-Armas sensilla, distal pair elongate (Lowe & Fet, 2024); male fingers with weak to strong undulation (scalloping) of proximal dentate margins. *Pectines*: fulcra present; internal fulcra present, elliptic; accessory internal fulcra absent; basal teeth and basal middle lamella unmodified; pectinal tooth counts:♂ 24–37,♀ 19–29. *Legs*: tibial spurs present on legs III–IV; bristle combs present on basitarsi I–III; ventral surface of telotarsi without median spinules, with two submedian rows of < 25 macrosetae; prolateral and retrolateral pedal spurs present on all legs, prolateral spurs basally bifurcate. *Hemispermatophore*: trunk of moderate length for buthids; capsule with 3-lobed sperm hemiduct; basal lobe hook-like, variable in length; flagellum folded, with shorter, broad laminate pars recta, and longer, narrow cylindrical pars reflecta.

Remarks. Hendrixson (2006: 37) diagnosed the genus as having central lateral and posterior median carinae of the carapace fused in a lyre-shaped configuration. Although these pairs of carinae may appear to be connected by transverse series of granules in some individuals (e.g., Figs. 13, 118), in others they are not (e.g., Figs. 8–12, 15). The lyre-shaped configuration is diagnostic for the genus *Buthus* Leach, 1815, not for *Androctonus* (Levy & Amitai, 1980: 14, 21; Barahoei et al., 2022: 198; Sissom, 1990: 100; Tikader & Bastawade, 1983: 242; Vachon 1952: 402). The same error was propagated by Desouky & Al Alshammari (2011: 195) in text copied from Hendrixson (2006).

Androctonus omanensis sp. n.

(Figs. 1–115, 163–166, 168–174, 179–200, Tabs. 1–2, 4)
http://zoobank.org/urn:lsid:zoobank.org:act:B33BDA9D-491D-4277-95EE-CBDCBE5172C8

Prionurus crassicauda: Pocock, 1895: 202 (in part?).
Buthus crassicauda: Finnegan, 1932: 92 (in part?).
Androctonus crassicauda: Vachon, 1966: 210 (in part); Vachon, 1979: 33–34 (in part); Levy & Amitai, 1980: 23, Appendix (in part); Vachon & Kinzelbach, 1987: 98 (in part); Al-Safadi, 1992: 96 (in part); El-Hennawy, 1992: 101, 109–110 (in part); Lowe, 1993: 2; Wood, 1993: 17; Fet & Lowe, 2000: 72 (in part); Fet et al., 2005: 2; 11 (in part); Hendrixson, 2006: 38–43 (in part); Lowe, 2010a: 43, 53, fig. 132; Lowe, 2010b: 10; Lowe, 2010c: 17; Amr et al., 2016: 19; Barahoei et al., 2020: 380 (in part); Amr et al., 2021: 94, tab. 16 (in part); Ythier, 2021: 1 (in part); Ythier & Lourenço, 2022: 240 (in part); Lowe & Fet, 2024: 4, 15, 63–64, 78, 81–82, 84, figs. 25–27, 338, 531, 691–692, 723–724, 754, tabs. 1–2.
Androctonus australis: Levy & Amitai, 1980: Appendix (in part, record from Muscat).
Androctonus cf. *crassicauda*: Lowe & Tang, 2024: 3 (in part), 8 (in part), 41, figs. 218–229.

Type locality and type depository. **Oman**, Barka, in wet falaj channel in garden, 23.70°N 57.90°E; NHMB.

Type material examined

Holotype ♂, **Oman**, Barka, in wet falaj channel in garden, 23.70°N 57.90°E, 15.IX.1995, leg. I. M. Al-Kasmi, NHMB.

Paratypes. **Oman**: 1♀, leg. A. B. Paltrinieri 610.11, NHMB 52/20; 1♂, leg. A. B. Paltrinieri 610.10, NHMB 50/20; 3♂, PDO medical clinic, NHMB; 1♂, Ras al Haimah, 23.62°N 58.50°E, VI.1971, leg. M. D. Gallagher MDG 2444, MNHN; 1♀, Ras al Hamra, near Muscat, on sand and rock, 23.62°N 58.52°E, V.1978, Petroleum Development Oman, MDG 4961, MNHN RS 7295; 1♀, Salalah, Ruus al Jibaal, under rock on soil at foot of mountain, 26.03°N 56.37°E, 168 m a. s. l., 28.II.1979, leg. T. B. Larsen MDG 5192, MNHN RS 7363; 1♀, Madinat Qaboos, 23.60°N 58.43°E, VIII.1979, leg. A. B. Paltrinieri 610.900, ONHM 610.9; 1♀, Lansab, in house on limestone hill, 23.55°N 58.33°E, 30 m a. s. l., 4.VIII.1979, leg. D. H. Insall & M. D. Gallagher MDG 5375, MNHN RS 7410; 1♀, Thamarit, Dhofar, sand and rock desert, 17.63°N 54.02°E, 350 m a. s. l., I.1980, leg. N. Barnes & M. D Gallagher MDG 5951, MNHN; 1♀, Khabura, Durham Project farm, under piece of polystyrene near house, 23.98°'N 57.10°E, 10 m a. s. l., 14.I.1980, leg. R. P. Whitcombe, NHMB 642.000, 0642; 1♀, Wattayeh, near Muscat, in house, 23.60°N 38.52°E, 9 m a. s. l., 11.III.1980, 23:00 h, leg. M. D. Gallagher MDG 5964, NHMB 350; 1♂, 3 miles W of Thamarit, under object on sand, 17.67°N 53.97°E, 450 m a. s. l., 28.III.1980, leg. J. N. Barnes 43, NHMB; 1♀, near Thamarit, Dhofar, under rock, 17.67°N 54.03°E, 450 m a. s. l., 30.III.1980, leg. J. N. Barnes 59, NHMB; 1♂1♀, Ra's al Hamra, near Muscat, mating pair, 23.63°N 58.50°E, 50 m a. s. l., X.1980, leg. D. Harvey & M. D. Gallagher MDG 6063, MNHN RS 8387; 1♀, Yalooni, Jiddat al Harasis, 19.95°N 57.10°E, 140 m a. s. l.,

I.1981, leg. K. O. Stanley Price & M. D. Gallagher MDG 6138, MNHN RS 8390; 1♀, Yalooni, Jiddat al Harasis, 19.95°N 57.10°E, 140 m a. s. l., II.1981, leg. M. D. Gallagher MDG 6138A, MNHN RS 8391; 1♀, Jiddat al Harasis, on sand, 19.63°N 56.72°E, 150 m a. s. l., 13.II.1981, leg. M. D. Gallagher MDG 6109, MNHN RS 8394; 1♀, Ghubara, central Oman, on sand, 19.45°N 56.03°E, 175 m a. s. l., 14.II.1981, leg. M. D. Gallagher MDG 6114, MNHN RS 8397; 1♂, Wadi al Ghubara, on sand, 18.63°N 56.05°E, 15.II.1981, leg. M. D. Gallagher MDG 6117, MNHN RS 8392; 1♀, Wadi al Ghubara (Shimal), on sand, 19.12°N 56.45°E, 15.II.1981, leg. M. D. Gallagher MDG 6120, MNHN RS 8395; 1♂1♀, Wadi Bu Mudhabi, Jiddat al Harasis, under barrel on sand, 19.88°N 56.17°E, 130 m a. s. l., 23.II.1981, leg. M. D. Gallagher MDG 6141-1,2, MNHN RS 8389; 1♂, Wadi Haytum, on sand, 19.03°N 56.72°E, 23.II.1981, leg. M. D. Gallagher MDG 6129, MNHN RS 8396; 1♀, Qurm, near Muscat, on dust under object, 23.16°N 58.48°E, 3 m a. s. l., 10.III.1981, 17:00 h, leg. M. D. Gallagher MDG 6146, MNHN RS 8393; 1♂, near Qurm, W of Muscat, 23.62°N 58.48°E, 20 m a. s. l., leg. E. M. Povall MDG 6777, NHMB; 1♂, Yalooni, Jiddat al Harasis, sand on stony plateau in house, sand on stony plateau, 19.95°N 57.12°E, 154 m a. s. l., 22.IV.1982, leg. M. D. Gallagher MDG 6428, NHMB; 1♀, Madinat Qaboos, 10 km W of Muscat, 23.60°N 58.47°E, 50 m a. s. l., 25.IV.1982, A. Jones MDG 6430, NHMB; 1♀, Madinat Qaboos, W of Muscat, rock and sand, 23.60°N 58.50°E, 50 m a. s. l., X.1982, leg. R. M. Lawton MDG 6774, NHMB; 1♀, Ra's Al Hamra, near Muscat, in house on sand, 23.63°N 58.50°E, 20 m a. s. l., 1983, Public Health Dept MDG 6937, NHMB; 1♂, Thamarit, under sheet of wood on soft sand, 17.70°N 53.98°E, 24.V.1983, leg. J. N. Barnes 127, NHMB; 2♂2♀, Ra's Al Hamra, 23.63°N 58.50°E, 100 m a. s. l., 1984, PDO Public Health Dept, NHMB; 1♂, Jiddat Al Harasis, 19.95°N 57.10°E, 170 m a. s. l., 13.VIII.1984, leg. T. Tear, NHMB; 1♂, Mina Al Fahal, W. of Muscat, 23.62°N 58.52°E, X.1984, Public Health Office, NHMB; 1♂, Tibat, Musandam region, 26.07°N 56.12°E, 20 m a. s. l., 24.X.1984, leg. M. D. Gallagher, GLPC; 1♀, Rumais, Batinah, 23.67°N 57.98°E, 20 m a. s. l., 15.VII.1985, per Omani Carrier, NHMB 349; 1♂, Qurm Creek, hill above creek in first floor of house, 23.62°N 58.48°E, 1.IX.1985, leg. P.L. Giacometti, NHMB 443; 1♂, Capital Area, Al Khuwayr, 23.58°N 58.42°E, 10.X.1985, leg. J. E. Clarke, NHMB; 1♀, Ibra, wadi, 22.68°N 58.47°E, 542 m a. s. l., leg. W. Büttiker, Oman Eastern Sands Project, NHMB 706.00; 1♀, Mintirib, wadi, 22.43°N 58.80°E, 268 m a. s. l., 15.I.1986, leg. W. Büttiker, Oman Eastern Sands Project, NHMB 690.00; 1juv., Mintirib, 22.43°N 58.80°E, 268 m a. s. l., 15.I.1986, leg. W. Büttiker, Oman Eastern Sands Project, NHMB 883.000; 1♀, Mintirib, Res. camp, 22.42°N 58.82°E, 269 m a. s. l., 18 Jan-1.II.1986, leg. W. Büttiker, Oman Eastern Sands Project, NHMB 709.00; 1♀, Wahiba Sands, 21.15°N 58.38°E, 2.II.1986, leg. M. D. Gallagher, Oman Eastern Sands Project, ONHM; 1♂, Qarhat Mu'ammar, camp, 21.63°N 59.30°E, 130 m a. s. l., 2.II.1986, leg. W. Büttiker, Oman Eastern Sands Project, NHMB 700.00; 1♂, Mintirib, Res. camp, 22.42°N 58.82°E, 269 m a. s. l., 8-10.II.1986, leg. W. Büttiker, Oman Eastern Sands Project, NHMB 696.00; 1 juv, Ras Dhabdhub, Camp, 21.53°N 58.82°E, 180 m a. s. l., 17.II.1986, leg. W. Büttiker, Oman Eastern Sands Project, NHMB; 1♂, Qarhat Mu'ammar, camp, 21.63°N 59.30°E, 130 m a. s. l., 24-26. II.1986, leg. W. Büttiker, Oman Eastern Sands Project, NHMB 691.00; 1♂, Wahiba Sands, Wadi Halfayn, under barrel on sand in old bedu camp under *Prosopis* trees, 21.08°N 58.25°E, 2. III.1986, leg. M. D. Gallagher, NHMB; 2♂, Wahiba Sands, 21.12°N 58.35°E, 60 m a. s. l., 7.III.1986, leg. M. D. Gallagher, Oman Eastern Sands Project, NHMB; 1♀, Wahiba Sands, 21.12°N 58.35°E, 60 m a. s. l., 7.III.1986, leg. M. D. Gallagher, Oman Eastern Sands Project, NHMB; 1♀1juv., Shaqq, camp, 21.12°N 58.37°E, 55 m a. s. l., 7.III.1986, leg. W. Büttiker, Oman Eastern Sands Project, NHMB 687.00; 1♂, Wadi Halfayn, Oman Eastern Sands Project, under *Prosopis* trees, 21.08°N 58.25°E, 8.III.1986, leg. M. D. Gallagher, NHMB; 1♂, 25 km W. of Shaqq, 21.12°N 58.15°'E, 10.III.1986, leg. W. Büttiker, Oman Eastern Sands Project, NHMB 688.00; 1♀, near Rusayl, capital area, 23.55°N 58.18°E, 17.IX.1986, Sultan of Oman's Land Forces 604.1, NHMB 51/20; 1♂, Sultan Qaboos University campus, Al Khod, crossing footpath of gravel & small stones, after dark, 23.57°N 58.12°E, 10.IV.1987, leg. S. M. Farook, NHMB Sc.1987.2; 1♂, Rumais, Al Batinah, in garden, 23.68°N 58.00°E, 8.V.1987, leg. A. Ahmed, ONHM 715.2; 1♂, Seeb, residential area, found climbing wall of house (old building), 23.68°N 58.15°E, 20.VI.1987, leg. A. Al Shariqi, NHMB Sc.1987.7; 1♀, Nakhl, found dead in fort, 23.27°N 57.83°E, 400 m a. s. l., 21.VI.1987, leg. J. Cain, NHMB 727; 1♀, Ghubra, Batinah coast, on sand and gravel, 23.27°N 57.70°'E, 15. VII.1987, leg. J. Cain, ONHM 745; 1♀, Barka, farmland, among leaves on ground, 23.70°N 57.97°E, 23.XI.1987, leg. A. Ali Sc.1987.19, NHMB 49/20; 1♂, Oman, 1988, leg. M. D. Gallagher, NHMB 1224; 1♀, near Muscat, 1988, Omanis, ONHM 1080; 1♀, Samad area, 22.80°N 58.15°E, 15.III.1988, leg. P. Yule, ONHM 928; 1♀, under artifact at old bedu camp, 22.40°N 57.05°E, 17.III.1988, 13:00 h, M. D. Gallagher MDG 8035, ONHM 1067; 1♂, Medinat Qaboos, among old decaying plant material near old wall of house, 23.60°N 58.47°E, 30. IV.1988, leg. S. M. Farook, NHMB Sc.1988.15; 1♀, near Seeb airport, killed in house on stony plain, 23.58°N 58.27°E, 20 m a. s. l., 15.VI.1988, leg. J. Cain, ONHM 996; 1♀, Al Khod, limestone ground, 23.60°N 58.08°E, VIII.1988, leg. M. J. Ebejer, ONHM 1102; 1♂3♀, Yalooni, Jiddat Al Harasis, 19.95°N 57.10°E, 150 m a. s. l., 1.VIII.1988, NHMB 1185.1-4; 1♀, Sultan Qaboos University campus, Al Khod, climbing wall near door, outside chemistry dept, 2nd floor, 23.57°N 58.12°E, 22.VIII.1988, leg. S. M. Farook, NHMB Sc.1988.19; 1♂, Azaiba, 23.60°N 58.37°E, 4.X.1988, leg. H. A. Al-Hasani, ONHM 1111; 1♀, Yalooni, 19.95°N 57.10°E, 150 m a. s. l., 1989, ONHM 1452; 1♂, Seeb, 23.68°N 58.15°E, 5.V.1989, leg. C. Hilary Fry, NHMB 15; 1♀, Thamrait & Matafah, on muddy road, dead, 17.65°N 54.03°E, 18.VIII.1989, leg. I. Brown & I. Gristad, NHMB 1348; 1♀, near Barka, on farm, 23.67°N 57.85°E, 50 m a. s. l., 26.V.1990, leg. B.W. Ritchie, NHMB 1604; 2♀, Shiafa Camp, near Izki, 22.93°N 57.78°E, 1.IX.1990, leg. N. Stafford, NHMB 18; 1♀, Huqf, Jiddat Al Harasis, in old *Prosopis* log, 1 km from escarpment, 19.93°N 57.33°E, 7.I.1991,

leg. A. S. Gardner, NHMB 19; 2♀, Dibab, under stone, on sandy, wooded plain, 23.10°N 59.03°E, 13.II.1991, leg. A. S. Gardner, NHMB 26; 1♂, west bank of Wadi Ateena, between Fasad & Shisr, 18.25°N 53.22°E, 320 m a. s. l., 29.III.1991, leg. R. P. Whitcombe, NHMB 1937; 1♀, Qarhat Mu'ammar, under dead log on sand, *Prosopis* woodland, 21.63°N 59.30°E, 20.IX.1991, leg. A. S. Gardner, NHMB 32; 1♂, Qarhat Mu'ammar, *Prosopis* woodland, field base, 21.63°N 59.30°E, 21.I.1992, A. S. Gardner, GLPC 37; 1♂, Yalooni, 19.93°N 57.10°E, X.1992, YAL 391, NHMB; 1♀, Yalooni, 19.93°N 57.10°E, X.1992, YAL 397, NHMB; 1♀, Barka, wadi, 23.70°N 57.88°E, 6.XI.1992, leg. Mariam, NHMB 43; 1♀, Madinat Qaboos, under flowerpot, 23.60°N 58.47°E, 100 m a. s. l., IV.1993, leg. S. Dias, NHMB; 1♂, Al Khuwayr south, 23.58°N 58.43°E, 28.IX.1993, leg. M. Jones, NHMB 2216; 1♀, Darsait, 23.62°N 58.53°E, 1.X.1993, Wafa, VF; 1♀, Wadi Bowshar, excavated from burrow in sand, edge of wadi, sandy wadi, *Prosopis* trees, 23.55°N 58.40°E, 50 m a. s. l., 4.X.1993, 21:30 h, leg. G. Lowe, M. D. Gallagher & T. Cope, GLPC; 6♂4♀, Quryat, UV detection, coastal sand dunes, on sand surface, warm & humid, coarse sand, scattered vegetation, trees, 23.23°N 58.91°E, 20 m a. s. l., 9.X.1993, 19:26 h, leg. G. Lowe & M. D. Gallagher, GLPC; 8♂7♀, Batinah Plain; 10-15 km W of Barka, Abyad pipeline road, UV detection, coastal sand dunes and sand flats, *Acacia* woodland, coarser sand, scattered vegetation, most scorpions near or at base of vegetation, 23.68°N 57.76°E, 50 m a. s. l., 13.X.1993, 19:03 h, leg. G. Lowe, A. S. Gardner & S. M. Farook, GLPC; 3♂13♀, Batinah Plain; 10-15 km W of Barka; Abyad pipeline road, UV detection, coastal sand dunes and sand flats, edge of *Acacia* woodland, less vegetation, 23.69°N 57.73°E, 50 m a. s. l., 13.X.1993, 21:05 h, leg. G. Lowe, A. S. Gardner & S. M. Farook, GLPC; 1♂3♀, Batinah Plain, 10-15 km W of Barka; Abyad pipeline road, UV detection, coastal sand dunes, near bases of vegetation, fine aeolian sand, 23.70°N 57.68°E, 50 m a. s. l., 13.X.1993, 22:34 h, leg. G. Lowe, A. S. Gardner & S. M. Farook, NHMB; 1♀, Yalooni camp, Yalooni, 19.93°N 57.10°E, 16.X.1993, leg. M. Lawrence, NHMB; 1♂, E of Thumrait; road to Marmul, UV detection, base of bush, first large wadi system, 1 km transect of wide open gravel wadi, tall vegetation, disturbed area, camel herds, 17.66°N 54.15°E, 500 m a. s. l., 19.X.1993, 19:45 h, leg. G. Lowe, NHMB; 1♂, Al Khod, Muscat, 23.55°N 58.12°E, 50 m a. s. l., 20.X.1993, leg. K. M. Azam, NHMB; 3♀, Yalooni, *Prosopis* woodland, on gravel plain, 19.95°N 57.10°E, 150 m a. s. l., 21.X.1993, leg. M. Fisher, NHMB; 2♀, Bayt Al Barakah, breeding center, 23.72°N 58.06°E, 0 m a. s. l., X.1993, leg. R. Woods, ONHM; 1♀, 1 juv, Bayt Al Barakah, breeding center, 23.72°N 58.06°E, 0 m a. s. l., X.1993, leg. R. Woods, NHMB; 1♂, Yalooni, limestone plateau with sand, trees, 19.93°N 56.10°E, 154 m a. s. l., 4.XI.1993, leg. C. J. V., YAL 521, NHMB; 1♂, Qurm, in house, 23.62°N 58.48°E, 20. XI.1993, leg. A. Abdullah Suleiman, NHMB; 1♀, Madinat Qaboos, under flowerpot on balcony of house, damaged by cat, 23.60°N 58.47°E, 100 m a. s. l., 11.XI.1993, leg. J. Hatch, ONHM; 1♂, near Sohar, in house, 24.35°N 56.72°E, III.1994, S. Musabah, ONHM; 1♂, Jiddat Al Harasis, under barrel in sandy depression, 19.87°N 57.10°E, 14.III.1994, leg. M. D. Gallagher MDG 8558, NHMB; 1♀, Jiddat Al Harasis, under metal object in sandy depression, 19.50°N 57.05°E, 150 m a. s. l., 14.III.1994, leg. M. D. Gallagher & M. W. Lawrence MDG 8557, NHMB; 1♀, Jiddat Al Harasis, under barrel in sandy depression, 19.48°N 57.05°E, 150 m a. s. l., 14.III.1994, 14:30 h, leg. M. D. Gallagher & M. W. Lawrence MDG 8556, GLPC; 2♂, Yalooni, in area of scattered trees, woodland, active on sand, near & under twigs fallen from *Prosopis* trees, clear sky, new moon, slight mild breeze, 19.93°N 57.08°E, 154 m a. s. l., 15.III.1994, 22:00 h, leg. M. D. Gallagher MDG 8564.1-2, NHMB; 1♂1♀, near Yalooni, Jiddat Al Harasis, under barrel on sand on stony plateau, 19.95°N 57.12°E, 154 m a. s. l., 16.III.1994, M. D. Gallagher MDG 8567, 8566, ONHM; 1♂1♀, Yalooni, Jiddat Al Harasis, UV detection, at entrance to burrow in sand mound, under *Acacia ehrenbergiana*, 19.95°N 57.12°E, 154 m a. s. l., 16.III.1994, 22:00-22:15 h, leg. M. W. Lawrence, M. D. Gallagher & G. Jones MDG 8572, ONHM; 1♀, N of Yalooni, under barrel on sand with beetles, 20.00'N 57.07°E, 150 m a. s. l., 17.III.1994, 14:00 h, leg. M. D. Gallagher MDG 8570, NHMB; 1♀, 12 km N of Yalooni, under barrel on sand, evidence of human occupation of vegetated depression on stony plateau 20.03°N 57.05°E, 150 m a. s. l., 17.III.1994, leg. M. D. Gallagher MDG 8571, NHMB; 1♂, Lasail, 24.32°N 56.41°E, IV.1994, leg. S. Musabah, NHMB; 1♂, Yalooni, on house, 19.93°N 57.10°E, 154 m a. s. l., 6. IV.1994, leg. M. W. Lawrence, NHMB; 1♂, Khawr Sallan, at entrance to small burrow in earth bank above sabkha, 24.40°N 56.72°E, 2 m a. s. l., 7.IV.1994, leg. C. J. N. Roberts & M. D. Gallagher MDG 8596, ONHM; 1♀, S margins of Al Abyad dune field, 23.57°N 57.72°E, 50 m a. s. l., 14.V.1994, leg. A. S. Gardner, NHMB; 1♀, 20.VII.1994, per M. D. Gallagher, NHMB; 1♀, near Madinat Qaboos, on porch of house on dunes, 23.59°N 58.48°E, 8.VIII.1994, 07:15 h, leg. V. Newns, NHMB; 1♂, Magan, 24.42°N 56.58°E, 13.VIII.1994, leg. S. Wilde & S. Kinver, ONHM; 1♂, Madinat Qaboos, in house on sand near rocky wadi, 23.60°N 58.47°E, 15.IX.1994, J. Johnstone, NHMB; 1♂, road to Jamma, on rock, near area of low dunes, north of low hills, 23.55°N 57.50°E, 150 m a. s. l., 25.IX.1994, leg. G. Lowe & M. D. Gallagher, NHMB; 1♂, Al Hayl, Muscat, sandy area with *Prosopis* trees, 23.63°N 58.26°E, 28.IX.1994, leg. A. S. Gardner, NHMB; 1♀, Bukha, Musandam Peninsula, UV detection on rock ledge at base of cliffs and stone wall, tree stands at north end of village, 26.15°N 56.16°E, 0 m a. s. l., 29. IX.1994, leg. G. Lowe, GLPC; 2♂1♀, east Wahiba Sands, *Prosopis* woodland, humpy dunes to hard sandy flats, sabkha, 21.66°N 59.30°E, 95 m a. s. l., transect 0.83 km E to 0.4 km W, 4.X.1994, leg. G. Lowe & M. D. Gallagher, GLPC; 1♂, Al Khod, 23.57°N 58.12°E, 50 m a. s. l., 20.XI.1994, leg. S. Said Mayid, NHMB; 1♂, Wahiba Sands, 22 km N of field base, UV detection, on sand dunes under *Prosopis cineraria* woodland, 21.84°N 59.31°E, 20 m a. s. l., 29.XII.1994, 19:00 h, leg. B. Skule & M. D. Gallagher MDG 8655, NHMB; 2♀, Bayt Al Barakah Mammal Breeding Centre, killed 6.VII.1995, 23.70°N 58.10°E, 30 m a. s. l., 1995, leg. R. Wood, NHMB; 1♀, Yalooni, 19.93°N 57.10°E, 17.V.1995, leg. M. W. Lawrence YAL 579, ONHM; 1♀, near Seeb, between fort roundabout and beach, moving rapidly in open, 23.60°N 58.25°E, 15 m a. s. l., 1.

VI.1995, leg. J. Dundon, NHMB; 1♂, Izki, in workshop area, 22.95°N 57.78°E, 590 m a. s. l., 24.VIII.1995, leg. J. Dundon, NHMB; 1♀, Izki area, 22.95°N 57.78°E, 590 m a. s. l., 4. IX.1995, leg. J. Dundon, NHMB; 1♀, between Ghabah & Adam, UV detection on sand, sandy wadi on open gravel plain, trees and bushes, 22.16°N 57.50°'E, 250 m a. s. l., 16.IX.1995, 22:00-23:00 h, leg. G. Lowe & J. Dundon, ONHM; 1♀, wadi south of Nizwa roundabout, near main road, UV detection, sandy wadi, 22.74°N 57.56°E, 380 m a. s. l., 17.IX.1995, 20:30 h, leg. G. Lowe, NHMB; 1♂1♀, Wadi Matam, south of Sinaw, soft sandy wadi, 21.79°N 58.28°E, 155 m a. s. l., 19.IX.1995, 18:30 h, leg. G. Lowe & M. D. Gallagher, NHMB; 2♂, Wadi Andam, road south of Sinaw, sandy wadi, UV detection at bases of trees, strong winds, scattered *Acacia tortilis*, *Prosopis cineraria*, 21.47°N 58.25°E, 90 m a. s. l., 19.IX.1995, 20:30 h, G. Lowe & M. D. Gallagher, GLPC; 1♂1♀, N edge of Duqm, UV detection, sandy area with scattered trees, sandy wadi with trees, saltbush, 19.66°N 57.64°E, 30 m a. s. l., 23.IX.1995, leg. G. Lowe & M. D. Gallagher, NHMB; 1♀, E. of Duqm, UV detection on ground, densely vegetated wadi, 19.65°N 57.67°E, 30 m a. s. l., 23.IX.1995, 23:50 h, leg. G. Lowe &M. D. Gallagher, ONHM; 8♂5♀, near Yitti, UV detection, on sand near bases of bushes and trees, burrows, wadi near village, soft sandy soil, rocky slopes at edge of wadi, 23.51°N 58.64°E, 0 m a. s. l., 1.X.1995, G. Lowe, M. D. Gallagher & A. Al-Baluchi, GLPC, ONHM (1♂); 1♀, Izki area, on open sandy ground, near farmland and gardens, 22.95°N 57.78°E, 590 m a. s. l., 29.X.1995, 21:00 h, leg. J. Dundon, NHMB; 1♀, Al Ghubra, in garden, 23.60°N 58.40°E, 15 m a. s. l., 17.XII.1995, leg. J. Neilson, ONHM; 1♀, 30 km S of Adam, in a sandy wadi, 22.10°N 57.52°'E, 19.III.1996, 23:30-01:00 h, leg. J. Dundon 118, NHMB; 1♂, Ghabah North area, south of Adam, in sandy wadi, 21.76°N 57.29°E, 150 m a. s. l., 19.III.1996, 20:30-21:15 h, leg. J. Dundon 117, NHMB; 1♂1♀, Yalooni, 19.93°N 57.10°E, 31.VIII.1996, leg. S. Brend, YAL 593, NHMB; 1♀, Ra's Al Hamra, in hills, 23.63°N 58.50°E, 10.XI.1996, leg. S. Fryer, ONHM; 1♀, Yalooni, Yalooni camp, 19.93°N 57.10°E, 1.VII.1997, leg. S. Brend, YAL 617, NHMB; 1♀, Thumrait, wadi, E of Thumrait, under rocks on sand & gravel, 17.70°N 53.98°E, 8.VII.1997, leg. J. N. Barnes, NHMB; 1♀, Thumrait, on garden wall under light, 17.70°N 53.98°E, 26.VIII.1997, 04:30 h, leg. J. N. Barnes, GLPC; 5♂, Dhuai, 21.10°N 58.37°'E, 70 m a. s. l., 21.X.1997, leg. M. D. Gallagher & I.D. Harrison MDG 8889, EV (1♂), ONHM; 2♀, Shisr, 18.25°N 53.65°E, 7.XI.1997, leg. S. Polak, NHMB; 1♀, Wadi Rawnub, under a large rock on sandy soil, 18.87°N 56.55°E, 9.II.1999, leg. I. Harrison, ONHM; 1♀, 5 km along road to Kitnah, 24.16°N 56.21°E, 15.II.2001, leg. M. P. T. Gillett, NHMB; 1♀, Madam Plain, camel station in sand on gravel plain, 24.94°N 55.88°E, 250 m a. s. l., 10.VIII.2001, leg. G. Feulner, GLPC; 1♂, hemispermatophore, south of Shalim, 18.04°N 55.62°E, leg. M. Stockmann, GLPC; 1♂, hemispermatophore, leg. W. Al Fath & D. Král, GLPC. **UAE**: 1juv., Al Fujayrah, area of sand and trees, about 800 yards from sea, 25.14°N 56.35°E, 29.VI.1972, leg. D. J. G. Williams, MNHN RS 6459, faded specimen; 1♂2♀, 1 juv, Al Fujayrah, sandy desert with shrubs, 25.14°N 56.35°E, X.1972, leg. D. J. G. Williams, MNHN RS 6505; 1♀, Ras al Khaymah, Trucial Coast, 25.77°N 55.94°E, VI.1973, leg. M. D. Gallagher MDG 2445, MNHN RS 6535; 1♂, subadult, Sharjah, Wadi Yudayah, Mileiha, 25.11ºN 55.78ºE, 24.XI.2013, 14G47-50, leg. P. Kučera, FKCP; 1♀, Dubai, Lahbab, Butti Bin Maktoum Bin Juma Al Maktoum's Farm, 25.04°N 55.58°E, 120 m a.s.l, 27.VII.2019, leg. B. Buzas, FKCP, UAE212; 1♂, Fujairah, Wadi Madab, Al Mayya Sanctuary, 25.14°N 56.32°E, 16 m a. s. l., 24.IX.2019, leg. N. J. Makevitage, FKCP, UAE256; 1♂, Dubai, Al Awir, 25.16°N 55.55°E, 81 m a. s. l., 26.I.2020, leg. N. J. Makevitage, FKCP, UAE436.

Comparative material.

Androctonus '*crassicauda*' complex. **Egypt**: 1♀, Sinai, Wadi Feran, III–VI.1914, leg. W. M. Mann (J. C. Phillips Exped.), MCZ; 1♀, near Abu Rawash, Giza, 1952, leg. G. Malakatis, USNM 57-1069. **Iraq**: 2♀, 26.I.1981, MNHN RS 8406. **Israel**: 1♀, Kefar, Shemuel, IV.1968, leg. S. Bleszynski, USNM; 1♂, Yas'ur, 32.89°'N 35.16°E, 6.VII.1970, leg. G. Levy Sc 1891, MCZ; 1♀, Beit Guvrin, 5.V.1973, leg. G. Tsabar, MCZ; 1♂, Judea, NW of Lahav, 5.III.1975, leg. H. Levi & P. Amitai, MCZ. **Jordan**: 1♂1♀, Wadi Rum, 13.I.1978, G.R.S.T.S., MZUF. **Saudi Arabia**: 1♂, leg. T. Ulke, USNM; 1 juv, Ras Mashab, 28.15'N 48.65°'E, III.1950, USNM; 2♂, between Ras Tanura and Ras Mishab, 27°N 49°E, X.1951, U.S. Navy Expedition, USNM; 1♂, east province, El Khobar, under board, margin of small sewage settling pond circled by Tamarisk, 105°F, 80% relative humidity, 10.IX.1978, 15:30 h, leg. J. A. Shetterly, MCZ; 1♀, nr Khaybar, 25.45°N 39.28°E, X.1985, leg. J. & P. Gasparetti, NHMB.

Androctonus amoreuxi amoreuxi. **Egypt**: 2♂1♀, Aswan, El Biyara, Kom Ombo, XI-XII.1962, leg. T. E. Lovejoy, USNM. **Senegal**: 1♂2♀, Dourabel Region, 17 km NE Dourabel to N'doulo, then 2 mi. N of N'doulo by dirt road, 12.XI.1965, leg. D. E. Harvey, USNM; 1juv.♀, Sin-Soloum Region, 20.XI.1965, leg. D. E. Harvey, USNM; 2♂, 1♀, Podor River Region, 26.III.1966, leg. D. E. Harvey, USNM; 1♀, Linguere Diourbel Region, 23.V.1966, leg. D. E. Harvey, USNM.

Androctonus amoreuxi hebraeus. **Egypt**: 1♂3♀, 1 juv, near Cairo, summer 1908, leg. A. J. Thompson, USNM 213, 864; 1♂, Sakara, X.1950, USNM 57-936; 2♂1juv.♀, near Sakara, Giza Province, under rocks in open desert, 5.XII.1950, leg. A. Roash & R. E. Kuntz, USNM 57-1135, 57-1142; 1 juv, Fouodiga Province, Baffim, 28.IX.1954, leg. W. H. Wells & B. H. Randall, USNM. **Israel**: 1♂1♀, Mamshit, 20.VI.1972, leg. P. Amitai MCZ Sc2287, Sc2290.

Androctonus australis. **Egypt**: 1♂, Bir Victoria, by Aly Tolba in open desert, 11.X.1951, leg. R. E. Kuntz, USNM 57-797; 1♀, Gebel Ahmar, 5 miles E. of Cairo, 12.X.1954, leg. W. H. Wells & B. H. Randall, USNM 57-905; 1♂1♀, 2008, GLPC. **Libya**: 2♂2♀, about 100 mi. inland from Tripoli, on sand in dune, III.1959–XII.1960, leg. P. F. Alexander, USNM. **Tunisia**: 1♂1♀, MZUF A.C.25 C.t.102, C.t.100.

Androctonus barahoeii. **Iran**: 4♂5♀, 35 km E of Gach Saran, Camp 11, 30.27°N 51.23°'E, 6.II.1964, leg. J. Neal, USNM; 1♂2♀1juv., 35 km E of Gach Saran, Camp 11, 30.27°N 51.23°'E, 9.II.1964, leg. J. Neal, USNM; 1♀, 35 km E of Gach Saran, Camp 11, 30.27°N 51.23°'E, 2 Sept 1964, leg. J.

Neal; 1♀ (paratype), Chahar Mahal & Bakhtiyari Prov., Aloni village, 31.54°N 51.07°E, 1883 m a. s. l. (Locality No. SH-3), XII .2007, leg. Pirali, FKCP; 1♂1♀ (paratypes), Markazi Prov., Delijan-Mahalat, 33.87°N 50.47°E, 1610 m a. s. l., V.2014, leg. Masihipour, Hayader & Behmam, FKCP.

Androctonus bicolor. **Egypt**: 1juv,, Western Desert Governorate, El Amiriya, 1.X.1954, leg. W. H. Wells & B. H. Randall, USNM 57-1066; 6♂10♀, Western Desert Governorate, El Amiriya, 14.IX.1954, leg. W. H. Wells & B. H. Randall, USNM. **Israel**: 1♀, Tel-Aviv, 32.03°N 34.46°E, 15.IX.1970, leg. A. Keller, MCZ Sc2230; 1♂, Nahal Oren, 1.VII.1970, leg. G. Levy, MCZ. **Libya**: 3♂2juvs. ♂, first escarpment inland from Tripoli about 250 mi., on rock, III.1959–XII.1960, leg. P. F. Alexander, USNM.

Androctonus caspius. **Iran**: 1♂1♀ (topotypes), Alborz Province, Hive village to Immazadeh Mousa, 36.06°N 50.65°E, 687 m a. s. l. (Locality No. Al-103), VI.2013, leg. Rabiei, Barzegar and Fallahpour, FKCP; 1♂1♀ (paratypes), Tehran Province, Firooz kooh, Semnan Rd, Pirdeh, 35.71°N 52.82°E, 2559 m a. s. l., V.2012, leg. Rabiei, Barzegar and Fallahpour, FKCP.

Androctonus crassicauda. **Iran**: 1♀, 10 km N Kashan, 13.V.1964, leg. J. Neal, USNM.

Androctonus mauritanicus. **Morocco**: 3♀, French Morocco, Safi, under rocks in cultivated fields, 22.IV.1943, leg. A. G. Humes, USNM 174363; 1♂, Marrakesh, under stone, VI.1960, leg. N. L. H. Krauss, USNM; 1♂, Nouasseur Air Base, 10.VIII.1962, leg. E. C. Trivette, USNM.

Androctonus orientalis. **Iran**: 1♀, Baluchistan, 85 km N of Zahedan, 10-11.II.1963, leg. L. H. Herman, USNM; 1 juv ♂, Kerman, 5 km NE of Bandar Abbas, 16-19.III.1963, leg. L. H. Herman, USNM; 1♂, 4km N of Lar, 25.VII.1965, leg. J. Neal, USNM.

Androctonus sumericus. **Iran**: 1♂, Awhaz, 1943-1944, leg. S. Pollock, USNM; 2♀, Khuzestan Province, 16 km S of Masjed Soleyman, under rocks, 25.II.1964, leg. J. Neal, USNM.

Androctonus transcaucasicus. **Iran**: 1♀, near Khoy, X.1959, leg. J. Drea & T. O'Connell, USNM; 1♀, East Azerbaijan Prov., Jolfa, 28.VII.1964, leg. J. Neal, USNM 71.21.

Etymology. Named after the country of occurrence.

Diagnosis ♂♀. Adult total length: ♂ 65–90 mm (mean ± SD: 76 ± 6 mm, N = 51), ♀ 70–100 mm (84 ± 7 mm, N = 52); base color typically uniform dark brown to almost black, but ranging to pale brown or yellowish; legs with tarsi more pale than proximal segments; metasoma robust, wider posteriorly, segment IV W/ segment I W: ♂ 1.2–1.3, ♀ 1.1–1.3; metasoma IV L/W: ♂ 1.0–1.2, ♀ 1.1–1.2; metasoma V L/W: ♂ 1.2–1.4, ♀ 1.3–1.5; metasoma IV L/D: ♂ 1.1–1.4, ♀ 1.2–1.4; metasoma V L/D: ♂♀ 1.5–1.8; metasoma V D/ carapace L: ♂♀ 0.6–0.7; segments II–III with median lateral carinae reduced to several posterior terminal granules, II with 1–5 granules (mode 3), III with 1–3 granules (mode 2); segments II–IV with dorsolateral carinae strongly elevated, bearing dentate granules, dorsal furrow deeply excavated; metasoma V ventrolateral carinae with dentate granules gradually increasing in size posteriorly, not abruptly enlarged and lobate; metasoma V dorsolateral carinae with blunt, rounded granules anteriorly; metasoma I dorsal surface smooth, metasoma II–IV lateral surfaces with moderately dense, fine granulation; metasoma V with 1–2 very weak lateral anal lobes; ventral surface of telson vesicle with coarse granulation; fixed finger trichobothrium *db* proximal to *est*; hemispermatophore basal lobe long, digitate; pedipalp segments robust, femur L/W: ♂ 2.3–2.9, ♀ 2.4–2.8; patella L/W: ♂♀ 2.1–2.7; chela robust, with broad manus, chela L/W: ♂ 3.3–4.2, ♀ 3.5–4.6; L/D ♂ 3.0–3.6, ♀ 3.2–3.4; manus with carinae obsolete; internal surface of manus with fine granulation, stronger in male; dentate margins of fingers proximally undulate, leaving gap when closed, weaker in female, stronger in male; number of subrows of median denticles, including proximal subrow (♂♀): movable finger 13–15, fixed finger 12–15; pectinal tooth count: ♂ 29–34,♀ 24–31; internal fulcra of pectines with single microseta; prolateral basitarsal spurs with simple, undivided basal tooth, sparsely to moderately setose, leg III spur with 6–29 macrosetae (≤ 25 in 97% of cases; median 17).

Comparisons. Other species in the *A*. '*crassicauda*' complex differ from *A*. *omanensis* **sp**. **n**. according to the following characters:

(1) *A*. *azerianus* Yağmur & Kovařík, 2025: (i) metasoma not as dilated posteriorly, segment IV W/ segment I W: ♂ 1.1, ♀ 1.0; (ii) metasoma V not as deep, D/ carapace L: ♂♀ 0.5, L/D ♂♀ 2.0; (iii) more elongate pedipalp segments: femur L/W ♂ 3.2, ♀ 3.1; patella L/W ♂♀ 2.8; chela L/ W ♂ 4.4, ♀ 4.8; (iv) pedipalp chela not as deep, L/D ♂ 3.8, ♀ 4.3; (v) internal surface of pedipalp chela manus almost smooth, with only scattered fine granules; (vi) lateral inframedian carinae weakly developed as fine granules on middle part of metasoma II.

(2) *A*. *barahoeii* Kovařík & Yağmur, 2025: (i) metasoma not as dilated posteriorly, segment IV W/ segment I W: ♂ 1.1, ♀ 1.0–1.1; (ii) metasoma V not as deep, D/ carapace L: ♂ 0.6, ♀ 0.5; (iii) ♂ pedipalp femur more elongate: L/W 3.0–3.3; (iv) ♀ pedipalp chela more elongate: L/W 4.9–5.0; (v) pedipalp chela not as deep, L/D ♂ 3.5–3.9, ♀ 4.1–4.4; (vi) lateral surfaces of metasomal segments smooth; (vii) enlarged, lobate dentition on posterior ventrolateral carinae of metasoma V.

(3) *A*. *caspius* Kovařík et al., 2025: (i) metasoma not as dilated posteriorly, segment IV W/ segment I W: ♂ 1.1–1.2, ♀ 1.1; (ii) metasoma V not as deep, D/ carapace L: ♂ 0.5–0.6, ♀ 0.5, L/D ♂♀ 1.8–1.9; (iii) ♂ pedipalp more elongate: patella L/W 2.7–2.8, femur L/W 3.2–3.3, chela L/W 4.4–4.7; (iv) pedipalp chela not as deep, L/D ♂ 3.8–4.2, ♀ 4.1–4.3; (v) lateral surfaces of metasomal segments smooth; (vi) enlarged, lobate dentition on posterior ventrolateral carinae of metasoma V; (vii) internal surface of pedipalp chela manus sparsely granulate, almost smooth.

(4) *A*. *crassicauda* (Olivier, 1807): (i) metasoma not as dilated posteriorly, segment IV W/ segment I W: ♂♀ 0.9–1.0; (ii) metasoma V not as deep, D/ carapace L: ♂♀ 0.4–0.5, L/D ♂ 2.0–2.1, ♀ 2.1–2.3; (iii) dorsolateral carinae of metasoma V anteriorly serrate, with sharp, dentate granules; (iv) generally smaller denticles on posterior part of ventrolateral carinae of metasoma V.

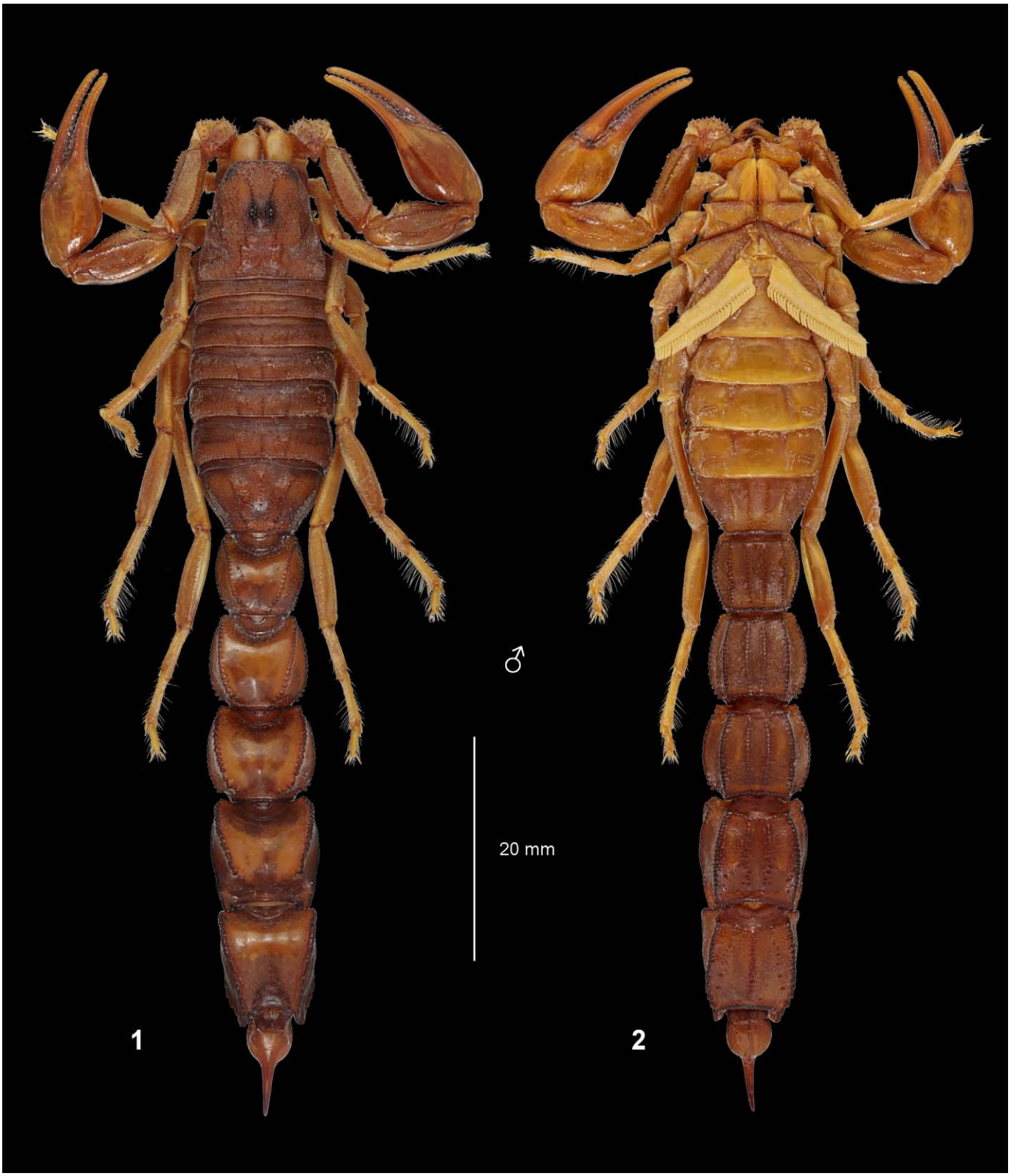

Figures 1–**2**. *Androctonus omanensis* **sp**. **n**., holotype male. Barka, 15.IX.1995. Habitus in dorsal (1) and ventral (2) views. Scale bar: 20 mm.

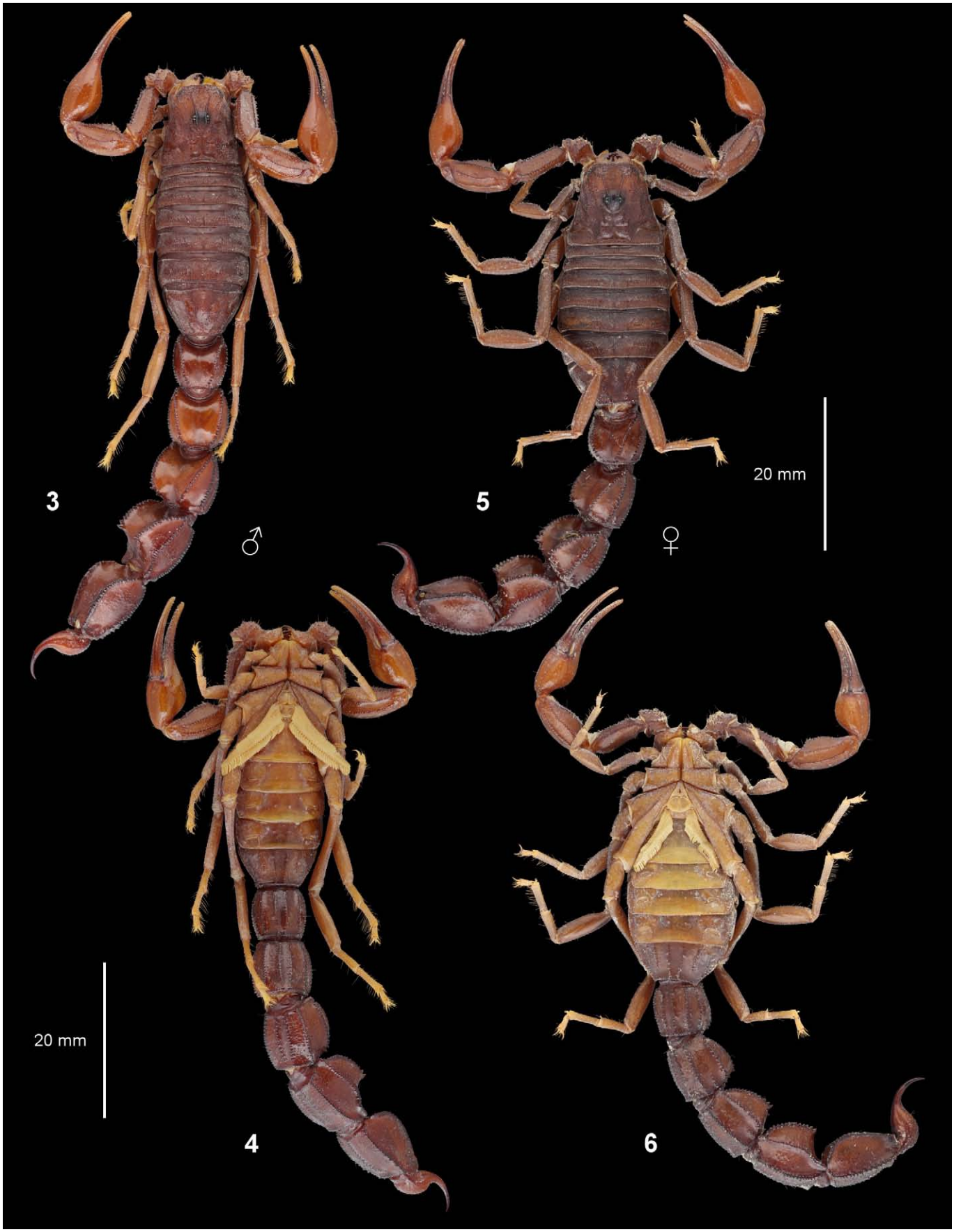

Figures 3–**6**. *Androctonus omanensis* **sp**. **n**., paratype male, Dhuai, 21.X.1997 (3–4) and paratype female, Shiafa camp, Izki, 1.IX.1990 (5–6). Habitus in dorsal (3, 5) and ventral (4, 6) views. Scale bars: 20 mm.

Figures 7–**12**. *Androctonus omanensis* **sp**. **n**., color variation in paratypes. Habitus in dorsal view. **Figure 7**. Adult female, Wadi Ateana, Fasad-Shisr, 29.III.1991. **Figure 8**. Juvenile male, Yalooni, Jiddat al Harasis, 16.III.1994. **Figure 9**. Subadult male, Wahiba (Sharqiyah) Sands, 4.X.1994. **Figure 10**. Adult male, Madinat Qaboos, 15.IX.1994. **Figure 11**. Subadult female, Wadi Bowshar, 4.X.1993. **Figure 12**. Subadult female, Madinat Qaboos, 8.VIII.1994. Scale bars: 10 mm.

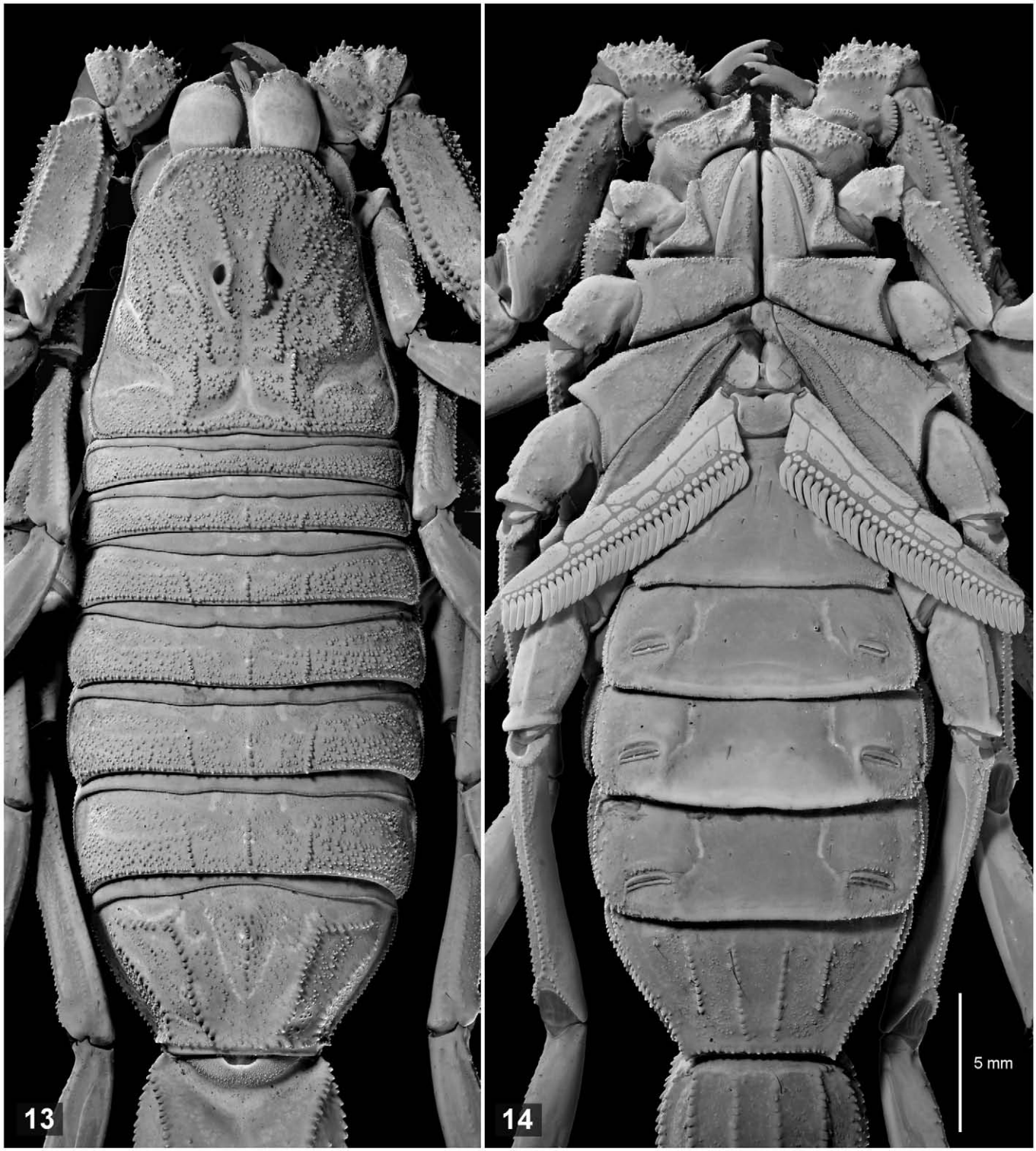

Figures 13–**14**. *Androctonus omanensis* **sp**. **n**., holotype male. Prosoma and mesosoma in dorsal (13) and ventral (14) views. Scale bar: 5 mm. UV fluorescence.

(5) *A*. *ishtar* Yağmur et al., 2025: (i) metasoma not as dilated posteriorly, segment IV W/ segment I W: ♂ 1.1, ♀ 1.0; (ii) metasoma V not as deep, D/ carapace L: ♂♀ 0.5, L/D ♂♀ 2.0; (iii) enlarged, lobate dentition on posterior ventrolateral carinae of metasoma V; (iv) pedipalp fixed finger with trichobothrium *est* level with, not distal to *db*; (v) lateral surfaces of metasomal segments smooth.

(6) *A*. *kunti* Yağmur, 2023: (i) metasoma not as dilated posteriorly, segment IV W/ segment I W: ♂♀ 1.1; (ii) metasoma V not as deep, D/carapace L: ♂♀ 0.5; (iii) ♂ pedipalp more elongate: femur L/W 3.1; patella L/W 2.8; chela L/W 4.5; (iv) ♀ pedipalp chela more elongate, L/W 4.6; (v) pedipalp chela not as deep, L/D ♂♀ 4.3; (vi) enlarged, lobate dentition on posterior ventrolateral carinae of metasoma V; (vii) lateral

surfaces of metasomal segments smooth.

(7) *A. orientalis* Birula, 1900: (i) ♂ metasoma not as dilated posteriorly, segment IV W/ segment I W 1.1; (ii) ♂ metasoma V not as deep, L/D 1.9; (iii) ♂ metasoma I more elongate, L/W 1.0; (iv) dorsolateral carinae of metasoma V anteriorly serrate, with sharp, dentate granules.

(8) *A. sumericus* Al-Khazali & Yağmur, 2023: metasoma V not as deep, D/ carapace L : ♂ 0.5–0.6, ♀ 0.5, L/D ♂ 1.9, ♀ 1.8–2.2.

(9) *A. tihamicus* Alqahtani et al., 2023: (i) metasoma V not as deep, L/D ♂ 1.9–2.0, ♀ 1.9–2.4; (ii) ♀ metasoma V more elongate, L/W 1.6–1.9; (iii) average size of adults smaller, 60–85 mm total length; (iv) internal surface of pedipalp chela manus of male sparsely granulate, of female almost smooth.

(10) *A. transcaucasicus* Kovařík et al., 2025: (i) metasoma not as dilated posteriorly, segment IV W/ segment I W: ♂♀ 1.1; (ii) ♀ metasoma V not as deep, D/ carapace L 0.4, L/D 2.1; (iii) pedipalp femur more elongate: L/W ♂ 3.3, ♀ 3.1; (iv) pedipalp chela not as deep, L/D ♂ 3.9, ♀ 4.1; (v) lateral surfaces of metasomal segments smooth; (vi) enlarged, lobate dentition on posterior ventrolateral carinae of metasoma; (vii) internal surface of pedipalp chela manus smooth.

(11) *A. turkiyensis* Yağmur, 2021: (i) posterior metasomal segments not as deep, segment L/D: ♂ IV 1.4, V 2.1, ♀ V 1.8–2.0; (ii) posterior metasomal segments narrower, segment L/W: ♂ IV 1.2, V 1.5; ♀ IV 1.3; (iii) ♂ pedipalp femur more elongate, L/W 3.1; (iv) enlarged, lobate dentition on posterior ventrolateral carinae of metasoma V.

Graphical comparisons of morphometric ratios are plotted in Figs. 171–174. Horizontal bars indicate ranges of selected ratios of *A. omanensis* **sp. n.**, alongside the same ranges of eleven other species of the *A.* '*crassicauda*' complex. The plots reveal some general trends: *A. omanensis* **sp. n.** tended to have wider and deeper posterior metasomal segments and stockier pedipalps than other species. In many cases, ratios of *A. omanensis* **sp. n.** also had greater ranges of variation. This does not necessarily imply that it is a more variable species because the ranges characterize larger samples (48 ♂, 50 ♀), whereas ranges of the other species are based on smaller samples. When additional samples of other species are analyzed, their ranges are expected to expand and overlap more with the ranges of *A. omanensis* **sp. n.** This may modify some of the differential diagnoses listed above, although the general trends are likely to persist.

One of the other species, *A. tihamicus*, had moderately larger samples (5 ♂, 10 ♀), and ratios with much higher ranges of variation (Figs. 173–174, orange bars). The ranges of several ratios exceeded those of *A. omanensis* **sp. n.** This seemed anomalous because the *A. tihamicus* samples all originated from a single locality (Al-Qunfuda, Saudi Arabia; Alqahtani et al., 2022a; 2023), whereas *A. omanensis* **sp. n.** was represented by five or ten times as many samples from 95 localities spanning almost the entire length of Oman (> 900 km). It raises doubts about the accuracy of some of the published measurements of *A. tihamicus* (cf. discussion under Morphometric Analysis).

Description ♂♀ (adults). **Coloration** (Figs. 1–12, 115, 197–200). Base color variable, typically a darker shade of reddish- or orange-brown, or almost black, ranging to a lighter shade of brown, or pale yellowish-brown in some individuals; contrasting color patterns usually absent; in darker individuals, sternites III–VI, the distal parts of pedipalp fingers, and the leg basitarsi and telotarsi may be lighter; pectines pale, yellowish.
Carapace (Figs. 13, 15, 179). Weakly trapezoidal, W/L 0.97–1.17, posterior W/anterior W 1.90–2.85; median ocular tubercle prominent, superciliary carinae coarsely granulate; 5 pairs of lateral ocelli in Type 5 configuration (Loria & Prendini, 2014), with major PLMa, MLMa and ALMa, and minor PDMi arranged linearly below short granulated carina, minor ADMi above carina; anterior median carinae strongly developed, coarsely granulate, not reaching anterior margin of carapace; central median, central lateral and posterior median carinae moderately developed, granulate; anterior margin of carapace with row of coarse granules, posterior margin with row of fine granules; left and right areas of anterior preocular region coarsely granulate, central lateral flanks granulate to finely granulate, posterior lateral flanks finely granulate; other intercarinal surfaces bearing sparse fine granulation, shagreened, or smooth; posterior median and posterior lateral sulci smooth; carapace granulation weaker in females than males; anterior margin of carapace sparsely setose.
Chelicerae (Figs. 75–76, 189–190). Dorsal surface of manus with coarse and fine granules located anteriorly around several short microsetae; dorsointernal carina strong, granulate, bearing one macroseta; central and posterior dorsal surfaces of manus smooth; fingers robust with dentition typical of the genus (Vachon, 1963): movable finger external margin with large distal external and distal internal denticles, large subdistal and median denticles and two small basal denticles, internal margin with large median and basal denticles, fixed finger with large subdistal denticle and median and basal denticles fused into proximal bicusp, two large denticles on ventral surface, the distal larger, the proximal smaller; dorsal surface of movable finger smooth, with several microsetae, ventral surface smooth with numerous long macrosetae; dorsal surface of fixed finger smooth with several macrosetae at base, ventral surface smooth with numerous long macrosetae; ventral surface of manus smooth with numerous long macrosetae.
Coxosternal area (Figs. 14, 16). Anterior margins of coxae I–IV and posterior margins of coxae III–IV densely granulate, carinate; posterior margins of coxae I–II irregularly granulate; endite I densely granulate, endite II sparsely granulate; other coxal surfaces sparsely, finely granulate; coxal granulation weaker in females than males; sternum with sparse, fine granules or smooth, subtriangular, with deep posteromedian pit, genital opercula rounded triangular, with sparse, fine granules on anterior or posterior margins, or smooth.
Pectines (Figs. 14, 16, 86–90, 102–103, 191–192). Basal piece wider than long, with convex lateral margins and small anteromedian notch, surface smooth; pectines with 3 marginal lamellae, 7–9 middle lamellae; distal tips extending

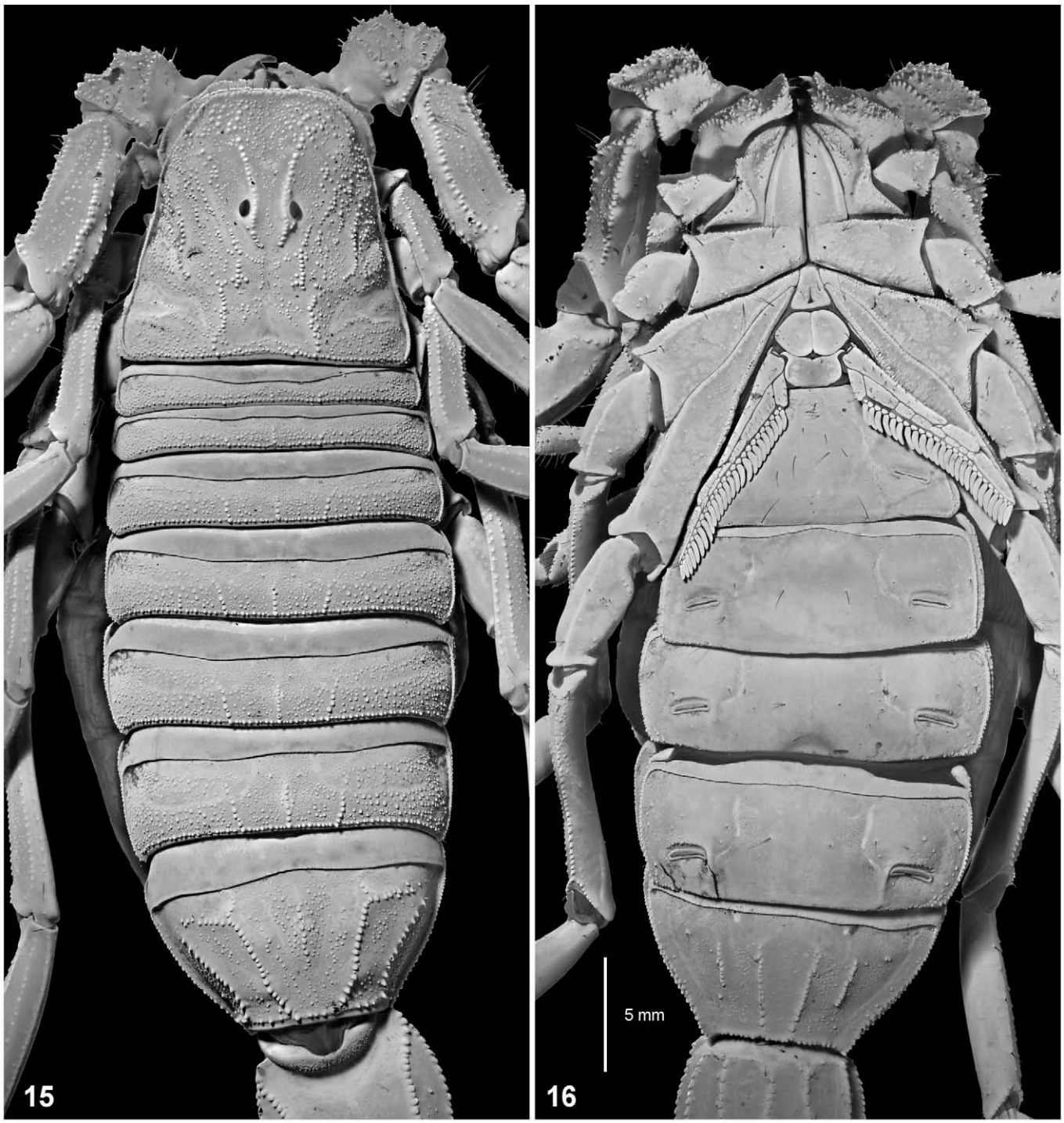

Figures 15–**16**. *Androctonus omanensis* **sp**. **n**., paratype female. Batinah coast, W of Barka, 13.X.1993. Prosoma and mesosoma in dorsal (15) and ventral (16) views. Scale bar: 5 mm. UV fluorescence.

to proximal third to half of trochanter IV in males, distal end of coxa IV in females; male combs with 29–34 teeth, female combs with 24–29 teeth, teeth longer in males than females; marginal and middle lamellae with sparse to moderately dense cover of macrosetae; fulcra with 3–7 macrosetae in males, 2–5 macrosetae in females; internal fulcra with single microseta.

Hemispermatophore (Figs. 77–79, 187–188). Flagelliform, trunk elongate, ca. 7 times length of capsule region; flagellum short with thicker, laminate pars recta and thinner cylindrical pars reflecta; sperm hemiduct with three lobes, posterior lobe large and laminate, median lobe small and acuminate, anterior lobe of intermediate length, tapered; posterior margin of median lobe overhanging posterior lobe, the two lobes fused along a median lobe carina; basal lobe a prominent, narrow, hook-like projection.

Mesosoma (Figs. 13–16, 179). *Tergites*: pretergites smooth with finely corrugated posterior margins; tergites with sparse to dense, medium-to-fine granulation; anterior surfaces with

Figures 17–**19**. *Androctonus omanensis* **sp**. **n**., holotype male. Metasoma and telson in dorsal (17), right lateral (18) and ventral (19) views. Scale bar: 10 mm. UV fluorescence.

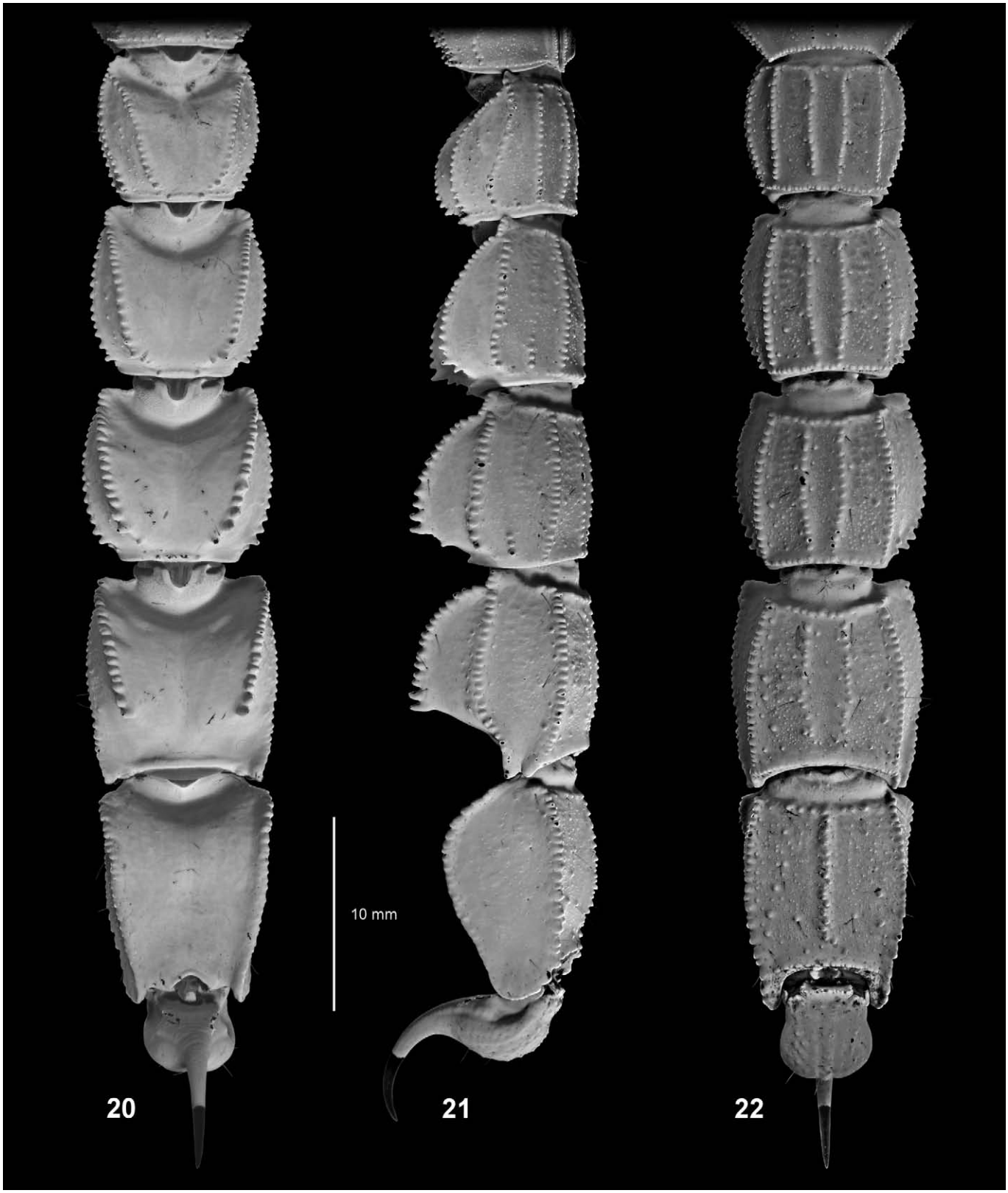

Figures 20–**22**. *Androctonus omanensis* **sp**. **n**., paratype female. Batinah coast, W of Barka, 13.X.1993. Metasoma and telson in dorsal (20), right lateral (21) and ventral (22) views. Scale bar: 10 mm. UV fluorescence.

finer granulation, becoming smooth or lightly shagreened near pretergite margins; tergite I without carinae or with trace of weak median carina; tergite II with weak median carina, traces of weak lateral carinae; tergites III–VI tricarinate with median and paired lateral carinae; all carinae on tergites I–VI granulate, confined to posterior 50–70% of tergites, lateral carinae anteriorly divergent; tergite VII with five carinae, median carina weak; tergite granulation and carination weaker in females than males; posterior margins of tergites I–VI bordered by dense rows of small granules; all tergites lacking macrosetae. *Sternites*: sternites III–VI medially smooth, may be shagreened or finely granulate along lateral margins; sternite VI with short, smooth or weakly granulate pairs of lateral carinae; posterior margins of sternites III–VI smooth; sternite VII texture varying from weakly shagreened or sparsely, finely granulated to smooth, with granulate pairs of median and lateral carinae, median pairs longer than lateral pairs; spiracles on sternites III–VI elongate, slit-like, each bordered anteriorly with smooth or granulate transverse carina; sternites III–VI with scattered, sparse macrosetae, sternite VII with 6 macrosetae, 4 on the carinae.

Metasoma (Figs. 17–22, 97, 99, 101, 104–109, 195–196). Robust, with short, stout segments; segments I–IV progressively increasing in width and depth; segment V relatively deep, D/L 0.55–0.68. *Carinae*: segment I with 10 complete carinae; segments II–III with 8 complete carinae, lateral inframedian carinae reduced to short posterior series of granules (granule counts: II 2.82 ±0.75 (range 1–5), III 1.98 ± 0.66, range 1–4; N = 168 carinae); segment IV with 8 carinae; segment V with 5 carinae. All carinae strong, granulate; dorsolateral carinae strongly raised on all segments, becoming progressively more elevated from segment I to segment IV; dorsolateral carinae on segments II–IV with posterior granules enlarged, dentate; dorsolateral carinae of segment V strongly granulate in anterior half, weakly granulate to smooth in posterior half; ventrolateral carinae of segment V with smaller granules in anterior half, larger granules in posterior half (Figs. 104–105); ventrosubmedian carinae on segment V obsolete, marked by isolated granules. Ventral anal margin with around 15 small, weak, transversely elongated granules; lateral anal margin non-lobate, or with 2–3 weakly incised lobes. *Intercarinal surfaces*: dorsal surfaces of all segments smooth, lustrous; dorsolateral surfaces smooth or with sparse fine granules on segments I–IV; lateral surfaces finely shagreened or smooth on segment I, sparsely, finely granulate to smooth on segments II–V (weaker in females); ventrolateral surfaces weakly, finely granulate or shagreened to smooth on segment I, densely, finely granulate to almost smooth on segments II–V; ventromedial surfaces of segments I–IV shagreened or densely, finely granulate. *Setation*: 2 pairs of macrosetae on ventrolateral and ventrosubmedian carinae of segments I–IV, 3 pairs on dorsolateral carinae of segment IV, 5 lateral and 4 ventral pairs on segment V.

Telson (Figs. 17–22, 195–196). Dorsal and lateral surfaces of vesicle smooth, ventral surface with weak coarse granulation; lateral profile pyriform. Aculeus thick, strongly curved, approximately same length as vesicle.

Pedipalps (Figs. 23–62, 98, 100, 180–186). *Femur*: dorsointernal, dorsoexternal and ventrointernal carinae strong, with contiguous, coarse, dentate granules; external carina strong, with dentate granules non-contiguous proximally; internal carina broad, with non-contiguous, large dentate granules arranged in band 2 granules wide; other carinae obsolete; dorsal, ventral and internal surfaces with sparse, fine granules, external surface smooth; distal external macrosetal cluster present as a dense compact linear strip with > 20 setae. *Patella*: dorsointernal, dorsomedian, ventroexternal, ventromedian, ventrointernal and internal carinae strong, coarsely granulate; dorsoexternal and external carinae strong, weakly granulate or smooth; dorsointernal, internal and ventrointernal surfaces with moderate to sparse fine granulation; dorsoexternal, external and ventroexternal surfaces smooth. *Chela*: fixed finger with digital (D1), dorsal secondary (D3) and dorsal marginal (D4) carinae strong; manus with D1 and D3 weak or obsolete, D4 absent; ventroexternal, ventromedian and ventrointernal carinae present on movable finger; other carinae absent; internal surface of manus densely, finely granulate, other surfaces smooth, lustrous; 13–15 denticle subrows on dentate margin of movable finger, 12–15 on dentate margin of fixed finger, subrows usually flanked by internal and external accessory denticles, except for proximal subrow in some cases; proximal dentate margins of fingers weakly undulate or scalloped, leaving a gap with fingertips closed, male gap slightly larger than female gap. *Trichobothriotaxy*: orthobothriotaxic, type Aβ (Vachon, 1974, 1975) (Figs. 51–62, 180–186).

Legs (Figs. 1–14, 63–74, 91, 193–194). *Femur*: I–III with inferior median carina denticulate-granulate; inferior prolateral and superior prolateral carinae granulate; superior median carina coarsely granulate, with irregular granulation proximally; femur IV with inferior median carina denticulate-granulate; inferior prolateral carina granulate, superior prolateral and superior median carinae weakly granulate; all prolateral surfaces sparsely granulate, with coarse granules on I, fine granules on II–IV; all retrolateral surfaces smooth except for sparse series of inferior retrolateral granules on I. *Patella*: I–IV with inferior median and inferior prolateral carinae weakly granulate or denticulate-granulate; prolateral median, superior prolateral and superior median carinae weakly granulate on II–III, weakly granulate or smooth on I and IV; all prolateral and retrolateral surfaces smooth. *Tibia*: I–III with regular series of long macrosetae on retrosuperior margin (bristle comb); III–IV with prominent tibial spurs. *Basitarsus*: I–III moderately compressed with flat retrolateral surfaces; regular series of long macrosetae (bristle combs) on retrosuperior and retroinferior margins; leg III retrosuperior series 16–25 (mean ± SD: 19.55 ± 2.56; median 20; N = 29); retrolateral spurs simple, prolateral spurs with non-bifurcate basal spiniform process, and numerous macrosetae, leg III setae 6–25 (mean ± SD: 15.41 ± 3.23; median 16; N = 126). *Telotarsus*: I–IV relatively short, laterodistal apices truncate,

Figures 23–**36**. *Androctonus omanensis* **sp**. **n**., paratype male. Duqm, 23.IX.1995. **Figures 23**–**34**. Right pedipalp chela (23–26), patella (27–30) and femur (31–34) in dorsal (23, 27, 31), external (24, 28, 32), ventral (25, 29, 33) and internal (26, 30, 34) views. **Figures 35**–**36**. Dentate margins of fixed (35) and movable (36) fingers of right pedipalp chela. Scale bar: 5 mm. UV fluorescence.

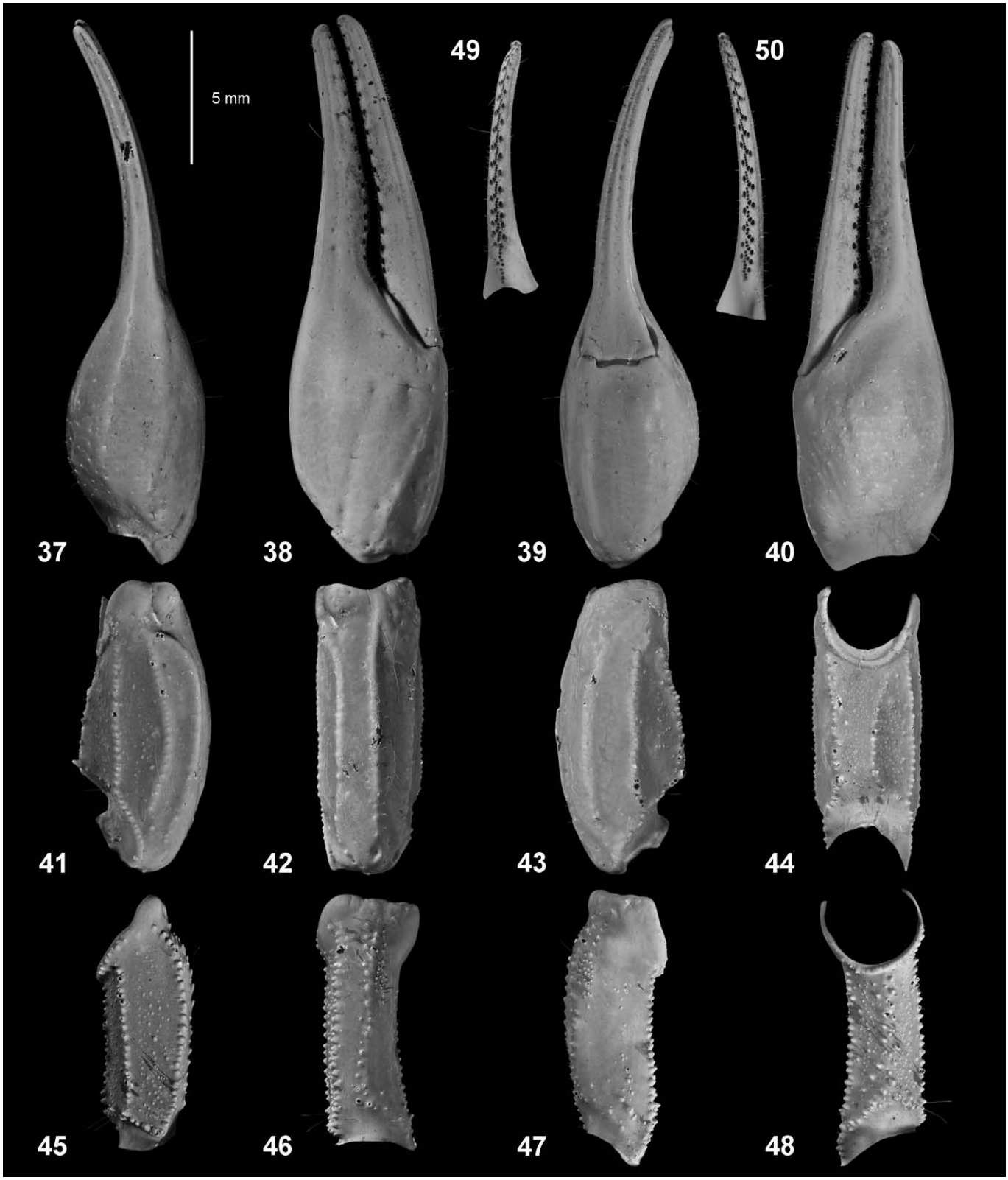

Figures 37–**50**. *Androctonus omanensis* **sp**. **n**., paratype female. Batinah coast, W of Barka, 13.X.1993. **Figures 37**–**48**. Right pedipalp chela (37–40), patella (41–44) and femur (45–48) in dorsal (37, 41, 45), external (38, 42, 46), ventral (39, 43, 47) and internal (40, 44, 48) views. **Figures 49**–**50**. Dentate margins of fixed (49) and movable (50) fingers of right pedipalp chela. Scale bar: 5 mm. UV fluorescence.

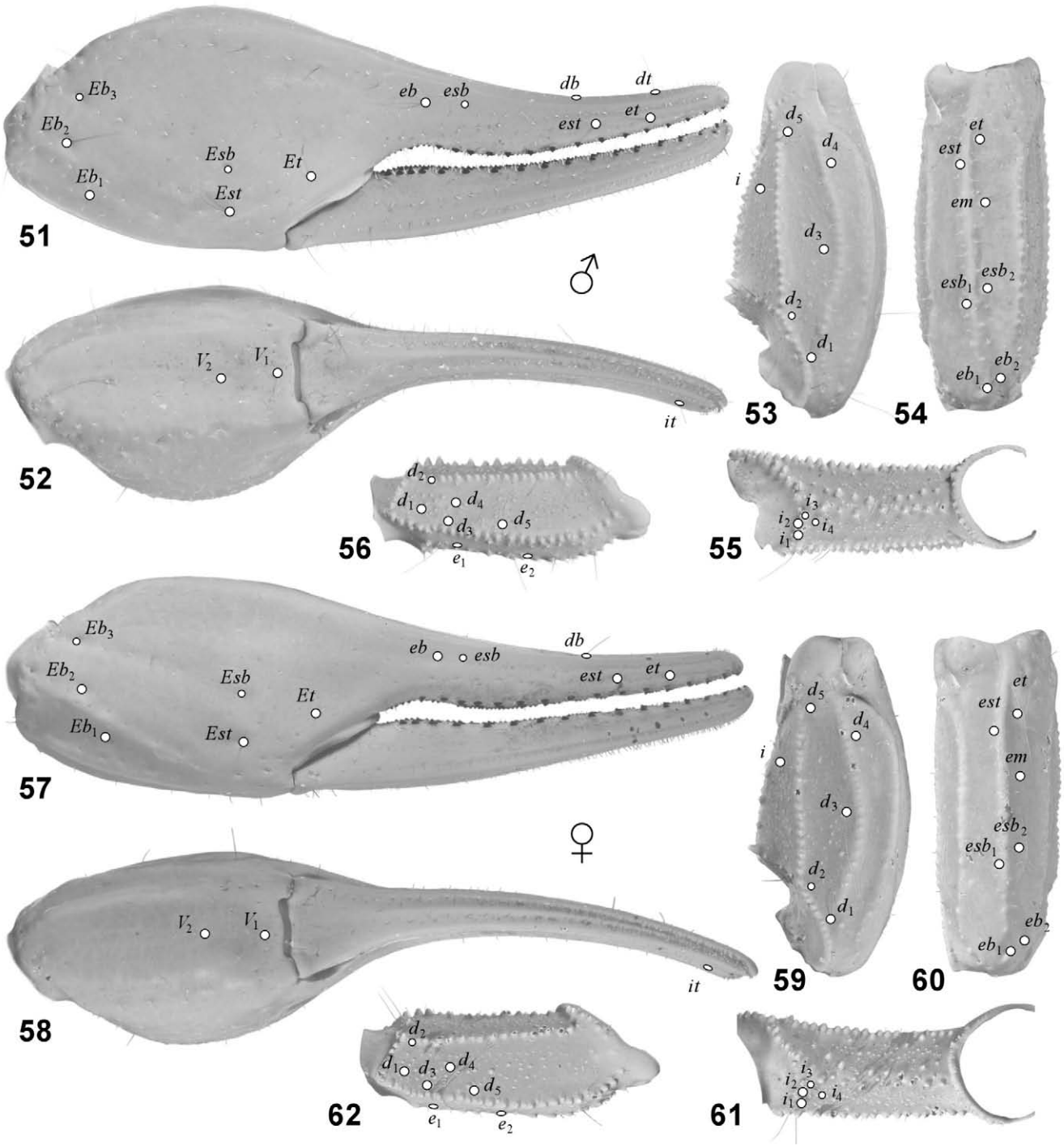

Figures 51–**62**. *Androctonus omanensis* **sp**. **n**., trichobothrial pattern. **Figures 51**–**56**. Paratype male. Duqm, 23.IX.1995. Right pedipalp chela (51–52), patella (53–54) and femur (55–56) in dorsal (53, 56), external (51, 54), ventral (52) and internal (55) views. **Figures 57**–**62**. Paratype female. Batinah coast, W of Barka, 13.X.1993. Right pedipalp chela (57–58), patella (59–60) and femur (61–62) in dorsal (59, 62), external (57, 60), ventral (58) and internal (61) views.

superior distal median lobe prominent; heavily setose, with long macrosetae arranged in prolateral, retrolateral and two ventral series; ungues long, curved and narrow.

Sexual dimorphism. Males generally with more robust, less elongate pedipalp chelae and metasomal segments II–V, and relatively longer pectines with higher pectinal tooth counts (Fig. 103, Tab. 4). The ranges of corresponding morphometric ratios and meristic counts overlapped between the two sexes.

Measurements. See Tables 1–2, 4.

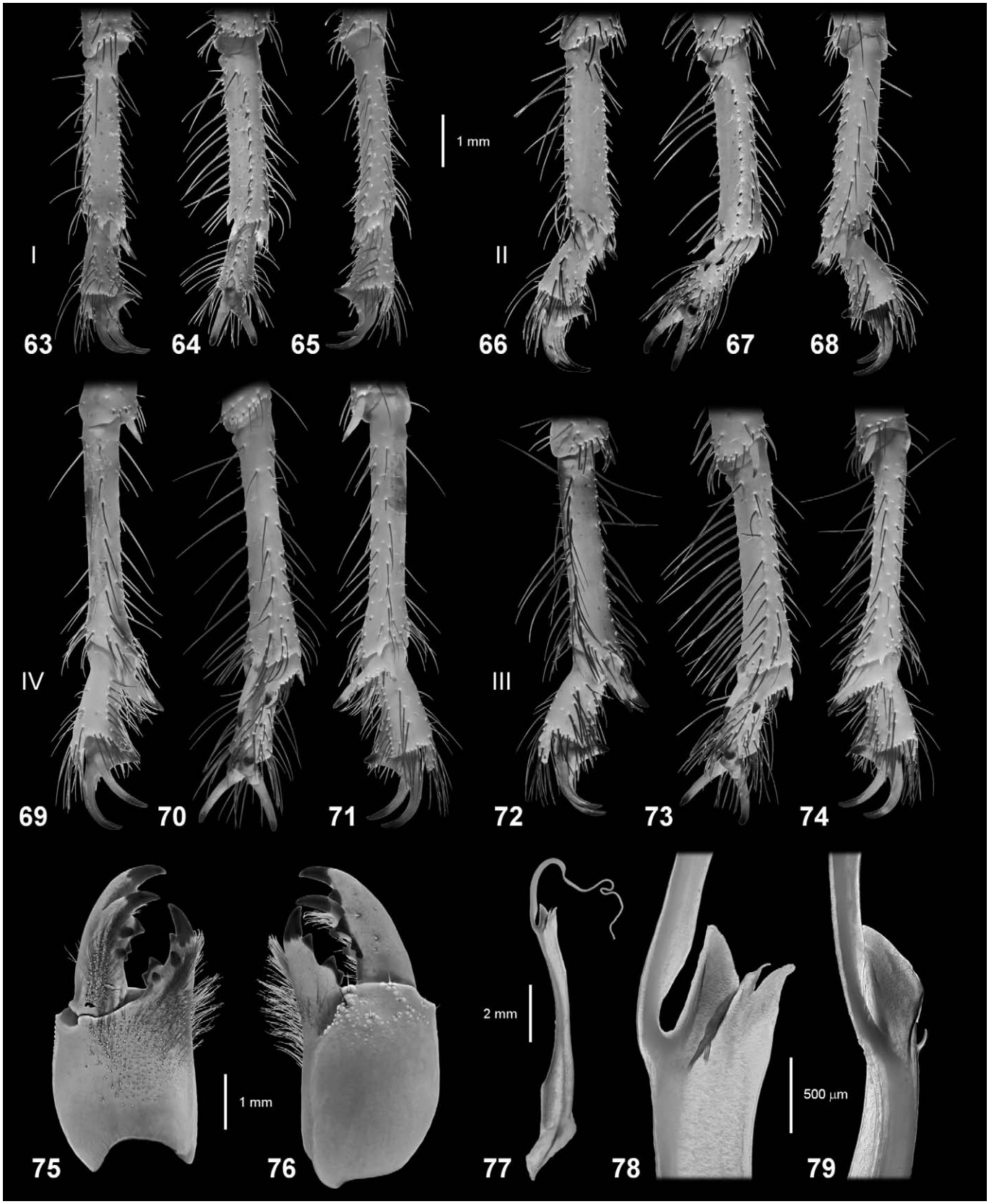

Figures 63–79. *Androctonus omanensis* **sp**. **n**., paratype males. **Figures 63–74**. Left basitarsi and telotarsi. Yitti village, 1.X.1995. Leg I (63–65), II (66–68), III (72–74) and IV (69–71) in retrolateral (63, 66, 69, 72), ventral (64, 67, 70, 73) and prolateral (65, 68, 71, 74) views. **Figures 75–76**. Right chelicera. Dhuai, 21.X.1997. Ventral (75) and dorsal (76) views. **Figures 77–79**. Right hemispermatophore. Shalim. Whole hemispermatophore (77), capsule region in convex (78) and posterior (79) views. Scale bars: 1 mm (63–74), 1 mm (75–76), 2 mm (77), 500 μm (78–79). UV fluorescence (63–76), white light (77–79).

Measurement (mm) or count		*A. omanensis* sp. n.			
		♂ holotype Barka 15.IX.1995	♂ paratype Izki 24.VIII.1995	♂ paratype Yalooni 13.VIII.1984	♂ paratype Wadi Ateena 29.III.1991
Carapace	L / W	10.2 / 11.3	8.3 / 9.4	9.4 / 10.3	9.6 / 9.6
Metasoma + telson	L	51	43	51	49
Metasoma I	L / W / D	6.8 / 7.6 / 6.4	5.6 / 5.9 / 5.1	6.7 / 7.1 / 6.0	6.3 / 6.8 / 6.0
Metasoma II	L / W / D	8.0 / 8.5 / 7.0	6.4 / 6.6 / 5.5	8.0 / 8.0 / 6.8	7.5 / 7.8 / 6.3
Metasoma III	L / W / D	8.1 / 9.3 / 8.2	6.9 / 7.6 / 6.0	8.4 / 8.7 / 7.6	7.5 / 8.7 / 7.3
Metasoma IV	L / W / D	9.7 / 9.3 / 8.4	7.9 / 7.6 / 6.6	9.9 / 8.8 / 7.6	9.6 / 8.6 / 7.5
Metasoma V	L / W / D	10.3 / 8.3 / 6.6	8.7 / 6.9 / 5.2	10.1 / 7.4 / 6.0	10.3 / 8.1 / 6.0
Lateral granules Met. II	left / right	3 / 4	4 / 3	3 / 3	3/ 4
Lateral granules Met. III	left / right	2 / 2	2/ 3	3 / 3	2/ 3
Telson	L / W / D	8.5 / 3.9 / 3.1	6.9 / 3.5 / 2.4	7.9 / 3.8 / 2.6	7.8 / 3.5 / 2.8
Pedipalp femur	L / W	8.1 / 3.1	6.6 / 2.5	7.7 / 2.9	7.9 / 2.7
Pedipalp patella	L / W	9.8 / 4.2	8.1 / 3.8	9.5 / 4.2	9.4 / 4.0
Pedipalp chela	L	17.1	14.2	16.7	16.5
Chela manus	L / W / D	6.5 / 4.7 / 5.3	5.8 / 3.7 / 4.3	6.5 / 4.4 / 5.1	6.3 / 4.3 / 4.6
Chela movable finger	L	11.1	9.6	10.7	10.8
Subrows: movable finger	left / right	14 / 15	15 / 14	13 / 13	14 / 14
Subrows: fixed finger	left / right	14 / 14	13 / 14	14 / 13	14 / 13
Pectine	L	10.7	8.7	10.14	10.24
Pectinal tooth count	left / right	31 / 32	30 / 29	30/ -	29 / 31
Leg III femur	L	10.3	8.7	9.9	10.8
Leg III patella	L	8.4	7.0	8.3	8.2
Basitarsus III RS setae	left / right	21 / 24	15 / 16	25 / 22	23 / 21
Basitarsus III spur setae	left / right	19 / 22	13 / 16	19 / 22	16 / 16
Total	**L**	**83**	**72**	**77**	**80**

Table 1. Morphometric and meristic data for representative male types of *Androctonus omanensis* **sp**. **n**. Abbreviations: L, length; W, width; D, depth; Met., metasoma; RS, retrosuperior. Carapace W is maximum (posterior) width. Pedipalp chela manus L is ventral length (Fig. 186). Lateral granule counts are for lateral inframedian carinae.

Variation.

Ontogenetic variation. Granulation on the carapace, tergites, coxae, and metasoma was weak in early juveniles, and became progressively stronger in later instars into adulthood. The dense granulation on the internal surface of the pedipalp chela manus and lateral surfaces of the metasomal segments was weak or absent in early juveniles. On the other hand, granulation on the telson vesicle was relatively stronger in juveniles compared to adults. The pedipalps, metasomal segments, and telson vesicle were slenderer in juveniles, and became progressively more robust in later instars (Figs. 92–97). For example, Figs. 98–99, upper panels, show a large increase in the morphometric ratios, pedipalp chela W/L and metasoma IV D/L, respectively, with increasing body size (as measured by carapace L). Size-scaling of chela L and metasoma IV L were isometric (Figs. 98–99, lower panels), implying allometric scaling of both chela W and metasoma IV D, which is shown in Figs. 100–101. Hierarchical cluster analysis of the bivariate scatter plots suggested that the samples included six instars, i.e., II–VII. Growth of pedipalp chela W was isometric over instars II–IV, and allometric over instars V–VII (Fig. 100). The allometric exponents exhibited sexual dimorphism, with chela W increasing as (carapace L)$^{3/2}$ in females, vs. (carapace L)^{2} in males. In adults, the chela of males was conspicuously wider than that of females. Growth of metasoma IV D was allometric over instars II–IV, and more strongly allometric over instars V–VII (Fig. 101). The allometric exponents of the later instars again exhibited sexual dimorphism, being higher in males. In adults, metasoma IV was somewhat deeper than that of females, although the difference was not conspicuous. Pectinal tooth count was ontogenetically invariant (Fig. 102), as in other buthids (Kovařík et al., 2016).

Metasoma V ventrolateral carinal dentition. Mean denticle depth was constant in the anterior part of the segment, and increased steadily in the posterior half of the segment in males (Fig. 104), and in the posterior three quarters of the segment in females (Fig. 105). Prominently enlarged, lobate denticles were absent. There was large variation between individuals of denticle depths at various anterior-posterior positions (CV ~ 30%–50%). Denticle depth scaled allometrically with denticle width, with weak exponents in both males (1.23) and females (1.22) (Figs.

Measurement (mm) or count		*A. omanensis* **sp. n.**			
		♀ **paratype W. of Barka 13.X.1993**	♀ **paratype Madinat Qaboos 25.IV.1982**	♀ **paratype Yalooni 1989**	♀ **paratype Thumrait 26.VIII.1997**
Carapace	L / W	11.7 / 13.1	12.11 / 12.91	10.88 / 11.35	10.62 / 11.50
Metasoma + telson	L	57	59	50	52
Metasoma I	L / W / D	7.2 / 8.2 / 7.0	7.5 / 8.2 / 7.0	6.8 / 7.0 / 6.3	6.7 / 7.3 / 6.2
Metasoma II	L / W / D	8.6 / 9.0 / 7.8	8.5 / 9.1 / 7.7	8.0 / 7.9 / 6.8	8.0 / 7.9 / 6.9
Metasoma III	L / W / D	9.0 / 9.7 / 8.7	8.9 / 9.9 / 8.6	8.3 / 8.7 / 7.6	8.3 / 8.4 / 7.5
Metasoma IV	L / W / D	10.7 / 9.8 / 8.8	10.6 / 9.9 / 9.0	10.0 / 8.5 / 7.7	10.0 / 8.1 / 7.5
Metasoma V	L / W / D	11.1 / 8.9 / 7.3	11.3 / 8.4 / 7.4	10.5 / 7.7 / 6.6	10.7 / 7.5 / 6.1
Lateral granules Met. II	left / right	3 / 4	3 / 3	3 / 3	6 / 3
Lateral granules Met. III	left / right	2 / 3	2 / 2	2 / 3	5 / 3
Telson	L / W / D	9.6 / 4.6 / 3.5	9.8 / 4.8 / 3.6	– / 4.3 / 3.4	9.3 / 4.1 / 3.1
Pedipalp femur	L / W	9.0 / 3.2	8.6 / 3.4	8.0 / 3.2	8.9 / 3.3
Pedipalp patella	L / W	10.4 / 4.8	10.8 / 4.7	9.9 / 4.3	10.3 / 4.2
Pedipalp chela	L	18.7	18.7	18.5	17.9
Chela manus	L / W / D	7.4 / 4.8 / 5.6	7.1 / 4.8 / 5.5	6.7 / 4.6 / 5.3	6.8 / 4.1 / 4.7
Chela movable finger	L	12.3	12.3	12.1	11.5
Subrows: movable finger	left / right	14 / 14	15 / 14	15 / 15	14 / 13
Subrows: fixed finger	left / right	12 / 14	14 / 13	14 / 15	15 / 14
Pectine	L	9.5	9.3	9.2	9.2
Pectinal tooth count	left / right	28/ 29	25 / 25	26 / 26	27 / 27
Leg III femur	L	10.8	11.8	10.6	10.2
Leg III patella	L	8.7	8.5	8.2	9.0
Basitarsus III RS setae	left / right	22 / 22	23 / 23	21 / 21	27 / 28
Basitarsus III spur setae	left / right	14 / 15	21 / 19	20 / 20	29 / 28
Total	**L**	**95**	**98**	**87**	**90**

Table 2. Morphometric and meristic data for representative female types of *Androctonus omanensis* **sp. n.** Abbreviations: L, length; W, width; D, depth; Met., metasoma; RS, retrosuperior. Carapace W is maximum (posterior) width. Pedipalp chela manus L is ventral length (Fig. 186). Lateral granule counts are for lateral inframedian carinae.

106–107). Denticle counts did not differ significantly between the sexes (P = 0.071, Mann-Whitney U test), and the mean count for sexes pooled was 20.80 ± 2.22, range 16–27 (N = 82).

Geographic variation. Geographic variation in morphometrics was investigated by multivariate analysis of 23 variables, normalized by carapace L to remove the effect of size and focus on shape differences: metasoma I–V L, W, D; pedipalp femur, patella and chela L, W; and pedipalp chela manus and movable finger L. Samples of 55 adult males, and 54 adult females were analyzed separately by PCA applied to standardized z-scores of logarithmically transformed data. The first three principal components (PC1–PC3), explained 64.41% of the variance in males, and 69.31% of the variance in females (Tab. 5). Specimen localities were divided into three groups by geographic region: I, north coast and mountains of Oman; II, interior desert plains of Oman; and III, the Empty Quarter dune systems of Oman, UAE and Saudi Arabia. Groups I and II were divided by the line: latitude° = 50.848° − 0.47799 × longitude°. A scatter plot of PC1 vs. PC2 for males shows separation of group III (= *A. ammophilus* **sp. n.**; see below), and overlap of groups I and II (= *A. omanensis* **sp. n.**) (Fig. 111). Linear discriminant functions constructed from PC1–PC3 of males enabled complete separation of group III from groups I and II (100% correct classification), but not of groups I and II from each other (26% of group I misclassified as II, 25% of group II misclassified as I). However, the plot of canonical scores showed partial separation of groups I and II along the CV2 axis (Fig. 112). Group I scores were significantly higher than group II scores ($P = 4 \times 10^{-5}$, Mann-Whitney U test). CV2 had a large positive PC3 coefficient (Tab. 8), and PC3 had a large positive pedipalp chela W loading (Tab. 6), indicating a difference in chela width. Indeed, chela W/ carapace L of group I was significantly larger than that of group II (P = 0.029, Mann-Whitney U test, α = 0.05). A geographic plot shows that some Batinah coast males have much wider chelae than any males from the interior (Fig. 114). These differences were not found in females, which tend to have narrower chelae than males (Fig. 113).

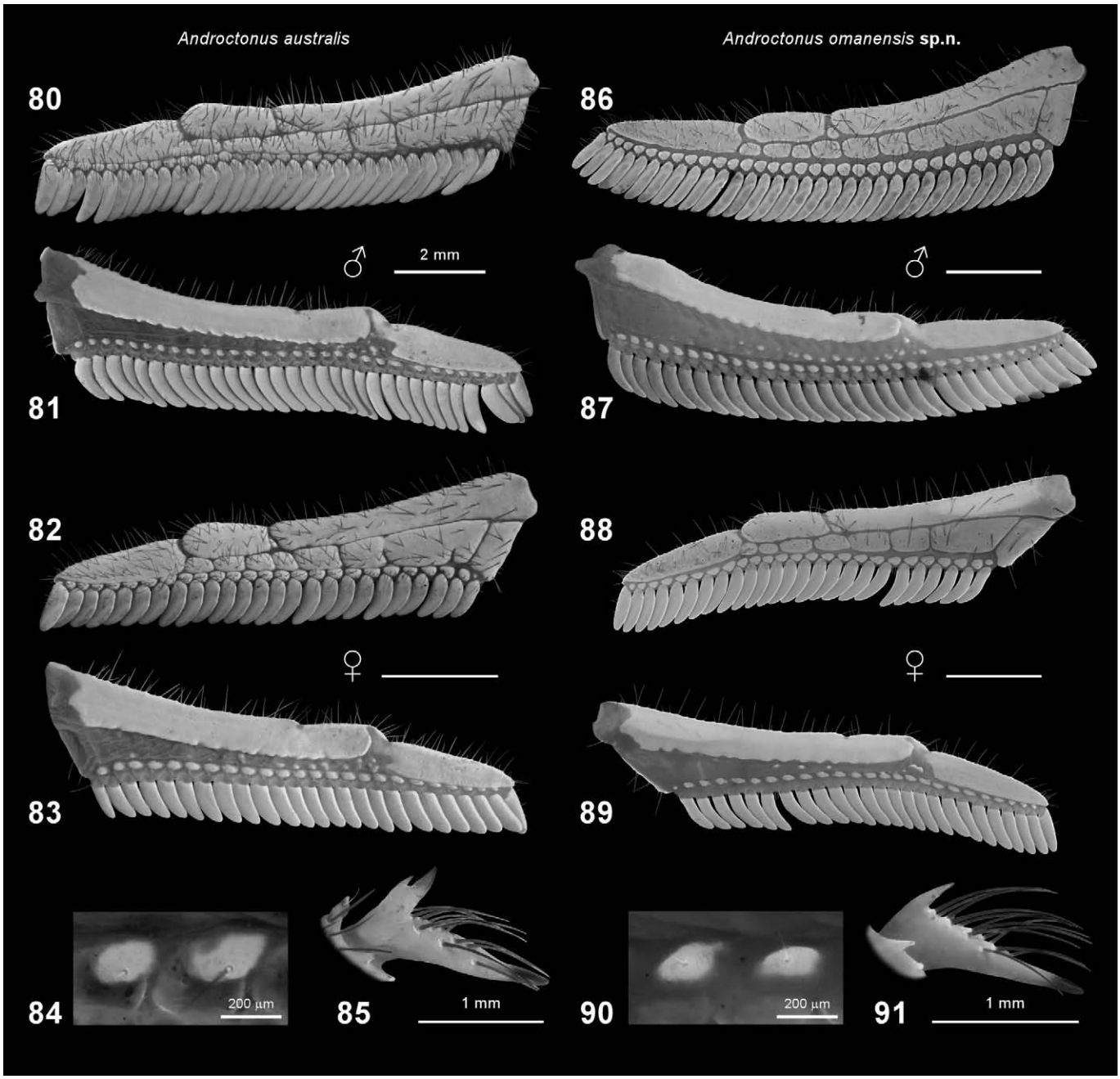

Figures 80–**91**. Pectines and prolateral basitarsal spurs. **Figures 80**–**84**. *Androctonus australis*. Egypt, 2008. Pectines of male (80–81) and female (82–83) in ventral (80, 82) and internal (dorsal) (81, 83) views, and internal fulcra of male (84). **Figures 86**–**90**. *A. omanensis* **sp**. **n**. Pectines of male, Batinah coast, W. of Barka, 13.X.1993 (86–87) and female, Lasail, IV.1995 (88–89) in ventral (86, 88) and internal (dorsal) (87, 89) views, and internal fulcra of male (90). **Figures 85**, **91**. Prolateral basitarsal spur, prolateral aspect, left leg III, male *A. australis* (85) and paratype male *A. omanensis* **sp**. **n**. (91) (Egypt, 2008, and W. of Barka, 13.X.1993, respectively). Scale bars: 2 mm (80–81, 82–83, 86–87, 88–89), 1 mm (85, 91), 200 µm (84, 90).

Coloration. Base color of carapace, tergites and metasoma varied greatly, from a dark reddish-brown or black to a much lighter shade of brownish-yellow or yellow (Figs. 7–12, 197–200). Lightness was not sexually dimorphic, with lighter and darker individuals in both sexes. The presence of lighter forms varied geographically: group I included both lighter and darker individuals, whereas group II included only darker individuals. Lightness was quantified by measuring the relative intensity of white light reflected from tergite VII of adults and subadults of either sex preserved in alcohol. Group I mean lightness (5.89 ± 2.74, N = 32) was significantly higher than group II mean lightness (2.95 ± 0.87, N = 24) ($P = 2.62 \times 10^{-6}$; t-test). A geographic plot shows the localization of lighter colored populations on the Batinah coast (Fig. 115). Although liquid preservation can cause color shifts, the lighter colored morphs cannot be dismissed as artefacts of fading due to long storage of specimens in alcohol, as light colored specimens were collected alive during fieldwork in Oman (e.g., Fig.

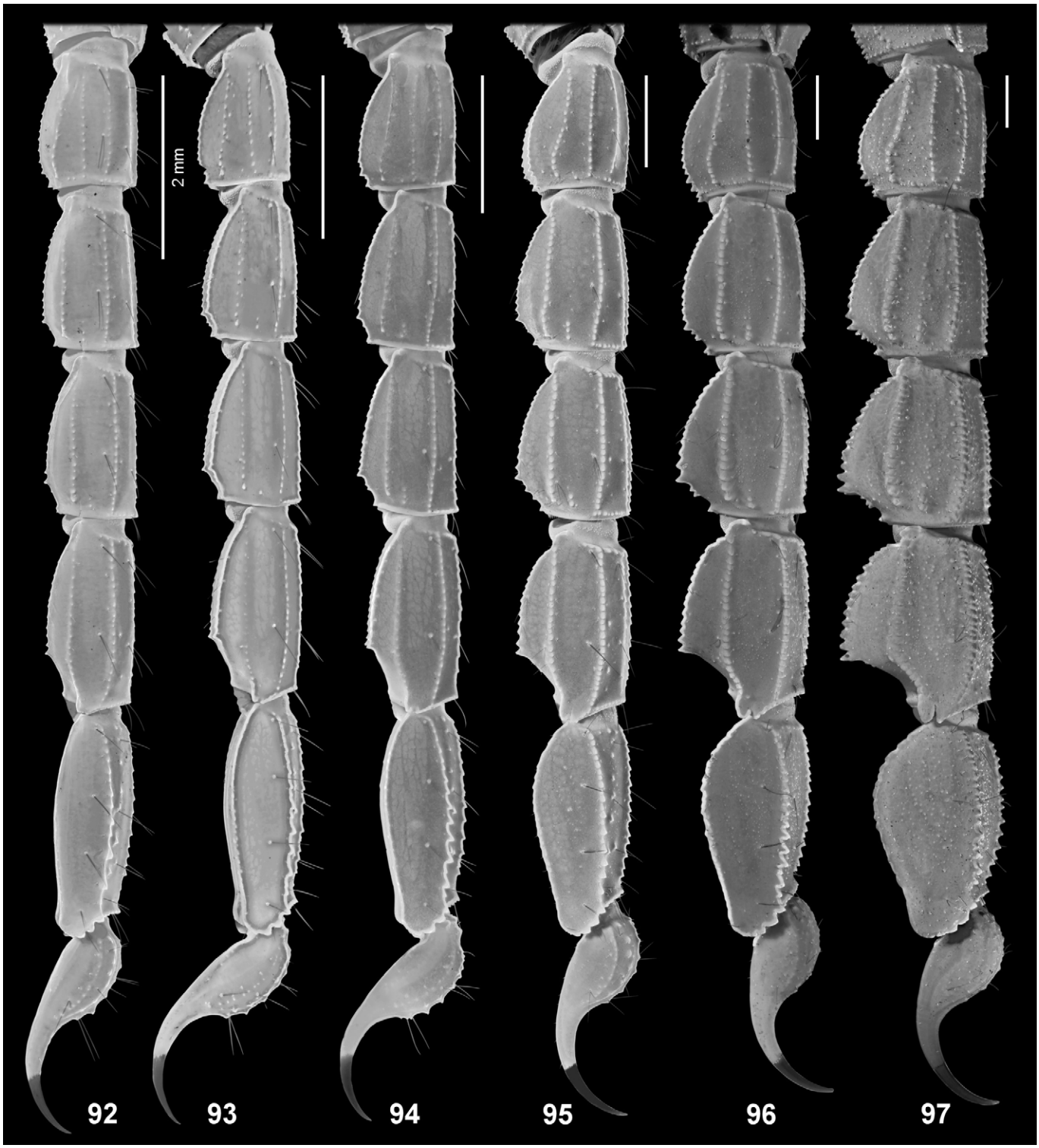

Figures 92–97. *Androctonus omanensis* **sp**. **n**. Ontogeny of metasoma and telson, right lateral views of juvenile to adult instars. **Figure 92**. Second instar paratype female, Quryat, 2.X.1993. **Figure 93**. Third instar paratype female, Wahiba (Sharqiyah) Sands, 2.II.1986. **Figure 94**. Juvenile paratype male, Tibat, Musandam, 24.X.1984. **Figure 95**. Immature paratype male, Batinah coast, W. of Barka, 13.X.1993. **Figure 96**. Subadult paratype female, Yalooni, 17.III.1994. **Figure 97**. Adult paratype female, Madinat Qaboos, 8.VIII.1984. Scale bars: 2 mm. UV fluorescence.

11). Moreover, fading in preservatives should be random and uncorrelated with geographic location. Coloration has been used as a diagnostic character for some species of the *A.* '*crassicauda*' complex, but it is not a stable character for diagnosis of *A*. *omanensis* **sp**. **n**.

Old records of the North African *A*. *australis* from Muscat (Levy & Amitai, 1980: 36, appendix) may be misidentified samples of pale morphs of *A*. *omanensis* **sp**. **n**. Vachon (1952: 405) listed as diagnostic characters for *A*. *australis* the presence of macrosetae on some of the internal fulcra of

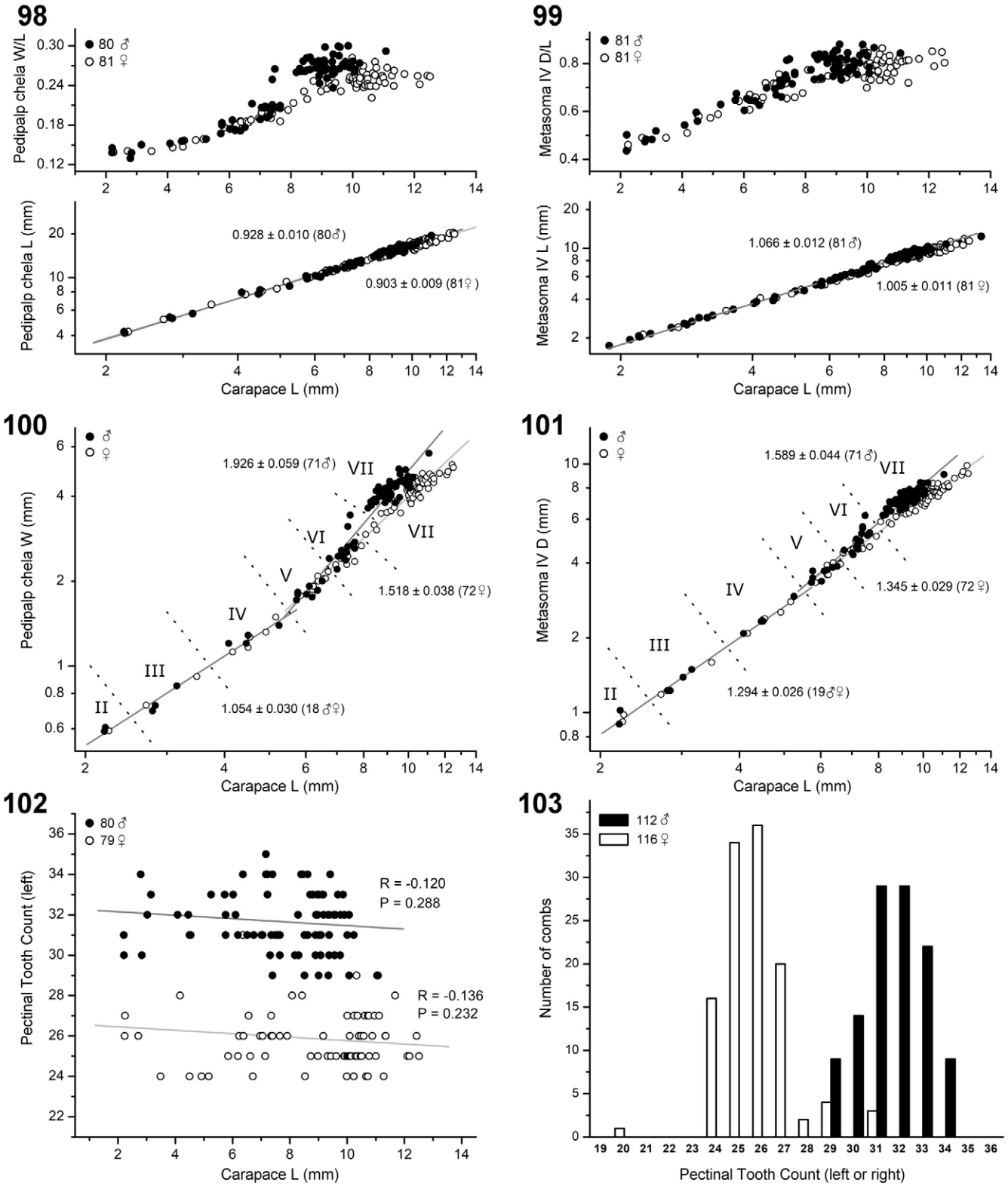

Figures 98–**103**. *Androctonus omanensis* **sp**. **n**. Ontogenetic variation of morphometrics and pectinal tooth counts. **Figs**. **98**–**101**. Allometric scaling in juveniles, immatures and adults. **Fig**. **98**. Scatter plot of morphometric ratio W/L (upper plot) and logarithmic scatter plot of length L (lower plot) of pedipalp chela vs. carapace L. **Fig**. **99**. Scatter plot of morphometric ratio D/L (upper plot) and logarithmic scatter plot of length L (lower plot) of metasoma IV vs. carapace L. **Fig**. **100**. Logarithmic **s**catter plot of pedipalp chela W vs. carapace L, with data partitioned into six instars (II–VII) according to hierarchical cluster analysis by UPGMA applied to Euclidean distances of the pair of variables. Lines are linear least squares regression fits to instars II–IV (both sexes), and V–VII (males and females separated), with slopes as labelled. **Fig**. **101**. Logarithmic **s**catter plot of metasoma IV D vs. carapace L. Instars partitioned and regression lines fit as in Fig. 100. **Figs**. **102**–**103**. Variation in pectinal tooth counts. **Fig**. **102**. Scatter plot showing ontogenetic variation of left pectinal tooth count. **Fig**. **103**. Histogram showing distributions of pectinal tooth counts in males (black bars) and females (open bars). Symbols (98–102): black circles, males; open circles, females.

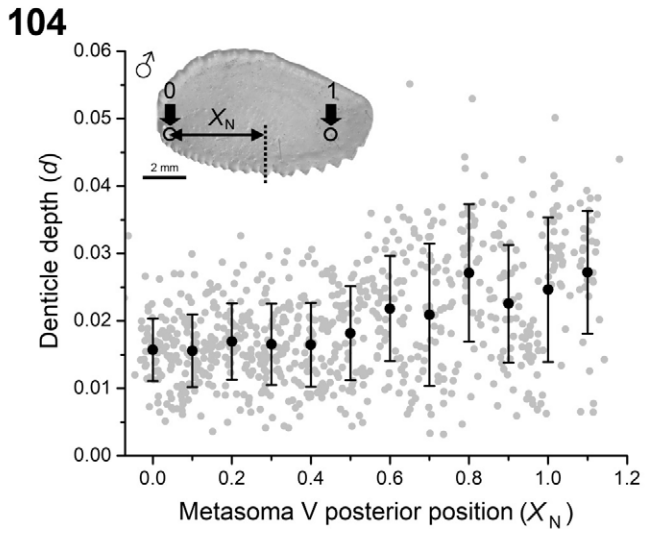

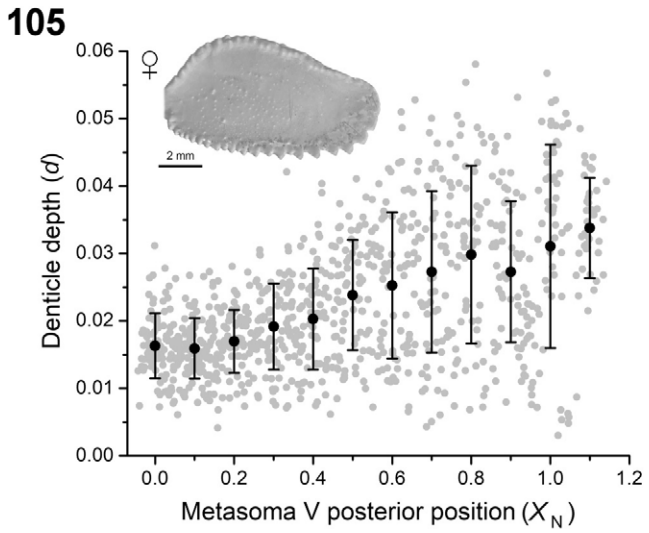

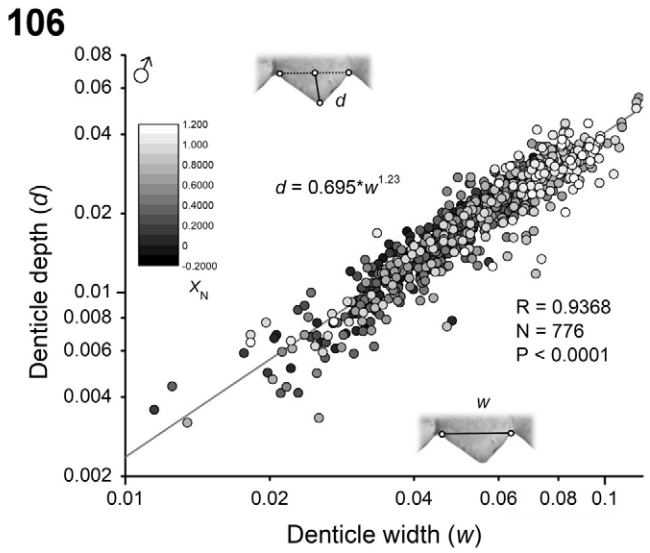

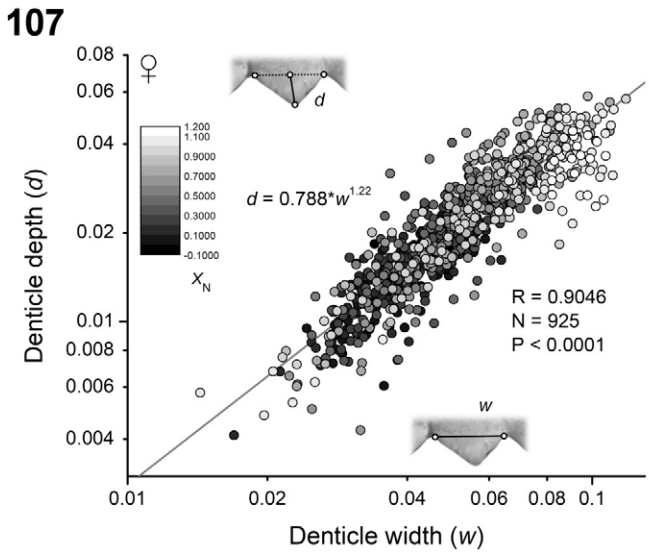

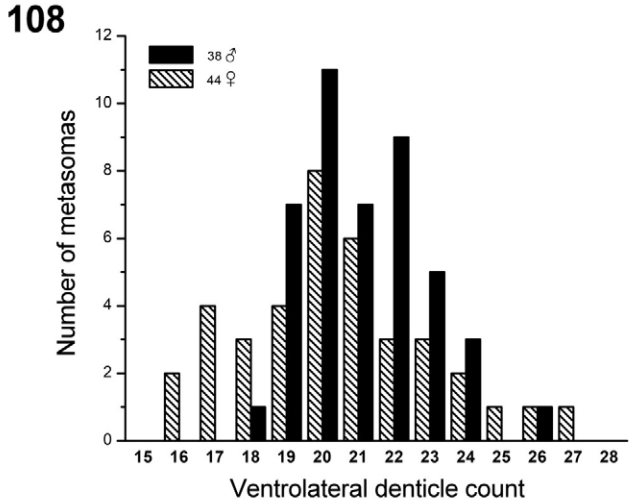

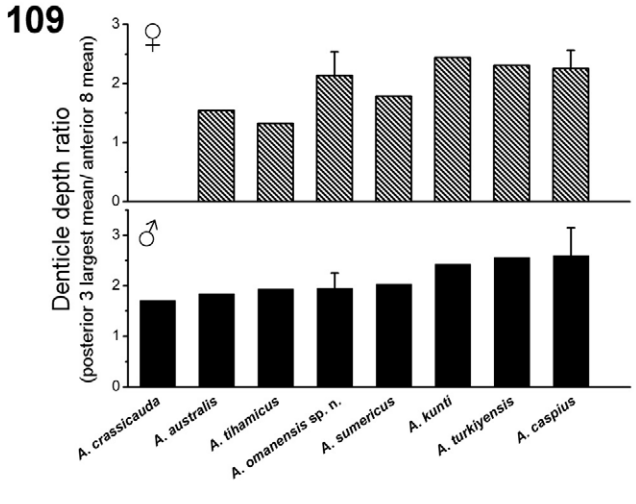

Figures 104–**109**. Variation in dentition of ventrolateral carinae of metasoma V. **Figures 104**–**108**. *Androctonus omanensis* **sp**. **n**. Data from 38 adult males (776 denticles), and 44 adult females (925 denticles). **Figures 104**–**105**. Scatter plots of normalized denticle depth (*d*; Figs. 106–107, upper insets) vs. normalized posterior position of denticle on metasoma V (X_N; Fig. 104, inset) in males (104) and females (105). Depths and positions normalized to distance between anterior and posterior landmark macrosetae (cf. Fig. 104, inset, arrows 0 & 1). Gray symbols: individual denticles; black symbols: mean depths of data in X_N bins of width 0.1; black bars: SD. Insets: metasoma V samples, lateral aspect, UV fluorescence: paratype male, Barka, 15.IX.1995 (104); paratype female, Ras al Hamra, 1983. **Figures 106**–**107**. Logarithmic scatter plots of denticle depth (*d*; upper insets) vs. denticle width (*w*; lower insets) in males (106) and females (107). Symbol fills: gray scale mapping of normalized posterior position (X_N). Lines: least squares linear regression fits. **Figure 108**. Histogram of showing distributions of denticle counts in males (black bars) and females (hatched bars). **Figure 109**. Histograms comparing ratio of measures of posterior denticle depth to anterior denticle depth, of *A*. *omanensis* **sp**. **n**. to similar species of *Androctonus* in males (lower plot) an females (upper plot). Posterior denticle depth is measured by mean depth of 3 largest denticles in posterior half of metasoma V, anterior denticle depth by mean depth of 8 most posterior denticles in anterior half of metasoma V.

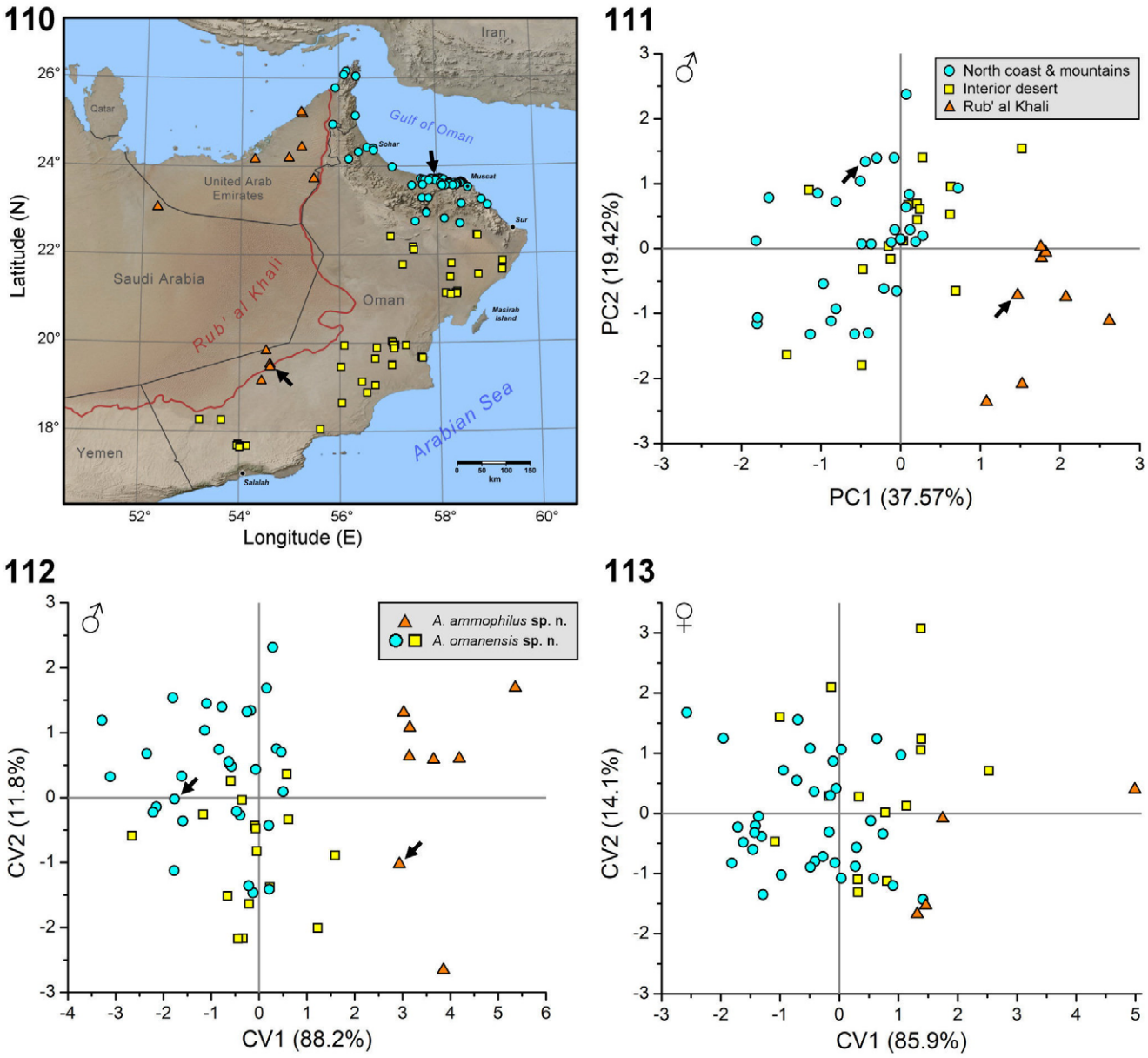

Figures 110–**113**: Distribution and multivariate morphometric analysis of *Androctonus* in Oman. **Figure 110**. Map of distribution records in Oman, adjacent Saudi Arabia, and United Arab Emirates: *A*. *omanensis* **sp**. **n**.: cyan circles (northern coast and Al Hajar mountains) and yellow squares (interior deserts of Oman); *A*. *ammophilus* **sp**. **n**.: orange triangles (Rub' al-Khali or Empty Quarter). Red line roughly indicates margin of Rub' al-Khali sands. **Figure 111**. Scatter plot of scores of first two principal components (PC1, PC2) explaining 57% of the variance, obtained from principal components analysis (PCA) of morphometric measurements of metasoma and pedipalps normalized to carapace L, of 54 males sampled from populations in Fig. 110. **Figure 112**–**113**. Scatter plots of canonical scores obtained from linear discriminant analysis (LDA) of first three principal components (PC1–3) obtained from PCA of 54 males (112) and 54 females (113) sampled from populations in Fig. 110. Symbols in Figs. 111–113 as in Fig. 110. Black arrows: type localities (110) and holotypes (111–112).

the pectines, and a bifurcated basal process on the prolateral basitarsal spurs. These characters were confirmed to be present in *A*. *australis* (Figs. 80–85), and absent in *A*. *omanensis* **sp**. **n**. (Figs. 86–91) (cf. Hendrixson, 2006: 42).

Distribution. *A*. *omanensis* **sp**. **n**. is common and widely distributed in Oman. In the north, it is been found on the Batinah coastal plain, in wadis at lower elevations of the Al Hajar mountains, and in coastal sites of the Musandam Peninsula, including adjacent United Arab Emirates (Fig. 110, cyan circles). In the interior desert plains of Oman, it has been found on the periphery of the Wahiba (Sharqiyah) Sands, on the broad alluvial fans extending south of the Al Hajar Mountains, on the central limestone plateau of Jiddat al-Harasis, and in the Nejd desert north of the Dhofar mountains in the south (Fig. 110, yellow squares).

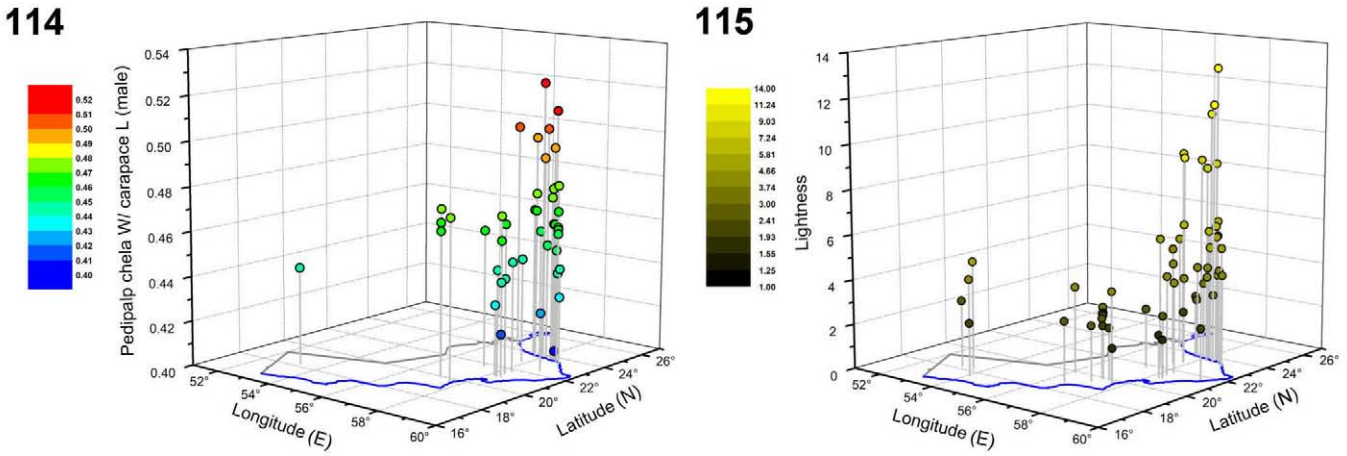

Figures 114–115: Geographic variation of pedipalp chela width and lightness of coloration of *A. omanensis* **sp. n. Figure 114**. 3. 3D scatter plot showing geographic variation of the morphometric ratio, pedipalp chela W/ carapace L, in 44 adult males. Ratios plotted as height on vertical axis, and as pseudocolor-mapped symbol fills. **Figure 115**. 3D scatter plot showing geographic variation of the lightness of coloration of 25 males and 34 females. Intensity of white light reflected from tergite VII of adults and subadults plotted as height on vertical axis, and as graded logarithmic black-yellow color-mapped symbol fills.

Ecology. *A. omanensis* **sp. n.** is arenicolous, inhabiting a variety of sandy substrates (Figs. 201–204). In UV detection surveys on the Batinah coastal plain, it was found to be abundant in low dunes of *Acacia* and *Prosopis* woodlands (Fig. 201). Individuals were often observed near entrances to burrows constructed in semi-consolidated sand near the bases of vegetation. In the Wahiba (Sharqiyah) Sands region, the species was found in low nabkha dunes associated with the belt of *Prosopis* woodlands along the eastern margins of the sands (Fig. 203), but not in the central sands with mega-ridge dunes (Al Hibal) where vegetation is sparse or absent. The majority of nighttime collections were made on the sand surface by UV detection, although some required excavation of burrows. Daytime collections were made by overturning objects resting on the sand surface (e.g., rocks, logs, timber, barrels), exposing scorpions sheltering in shallow scrapes or tunnels. Adaptation to sandy substrates is indicated by the compressed basitarsi I–III, equipped with rows of long macrosetae (bristle combs), a typical feature of psammophilous or semi-psammophilous scorpions (Fet et al., 1998; Prendini, 2001). In the Nejd desert around Thumrait, *A. omanensis* **sp. n.** occurred on sandy substrates (Fig. 204), but was also was reported to be common in "rocky areas" (J. N. Barnes, personal communication, 1992), although it is neither lithophilic nor lapidicolous. In rock-strewn areas, there may be sandy substrates in which arenicolous scorpions can excavate burrows. The species is frequently encountered around human habitation, probably because many buildings in Oman are situated near sandy terrain.

Androctonus ammophilus sp. n.

(Figs. 110–113, 116–163, 167–170, 175–178, Tabs. 3–4)
http://zoobank.org/urn:lsid:zoobank.org:act:65448290-7EE0-4EC5-9067-978ECFD609CA

Buthus crassicauda: Finnegan, 1932: 92 (in part?).
Androctonus crassicauda: Vachon, 1966: 210 (in part); Vachon, 1979: 33–35, fig. 4 (in part); Levy & Amitai, 1980: 29, Appendix (in part); El-Hennawy, 1992: 101, 109–110 (in part); Al-Safadi, 1992: 96–97, fig. 1 (in part); Tigar & Osborne, 1999: 174, 180, tab. 2 (?); Fet & Lowe, 2000: 72 (in part); Hendrixson, 2006: 38–43 (in part); Amr et al., 2021: 90, 94, tabs. 11, 16 (in part); Saji et al., 2021: 3757 (?); Ythier, 2021: 1 (in part); Ythier & Lourenço, 2022: 240 (in part).

Type locality and type depository. **Oman**, Montasar, 19.46°N 54.62°E; NHMB.

Type material examined
Holotype ♂, **Oman**, Montasar, 19.46°N 54.62°E, 14.IX.1997, leg. I. D. & S. Harrison, NHMB.
Paratypes. **Oman:** 1♀, Qitbit, 19°07'N 54°27'E, 26.III.1989, leg. S. M. Farook & A. S. Gardner, NHMB 8; 1♂, Qitabit, behind resthouse, 2 km, camping area, 19.12°N 54.45°E, 27.III.1989, leg. A. S. Gardner & S. M. Farook, NHMB 12; 5♀, Montesar, Wadi Muqshin, under fallen pieces of bark, twigs or branches, 19.45°N 54.62°E, 30.III.1989, leg. A. S. Gardner & S. M. Farook, GLPC 13; 1♂, Al Hafrah, new govt admin. centre, Saudi Arabia/ Oman border, dead in well, ca. 3

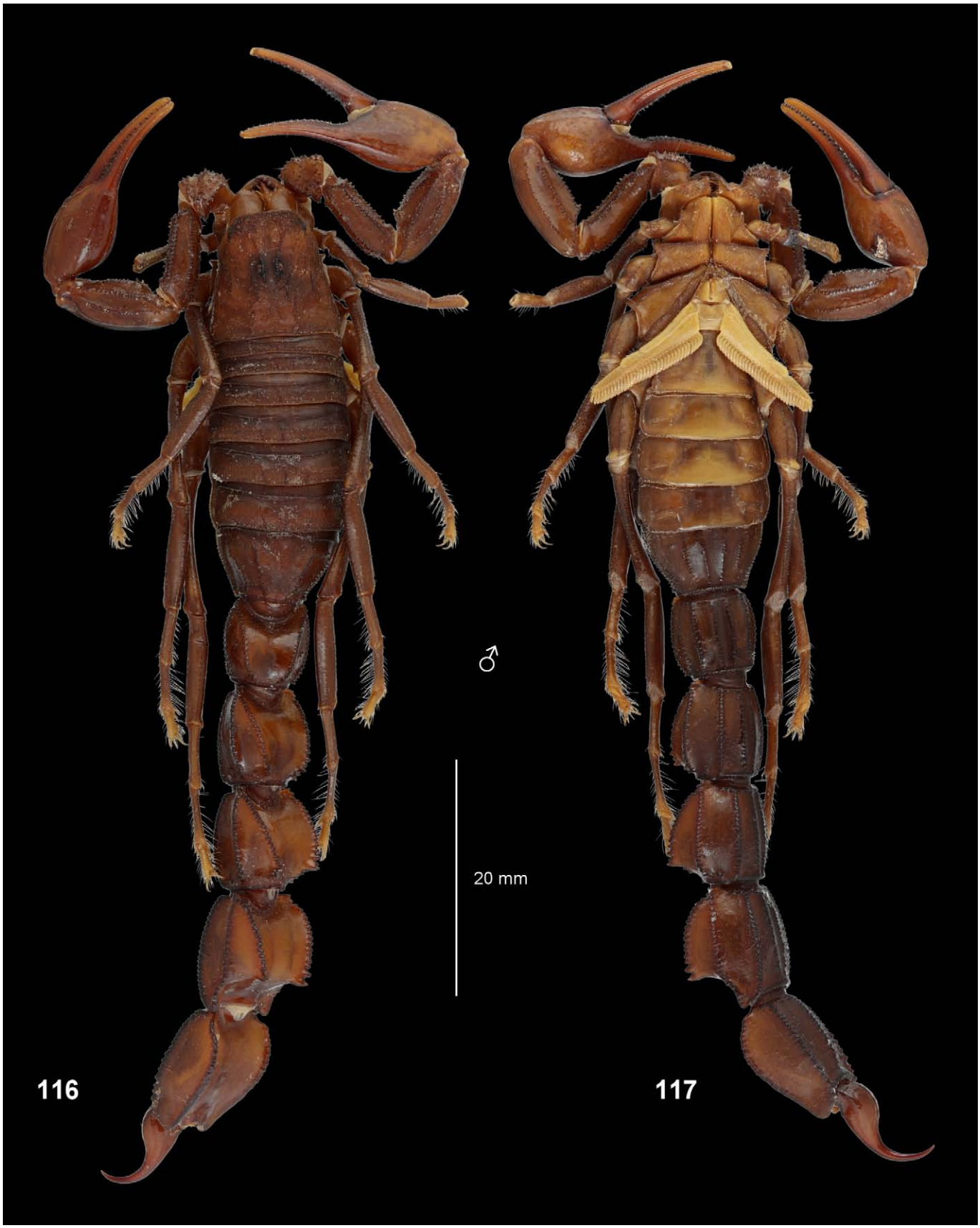

Figures 116–117. *Androctonus ammophilus* **sp. n.**, holotype male. Montasar, 14.IX.1997. Habitus in dorsal (116) and ventral (117) views. Scale bar: 20 mm.

m deep, 19.82°N 54.53°E, 18.VI.1990, leg. R.P. Whitcombe, NHMB 1696; 1♀, Montesar, under sheet of plywood on sand, 19.45°N 54.62°E, 20.IV.1991, leg. A. S. Gardner, NHMB 31; 1♀, Montesar, under oil drum on sand, 19.45°N 54.62°E, 12.I.1992, leg. A. S. Gardner S. M. Farook, NHMB 35; 1♀, Ramlat Muqshin, edge of Rub'Al-Khali, UV detection, large, rounded dunes, low dune system, 19.51°N 54.61°E, 195 m a. s. l., 6.X.1994, leg. G. Lowe & M. D. Gallagher, GLPC. **Saudi Arabia**: 1♂, Rub Al-Khali, Mihrad, 23.05°N 52.30°E, IV.1970, leg. F. Facchini Dono & B. Lanza, MZUF. **UAE**: 2♀, Abu Dhabi, leg. D. J. G. Williams, MNHN RS 5415; 1♂, Abu Dhabi, leg. D. J. G. Williams, MNHN RS 6500; 1♂, Sharja (Ash Shariqah), 25.22°N 55.23°E, 23.IX.1950, leg. H. Field, MCZ 1440; 2♂2♀, Abu Dhabi, Suwayhan, sandy ground near buildings, just before or after last light, 24.43°N 55.24°E, 15-30.VI.1970, leg. D. J. G. Williams, MNHN RS 5416; 1♀, Abu Dhabi, Suwayhan, found drowned in water, at night, just before or after last light, 24.43°N 55.24°E, 15-30.VI.1970, leg. D. J. G. Williams, MNHN RS 5417; 2♂, Liwa (Suwayh), 24.43°N 55.24°E, 6.IV.1971, leg. D. J. G. Williams, MNHN RS 6507; 2♀, Abu Dhabi, 24.15°N 54.28°E, VI.1971, leg. D. J. G. Williams, MNHN RS 6501; 2♂2♀, 1 juv, X.1971, leg. D. J. G. Williams, MNHN RS 6504; 3♂, Zaaba, camp area, 23.71°N 55.49°E, 4,6,8,10.VI.1972, leg. D. J. G. Williams, MNHN RS 6508; 1♂, Dubai, collected by Arab soldiers in the desert, 25.18°N 55.26°E, VIII.1972, M. D. Gallagher MDG 2184, MNHN RS 6502; 1♂, Bada Maza, S. of Abu Dhabi, X.1972, D. J. G. Williams, MNHN RS 6503; 1♂1♀, VII.1973, local collectors, MDG 2465, MNHN RS 6532; 3♂1♀, Abu Dhabi, Ile Zirkuh, 1978, leg. F. Leveque, MNHN RS 7298; 1♂1♀, Al Khatam, 24.18°N 54.98°E, 15.III.2009, leg. Osama, EAD, GLPC.

Etymology. The specific epithet (masculine) is derived from Greek, άμμος = sand, φιλία = love, in reference to the habitat and distribution in the sand dunes of the Rub' al-Khali (Empty Quarter).

Diagnosis ♂♀. Adult total length: ♂♀ 75–95 mm (mean ± SD: 84.5 ± 5.7 mm, N = 12); base color typically uniform dark brown to almost black; legs with tarsi more pale than proximal segments; metasoma robust, wider posteriorly, segment IV W/ segment I W: ♂ 1.2–1.3, ♀ 1.1–1.2; metasoma IV L/W: ♂ 1.0–1.3, ♀ 1.1–1.2; metasoma V L/W: ♂ 1.3–1.4, ♀ 1.4–1.5; metasoma IV L/D: ♂ 1.2–1.5 ♀ 1.2–1.4; metasoma V L/D: ♂ 1.6–1.9, ♀ 1.7–1.9; metasoma V D/ carapace L: ♂ 0.6, ♀ 0.5–0.6; segments II–III with lateral inframedian carinae reduced to several posterior terminal granules, II with 2 granules, III with 1–2 granules (mode 1); segments II–IV with dorsolateral carinae strongly elevated, bearing dentate granules, dorsal furrow deeply excavated; metasoma V ventrolateral carinae with dentate granules gradually increasing in size posteriorly, not abruptly enlarged and lobate; metasoma V dorsolateral carinae with blunt, rounded granules anteriorly; metasoma I dorsal surface smooth, metasoma II–IV lateral surfaces with moderately dense, fine granulation; metasoma V with 1–2 very weak lateral anal lobes; ventral surface of telson vesicle with coarse granulation; fixed finger trichobothrium *db* proximal to *est*; hemispermatophore basal lobe long, digitate; pedipalp segments robust, femur L/W: ♂ 2.6–3.0, ♀ 2.6–2.7; patella L/W: ♂ 2.3–2.7, ♀ 2.3–2.5; chela robust, with broad, deep manus, chela L/W: ♂ 3.5–4.1, ♀ 4.1–4.7; L/D ♂ 3.1–3.5, ♀ 3.4–4.0; manus with carinae obsolete; internal surface of manus with fine granulation; dentate margins of fingers proximally undulate, leaving gap when closed, weaker in female, stronger in male; number of subrows of median denticles, including proximal subrow (♂♀): movable finger 13–14, fixed finger 15; pectinal tooth count:♂ 29–34,♀ 22–27; internal fulcra of pectines with single microseta; prolateral basitarsal spurs with simple, undivided basal tooth, densely setose, leg III spur with > 25 macrosetae.

Comparisons. *A. ammophilus* **sp. n.** is most similar to *A. omanensis* **sp. n.**, from which it differs in the following combination of characters: (i) base color uniform dark brown to almost black, without pale color variants; (ii) generally less robust metasoma, posterior segments less deep, metasoma V L/D ♂ 1.6–1.9 (vs. 1.5–1.8), ♀ 1.7–1.9 (vs. 1.5–1.8), metasoma V D/carapace L ♀ 0.5–0.6 (vs. 0.6–0.7); ♀ legs more elongate, femur III/ metasoma I W 1.5–1.6 (vs. 1.0–1.6), femur II L/ metasoma IV D 1.4–1.6 (vs. 0.9–1.4), femur III L/ metasoma V D 1.7–2.0 (vs. 1.1–1.8); the two species have overlapping ranges of morphometric ratios of individual segments (Figs. 169–170), but can be separated by multivariate analysis and joint distributions of several morphometric ratios (Figs. 111–112, 168); (iii) generally fewer granules on lateral inframedian carinae of metasomal segments: segment II 2, segment III 1 (80%) or 2 (20%), vs. segment II 2–4 (96%), segment III 1 (24%), 2 (57%) or 3 (18%); (iv) leg III prolateral basitarsal spur with greater number of macrosetae, > 25 (vs. ≤ 25 in 97% of cases).

Other species in the *A.* '*crassicauda*' complex differ from *A. ammophilus* **sp. n.** according to the following characters:

(1) *A. azerianus* Yağmur & Kovařík, 2025: (i) metasoma not as dilated posteriorly, segment IV W/ segment I W: ♂ 1.1, ♀ 1.0; (ii) metasoma V not as deep, L/D ♂♀ 2.0; (iii) more elongate pedipalp segments: femur L/W ♂ 3.2, ♀ 3.1; patella L/W ♂♀ 2.8; chela L/ manus W ♂ 4.4, ♀ 4.8; (iv) pedipalp chela not as deep, L/D ♂ 3.8, ♀ 4.3; (v) internal surface of pedipalp chela manus almost smooth, with only scattered fine granules; (vi) lateral inframedian carinae weakly developed as fine granules on middle part of metasoma II; (vii) prolateral basitarsal spurs sparsely setose (Yağmur et al., 2025a: fig. 160).

(2) *A. barahoeii* Kovařík & Yağmur, 2025: (i) metasoma not as dilated posteriorly, segment IV W/ segment I W: ♂ 1.1, ♀ 1.0–1.1; (ii) ♀ pedipalp patella more elongate: L/W 2.5–2.6; (iii) ♀ pedipalp chela more elongate: L/W 4.9–5.0; (iv) pedipalp chela not as deep, L/D ♂ 3.5–3.9, ♀ 4.1–4.4; (v) enlarged, lobate dentition on posterior ventrolateral carinae of metasoma V; (vi) prolateral basitarsal spurs sparsely setose (Yağmur et al., 2025a: figs. 177–180).

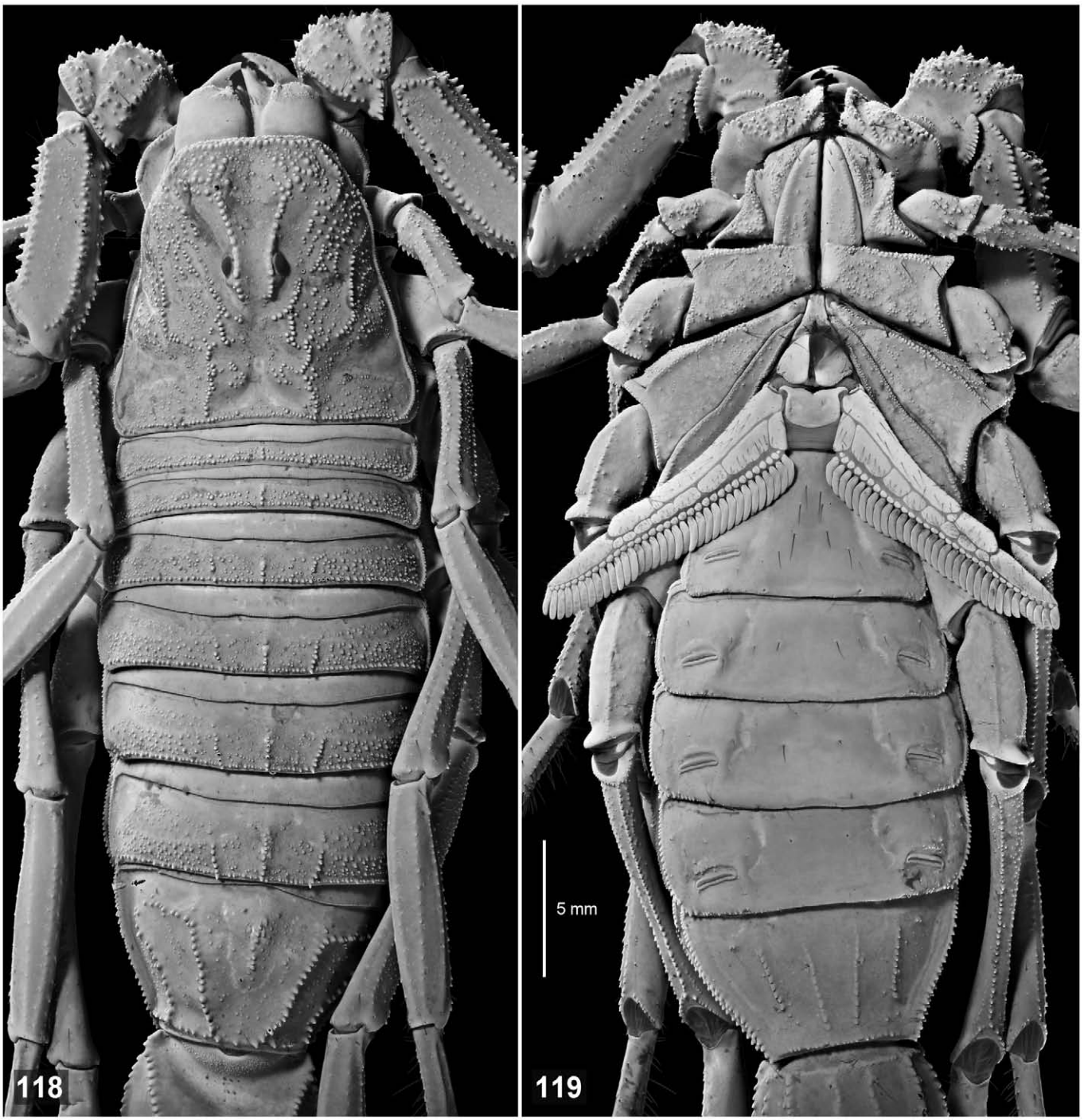

Figures 118–**119**. *Androctonus ammophilus* **sp**. **n**., holotype male. Prosoma and mesosoma in dorsal (118) and ventral (119) views. Scale bar: 5 mm. UV fluorescence.

(3) *A*. *caspius* Kovařík et al., 2025: (i) metasoma not as dilated posteriorly, segment IV W/ segment I W: ♂ 1.1–1.2, ♀ 1.1; (ii) pedipalp patella more elongate: L/W ♂ 2.7–2.8, ♀ 2.5–2.6; (iii) pedipalp femur more elongate: ♂ L/W 3.2–3.3, ♀ L/W 2.5–2.6; (vi) ♂ pedipalp chela more elongate, L/W 4.4–4.5; (v) pedipalp chela not as deep, L/D ♂ 3.8–4.2, ♀ 4.1–4.3; (vi) enlarged, lobate dentition on posterior ventrolateral carinae of metasoma V; (vii) prolateral basitarsal spurs sparsely setose (Yağmur et al., 2025a: figs. 177–180); (viii) internal surface of pedipalp chela manus sparsely granulate, almost smooth.

(4) *A*. *crassicauda* (Olivier, 1807): (i) metasoma not as dilated posteriorly, segment IV W/ segment I W: ♂♀ 0.9–1.0; (ii) metasoma V not as deep, L/D ♂ 2.0–2.1, ♀ 2.1–2.3; (iii) dorsolateral carinae of metasoma V anteriorly serrate, with sharp, dentate granules.

(5) *A*. *ishtar* Yağmur et al., 2025: (i) metasoma not as dilated posteriorly, segment IV W/ segment I W: ♂ 1.1, ♀ 1.0;

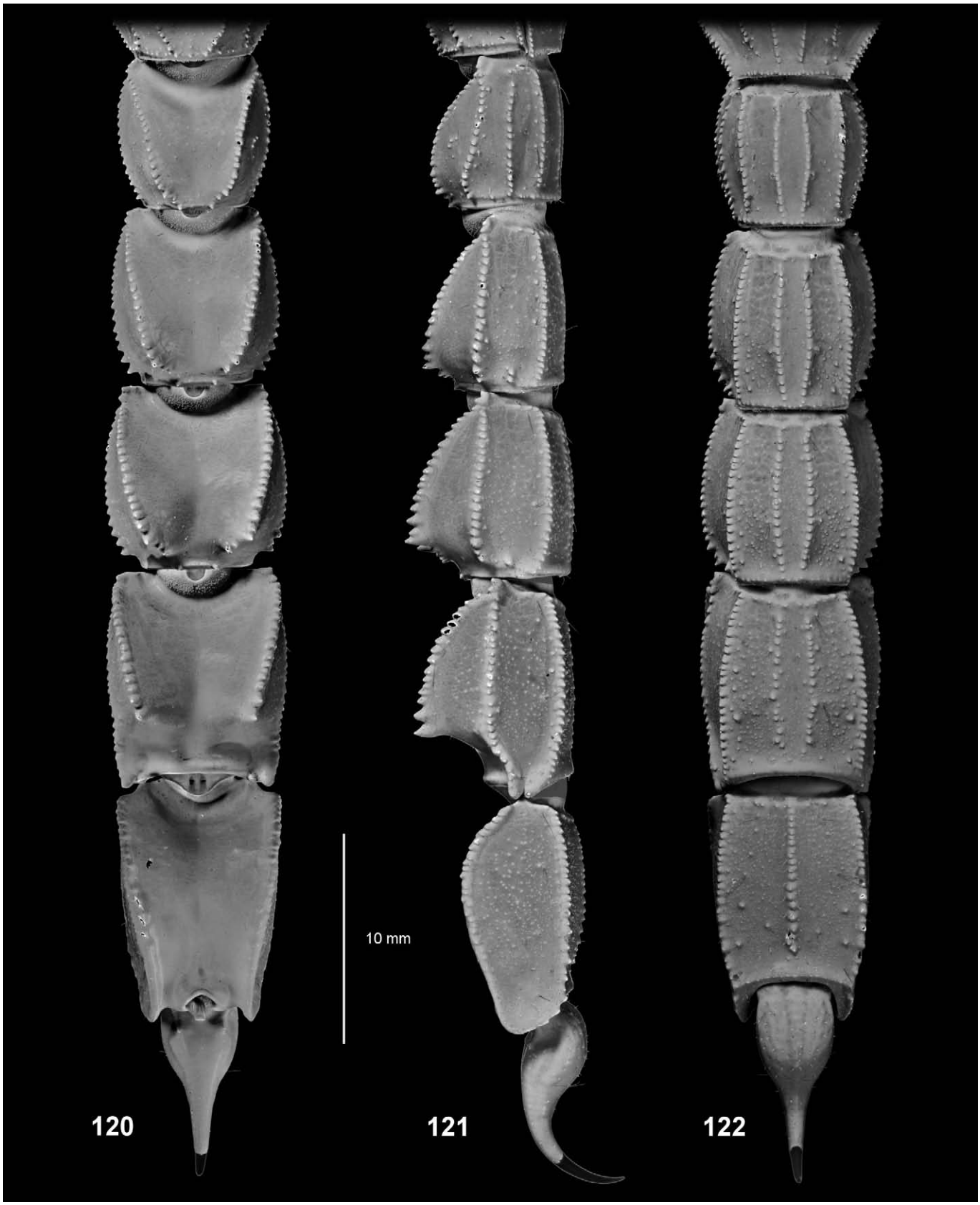

Figures 120–**122**. *Androctonus ammophilus* **sp**. **n**., holotype male. Metasoma and telson in dorsal (120), right lateral (121) and ventral (122) views. Scale bar: 10 mm. UV fluorescence.

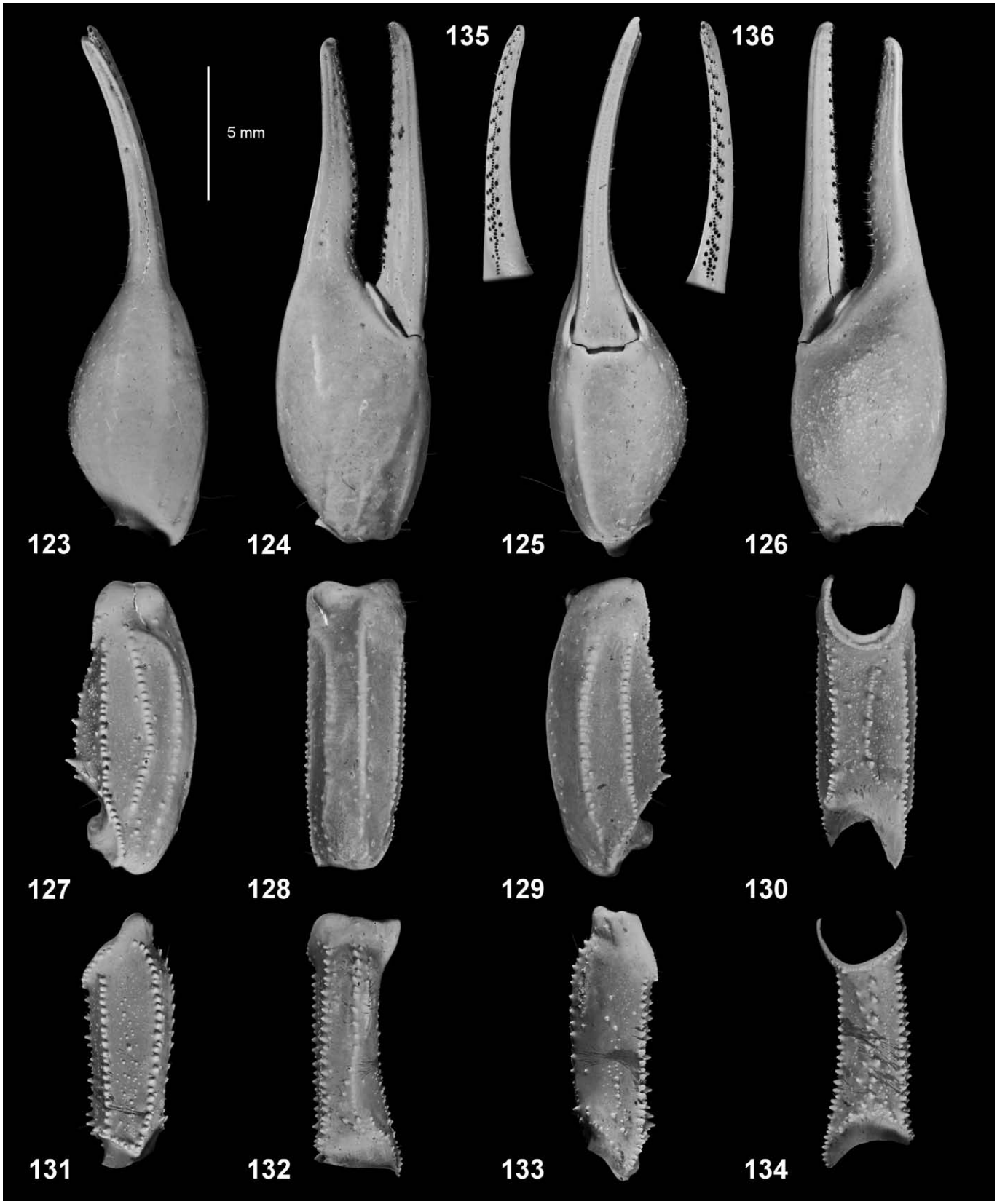

Figures 123–**136**. *Androctonus ammophilus* **sp**. **n**., paratype male. Al Hafrah, 18.VI.1990. **Figures 123**–**134**. Right pedipalp chela (123, 125–126), patella (127–130) and femur (131–134) in dorsal (123, 127, 131), external (128, 132), ventral (125, 129, 133) and internal (126, 130, 134) views. Left pedipalp chela in external view (124), shown as mirror image for comparison (right chela missing fixed finger trichobothria *est* and *et*). **Figures 135**–**136**. Dentate margins of fixed (135) and movable (136) fingers of right pedipalp chela. Scale bar: 5 mm. UV fluorescence.

(ii) metasoma V not as deep, D/ carapace L: ♂♀ 0.5, L/D ♂♀ 2.0; (iii) enlarged, lobate dentition on posterior ventrolateral carinae of metasoma V; (iv) pedipalp fixed finger with trichobothrium *est* level with, not distal to *db*; (v) prolateral basitarsal spurs sparsely setose (Yağmur et al., 2025b: fig. 8).

(6) *A. kunti* Yağmur, 2023: (i) metasoma not as dilated posteriorly, segment IV W/ segment I W: ♂♀ 1.1; (ii) metasoma V not as deep, D/carapace L: ♂♀ 0.5, L/D ♂ 2.0, ♀ 1.9; (iii) ♂ pedipalp more elongate: femur L/W 3.1; patella L/W 2.8; chela L/ manus W 4.5; (iv) pedipalp chela not as deep, L/D ♂♀ 4.3; (v) enlarged, lobate dentition on posterior ventrolateral carinae of metasoma V; (vi) prolateral basitarsal spurs sparsely setose (Yağmur, 2023: figs. 73–74).

(7) *A. orientalis* Birula, 1900: (i) ♂ metasoma not as dilated posteriorly, segment IV W/ segment I W 1.1; (ii) ♂ metasoma V not as deep, L/D 1.9; (iii) ♀ pedipalp chela wider, L/ W 3.7–3.9; (iv) dorsolateral carinae of metasoma V anteriorly serrate, with sharp, dentate granules; (v) prolateral basitarsal spurs sparsely setose (Yağmur et al., 2025a: figs. 113, 120).

(8) *A. sumericus* Al-Khazali & Yağmur, 2023: (i) pedipalp chela more robust, not as narrow: L/W ♂ 3.3–3.5, ♀ 3.3–3.9; (ii) ♀ pedipalp femur more elongate, L/W 2.7–2.9; (iii) prolateral basitarsal spurs sparsely setose (Al-Khazali & Yağmur, 2023: figs. 7, S9).

(9) *A. tihamicus* Alqahtani et al., 2023: (i) metasoma V not as deep, L/D: ♂ 1.9–2.0, ♀ 1.9–2.4; (ii) ♀ metasoma V narrower, L/W 1.6–1.9; (iii) average size of adults smaller, 60–85 mm total length; (iv) internal surface of pedipalp chela manus weakly granulate to almost smooth; (v) prolateral basitarsal spurs sparsely setose (Alqahtani et al., 2023: fig. 12, labeled as "*retrolateral*").

(10) *A. transcaucasicus* Kovařík et al., 2025: (i) metasoma not as dilated posteriorly, segment IV W/ segment I W: ♂♀ 1.1; (ii) ♀ metasoma V not as deep, D/ carapace L 0.4, L/D 2.1; (iii) pedipalp femur more elongate: L/W ♂ 3.3, ♀ 3.1; (iv) ♀ pedipalp patella more elongate, L/W 2.7; (v) pedipalp chela not as deep, L/D ♂ 3.9, ♀ 4.1; (vi) enlarged, lobate dentition on posterior ventrolateral carinae of metasoma V; (vii) prolateral basitarsal spurs sparsely setose (Yağmur et al., 2025a: figs. 307–310); (viii) internal surface of pedipalp chela manus smooth.

(11) *A. turkiyensis* Yağmur, 2021: (i) ♂ metasoma V not as deep, L/D 2.1; (ii) ♂ pedipalp patella narrower, L/W 2.8; (iii) enlarged, lobate dentition on posterior ventrolateral carinae of metasoma V; (iv) prolateral basitarsal spurs sparsely setose (Yağmur, 2021: figs. 65–68; 66–67 labeled as "*retrolateral*").

Graphical comparisons of morphometric ratios are plotted in Figs. 175–178. Horizontal bars indicate the ranges of selected ratios of *A. ammophilus* **sp. n.** alongside the same ranges of eleven other species of the *A.* '*crassicauda*' complex. Overall trends are similar to those of *A. omanensis* **sp. n.** (see above), i.e., somewhat wider and deeper posterior metasomal segments and stockier pedipalps than the other species, although the differences are less pronounced. This reflects the considerable overlap of ratios *A. ammophilus* **sp. n.** and *A. omanensis* **sp. n.** (Figs. 169–170).

Description ♂♂ (adults). **Coloration** (Figs. 116–117). Base color dark brown or almost black; sternites III–VI, distal parts of pedipalp fingers, and leg telotarsi lighter; pectines pale, yellowish.

Carapace (Fig. 118). Weakly trapezoidal, W/L 1.00–1.08, posterior W/anterior W 1.92–2.45; median ocular tubercle prominent, superciliary carinae coarsely granulate; 5 pairs of lateral ocelli in Type 5 configuration (Loria & Prendini, 2014), with major PLMa, MLMa and ALMa, and minor PDMi arranged linearly below short granulated carina, minor ADMi above carina; anterior median carinae strongly developed, coarsely granulate, not reaching anterior margin of carapace; central median, central lateral and posterior median carinae moderately developed, granulate; anterior margin of carapace with row of coarse granules, posterior margin with row of fine granules; left and right areas of anterior preocular region coarsely granulate, central lateral flanks granulate to finely granulate, posterior lateral flanks finely granulate; other intercarinal surfaces bearing sparse fine granulation, shagreened, or smooth; posterior median and posterior lateral sulci smooth; anterior margin of carapace sparsely setose.

Chelicerae (Figs. 158–159). Dorsal surface of manus with coarse and fine granules located anteriorly around several short microsetae; dorsointernal carina strong, granulate, bearing one macroseta; central and posterior dorsal surfaces of manus smooth; fingers robust with dentition typical of the genus (Vachon, 1963): movable finger external margin with large distal external and distal internal denticles, large subdistal and median denticles and two small basal denticles, internal margin with large median and basal denticles, fixed finger with large subdistal denticle and median and basal denticles fused into proximal bicusp, two large denticles on ventral surface, the distal larger, the proximal smaller; dorsal surface of movable finger smooth, with several microsetae, ventral surface smooth with numerous long macrosetae; dorsal surface of fixed finger smooth with several macrosetae at base, ventral surface smooth with numerous long macrosetae; ventral surface of manus smooth with numerous long macrosetae.

Coxosternal area (Fig. 119). Anterior margins of coxae I–IV and posterior margins of coxae III–IV densely granulate, carinate; posterior margins of coxae I–II irregularly granulate; endite I densely granulate, endite II sparsely granulate; other coxal surfaces sparsely, finely granulate; sternum with sparse, fine granules or smooth, subtriangular, with deep posteromedian pit, genital opercula rounded triangular, with sparse, fine granules on anterior or posterior margins, or smooth.

Pectines (Fig. 119). Basal piece wider than long, with convex lateral margins and small anteromedian notch, surface smooth; pectines with 3 marginal lamellae, 7–9 middle lamellae; distal tips extending to proximal third to half of trochanter IV in male; male combs with 29–34 teeth, marginal and middle lamellae with sparse to moderate cover of macrosetae; fulcra with 4–8 macrosetae in males; internal fulcra with single microseta.

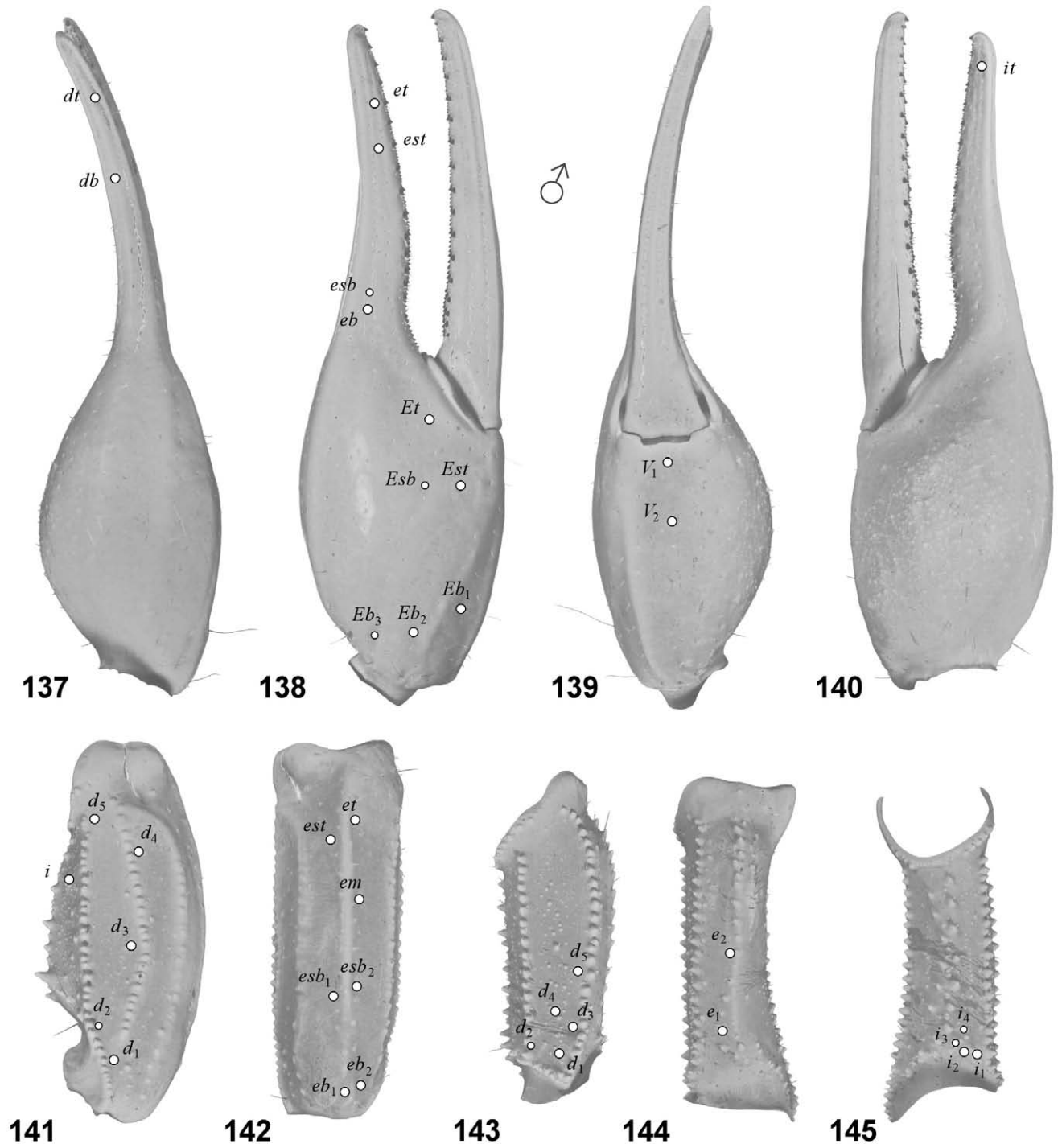

Figures 137–145. *Androctonus ammophilus* **sp. n.**, trichobothrial pattern, paratype male. Al Hafrah, 18.VI.1990. Right pedipalp chela (137, 139–140), patella (141–142) and femur (143–145) in dorsal (137, 141, 143), external (142, 144), ventral (139) and internal (140, 145) views. Left pedipalp chela in external view (138), shown as mirror image for comparison (right chela missing fixed finger trichobothria *est* and *et*).

Hemispermatophore (Figs. 160–162). Flagelliform, trunk elongate, ca. 8 times length of capsule region; flagellum short with thicker, laminate pars recta; sperm hemiduct with three lobes, posterior lobe large and laminate, median lobe small and acuminate, anterior lobe of intermediate length, tapered; posterior margin of median lobe overhanging posterior lobe, the two lobes fused along a median lobe carina; basal lobe a prominent, narrow, hook-like projection.

Measurement (mm) or count		*A. ammophilus* **sp. n.**			
		♂ **holotype Montesar 14.IX.1997**	♂ **paratype Al Hafrah 18.VI.1990**	♀ **paratype Abu Dhabi VI.1971**	♀ **paratype Abu Dhabi RS6500**
Carapace	L / W	10.4 / 11.0	10.6 / 11.1	11.7 / 12.1	11.4 / 12.3
Metasoma + telson	L	52	50	57	57
Metasoma I	L / W / D	7.2 / 7.2 / 6.0	7.4 / 7.3 / 6.1	7.5 / 7.8 / 6.5	7.2 / 7.6 / 6.5
Metasoma II	L / W / D	8.8 / 7.9 / 6.8	8.4 / 8.2 / 6.7	8.1 / 8.5 / 7.1	8.4 / 8.2 / 7.3
Metasoma III	L / W / D	8.7 / 8.6 / 7.6	8.9 / 8.9 / 7.8	8.4 / 9.2 / 8.0	8.1 / 8.9 / 8.0
Metasoma IV	L / W / D	10.2 / 8.5 / 7.6	10.8 / 8.9 / 7.9	10.1 / 9.1 / 8.2	10.4 / 8.7 / 8.1
Metasoma V	L / W / D	10.6 / 7.6 / 6.0	11.1 / 7.8 / 6.0	11.3 / 7. 9/ 6.7	11.0 / 8.1 / 6.6
Lateral granules Met. II	left / right	2 / 2	2/ 2	–	–
Lateral granules Met. III	left / right	1 / 1	1/ 1	–	–
Telson	L / W / D	8.4 / 3.7 / 3.0	8.4 / 3.6 / 3.0	10.4 / 4.7 / 3.7	10.3 / 4.4 / 3.3
Pedipalp femur	L / W	8.3 / 3.2	9.3 / 3.2	8.7 / 3.3	9.0 / 3.3
Pedipalp patella	L / W	10.3 / 4.4	11.5 / 4.3	10.7 / 4.7	10.5 / 4.7
Pedipalp chela	L	18.2	19.2	19.4	19.3
Chela manus	L / W / D	7.4 / 4.8 / 5.5	7.8 / 5.0 / 5.6	7.1 / 4.8 / 5.7	7.7 / 4.6 / 5.2
Chela movable finger	L	11.2	12.3	12.9	12.7
Subrows: movable finger	left / right	15 / 15	15 / 15	–	–
Subrows: fixed finger	left / right	14 / 14	14 / 15	–	–
Pectine	L	11.2	–	9.0	9.2
Pectinal tooth count	left / right	32 / 34	– / –	25 / 25	26 / 27
Leg III femur	L	11.9	11.5	11.5	11.3
Leg III patella	L	9.2	9.7	9.5	9.5
Basitarsal RS setae	left / right	24 / 25	– / 26	–	–
Basitarsal spur setae	left / right	28 / 30	33 / –	–	–
Total	**L**	**84**	**80**	**92**	**89**

Table 3. Morphometric and meristic data for representative male and female types of *Androctonus ammophilus* **sp. n.** Abbreviations: L, length; W, width; D, depth; Met., metasoma; RS, retrosuperior. Carapace W is maximum (posterior) width. Pedipalp chela manus L is ventral length (Fig. 186). Lateral granule counts are for lateral inframedian carinae.

Mesosoma (Figs. 118–119). *Tergites*: pretergites smooth with finely corrugated posterior margins; tergites with sparse to moderate, medium-to-fine granulation; anterior surfaces with finer granulation, becoming smooth near pretergite margins; tergite I with weak median carina; tergite II with weak median carina, traces of weak lateral carinae; tergites III–VI tricarinate with median and paired lateral carinae; all carinae on tergites I–VI granulate, confined to posterior 50–70% of tergites, lateral carinae anteriorly divergent; tergite VII with five carinae, median carina weak; posterior margins of tergites I–VI bordered by dense rows of small granules; all tergites lacking macrosetae. *Sternites*: sternites III–VI smooth; sternite VI with short, smooth or weakly granulate pairs of lateral carinae; posterior margins of sternites III–VI smooth; sternite VII smooth, with granulate pairs of median and lateral carinae, median pairs longer than lateral pairs; spiracles on sternites III–VI elongate, slit-like, each bordered anteriorly with smooth or granulate transverse carina; sternites III–VI with scattered, sparse macrosetae, sternite VII with 6 macrosetae, 4 on the carinae.

Metasoma (Figs. 120–122). Robust, with short, moderately stout segments; segments I–IV progressively increasing in width and depth; segment V moderately deep, D/L 0.52–0.61. *Carinae*: segment I with 10 complete carinae; segments II–III with 8 complete carinae, lateral inframedian carinae reduced to short posterior series of granules (II with 2 granules, III with 1 granule in 5/6 carinae); segment IV with 8 carinae; segment V with 5 carinae. All carinae strong, granulate; dorsolateral carinae moderately raised on all segments, becoming progressively more elevated, from segment I to segment IV; dorsolateral carinae on segments II–IV with posterior granules enlarged, dentate; dorsolateral carinae of segment V strongly granulate in anterior half, weakly granulate to smooth in posterior half; ventrolateral carinae of segment V with smaller granules in anterior half, slightly larger granules in posterior half; ventrosubmedian carinae on segment V obsolete, marked by isolated granules. Ventral anal margin with around 15 small, weak, transversely elongated granules; lateral anal margin non-lobate. *Intercarinal surfaces*: dorsal surfaces of

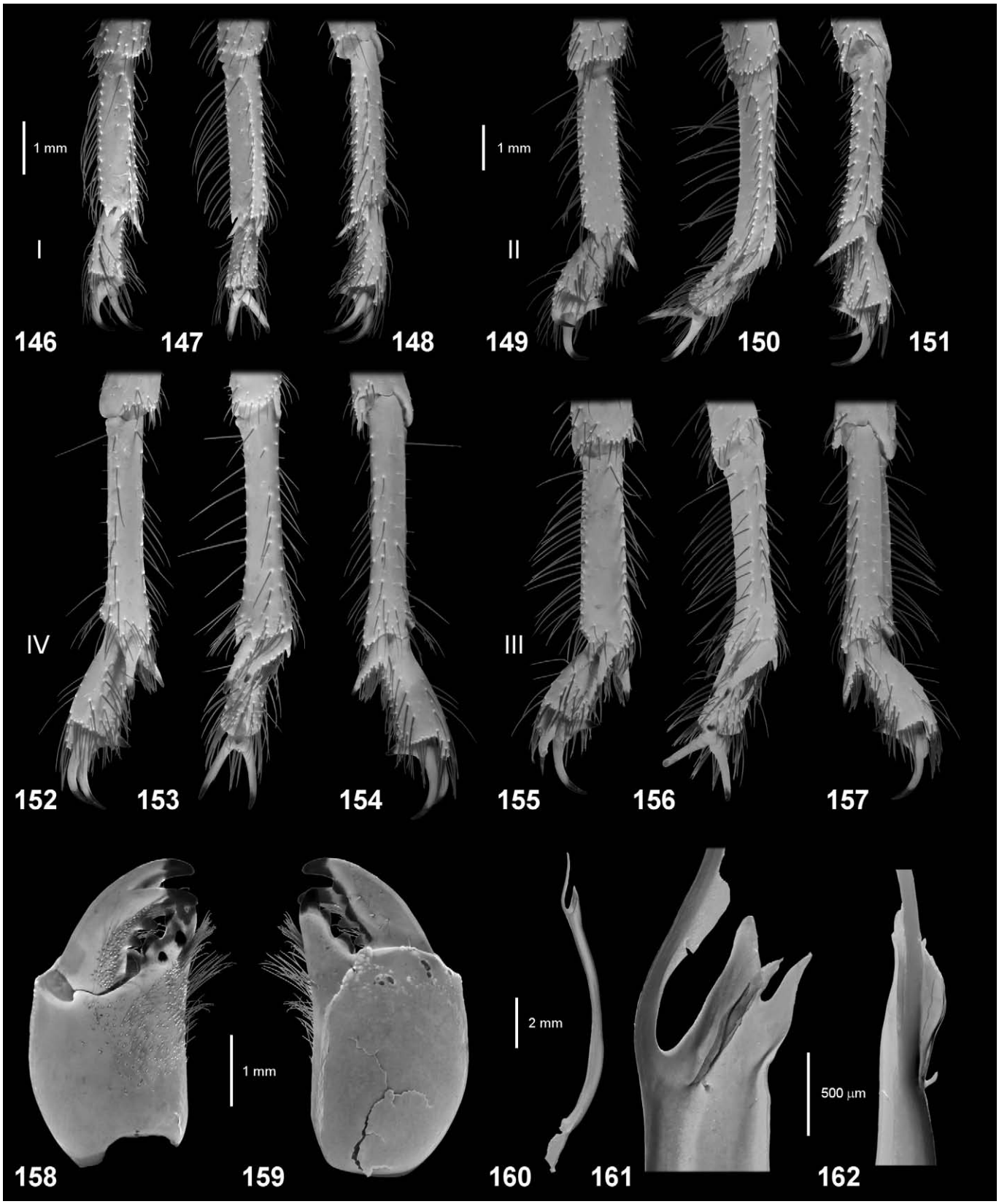

Figures 146–162. *Androctonus ammophilus* **sp. n. Figures 146–157**. Right basitarsi and telotarsi (shown as mirror image for comparison to Figs. 63–74). Leg I (146–148), paratype male, Qitbit, 26.III.1989; legs II (149–151), III (155–157) and IV (152–154), holotype male; in retrolateral (146, 149, 152, 155), ventral (147, 150, 153, 156) and prolateral (148, 151, 154, 157) views. **Figures 158–159**. Right chelicera, paratype male, Qitbit, 26.III.1989. Ventral (158) and dorsal (159) views. **Figures 160–162**. Right hemispermatophore. paratype male. Al Hafrah, 18.VI.1990. Whole hemispermatophore (160), capsule region in convex (161) and posterior (162) views. Scale bars: 1 mm (146–148), 1 mm (149–157), 1 mm (158–159), 2 mm (160), 500 µm (161–162). UV fluorescence (146–159), white light (160–162).

Ratio or count	*A. omanensis* **sp. n.**		*A. ammophilus* **sp. n.**	
	♂	♀	♂	♀
Carapace L/W	0.9–1.0 0.95 ± 0.03 (48)	0.9–1.0 0.92 ± 0.04 (50)	0.9–1.0 0.97 ± 0.02 (8)	0.9–1.0 0.95 ± 0.02 (4)
Carapace posterior W/ anterior W	1.9–2.8 2.29 ± 0.22 (48)	2.0–2.8 2.34 ± 0.20 (50)	1.9–2.5 2.16 ± 0.16 (8)	2.1–2.4 2.16 ± 0.14 (4)
Pectine L/ Carapace L**	1.0–1.2 1.07 ± 0.05 (48)	0.7–1.0 0.83 ± 0.05 (50)	1.0–1.1 1.09 ± 0.03 (7)	0.8 0.81 ± 0.03 (4)
Pedipalp chela L/W*	3.3–4.2 3.70 ± 0.19 (48)	3.5–4.6 4.01 ± 0.21 (51)	3.5–4.1 3.75 ± 0.21 (8)	4.1–4.7 4.28 ± 0.31 (4)
Pedipalp chela L/D*	3.0–3.6 3.25 ± 0.14 (48)	3.2–4.0 3.45 ± 0.17 (49)	3.1–3.5 3.3 ± 0.13 (8)	3.4–4.0 3.65 ± 0.25 (4)
Pedipalp chela movable finger L/ manus L*	1.5–1.9 1.62 ± 0.08 (48)	1.6–1.9 1.73 ± 0.09 (51)	1.5–1.7 1.59 ± 0.08 (8)	1.6–1.8 1.72 ± 0.12 (4)
Pedipalp femur L/W	2.3–2.9 2.65 ± 0.15 (48)	2.4–2.9 2.59 ± 0.14 (51)	2.6–3.0 2.79 ± 0.13 (8)	2.6–2.7 2.66 ± 0.09 (4)
Pedipalp patella L/W	2.1–2.7 2.33 ± 0.13 (48)	2.1–2.7 2.27 ± 0.10 (51)	2.1–2.7 2.33 ± 0.13 (8)	2.3–2.5 2.34 ± 0.10 (4)
Metasoma I L/W	0.9–1.0 0.94 ± 0.03 (48)	0.9–1.0 0.94 ± 0.04 (51)	0.9–1.1 1.00 ± 0.05 (8)	0.9–1.0 0.98 ± 0.09 (4)
Metasoma II L/W*	0.9–1.1 0.99 ± 0.04 (48)	0.9–1.1 1.01 ± 0.03 (51)	1.0–1.1 1.07 ± 0.04 (8)	1.0–1.1 1.03 ± 0.06 (4)
Metasoma III L/W*	0.9–1.0 0.92 ± 0.04 (48)	0.9–1.1 0.96 ± 0.04 (51)	0.9–1.0 0.98 ± 0.03 (8)	0.9–1.1 0.98 ± 0.09 (4)
Metasoma IV L/W*	1.0–1.2 1.09 ± 0.04 (48)	1.1–1.2 1.15 ± 0.04 (51)	1.1–1.3 1.19 ± 0.04 (8)	1.1–1.2 1.19 ± 0.06 (4)
Metasoma V L/W*	1.2–1.4 1.27 ± 0.06 (48)	1.3–1.5 1.38 ± 0.07 (51)	1.3–1.4 1.35 ± 0.06 (8)	1.4–1.5 1.44 ± 0.06 (4)
Metasoma III L/D*	1.0–1.1 1.06 ± 0.04 (48)	1.0–1.2 1.09 ± 0.04 (51)	1.0–1.2 1.14 ± 0.06 (8)	1.0–1.2 1.11 ± 0.10 (4)
Metasoma IV L/D*	1.1–1.4 1.24 ± 0.05 (48)	1.2–1.4 1.27 ± 0.06 (51)	1.2–1.4 1.33 ± 0.07 (8)	1.2–1.4 1.31 ± 0.07 (4)

Table 4. Variation in morphometric ratios in *Androctonus omanensis* **sp. n.** and *A. ammophilus* **sp. n.** Cited data are: range (minimum – maximum), mean ± SD, and number of samples. Variables exhibiting significant sexual dimorphism (Mann-Whitney U test, $P < 0.05$): *, female value larger; ** male value larger.

all segments smooth, lustrous; dorsolateral surfaces smooth or with sparse fine granules on segments I–IV; lateral surfaces smooth on segment I, smooth to shagreened or densely, finely granulate on segments II–V; ventrolateral surfaces smooth or weakly shagreened on segment I, shagreened or densely, finely granulate on segments II–V; ventromedial surfaces of segments I–IV smooth or shagreened. *Setation*: 2 pairs of macrosetae on ventrolateral and ventrosubmedian carinae of segments I–IV, 3 pairs on dorsolateral carinae of segment IV, 5 lateral and 4 ventral pairs on segment V.

Telson (Figs. 120–122). Dorsal and lateral surfaces of vesicle smooth, ventral surface with weak coarse granulation; lateral profile pyriform. Aculeus thick, strongly curved, approximately same length as vesicle.

Pedipalps (Figs. 123–145). *Femur*: dorsointernal, dorsoexternal and ventrointernal carinae strong, with contiguous, coarse, dentate granules; external carina strong, with dentate granules non-contiguous proximally; internal carina broad, with non-contiguous, large dentate granules arranged in band 2 granules wide; other carinae obsolete; dorsal, ventral and internal surfaces with sparse, fine granules, external surface smooth; distal external macrosetal cluster present as a dense compact linear strip with > 20 setae. *Patella*: dorsointernal, dorsomedian, ventroexternal, ventromedian, ventrointernal and internal carinae strong, coarsely granulate; dorsoexternal carinae strong, weakly granulate; external carina smooth; dorsointernal, internal and ventrointernal surfaces with moderate to sparse fine granulation; dorsoexternal surface with sparse fine granules,

No.	♂			♀		
	Eigenvalue	%	cumulative %	Eigenvalue	%	cumulative %
1	8.6403	37.57	37.57	10.3811	45.14	45.14
2	4.4673	19.42	56.99	4.0460	17.59	62.73
3	1.7073	7.42	64.41	1.5135	6.58	69.31
4	1.3077	5.69	70.1	1.1664	5.07	74.38
5	1.0353	4.5	74.6	0.9373	4.08	78.45
6	0.8414	3.66	78.26	0.6792	2.95	81.41
7	0.6718	2.92	81.18	0.6684	2.91	84.31
8	0.6546	2.85	84.02	0.5881	2.56	86.87
9	0.6261	2.72	86.75	0.4918	2.14	89.01
10	0.5202	2.26	89.01	0.4002	1.74	90.75
11	0.4667	2.03	91.04	0.3818	1.66	92.41
12	0.4127	1.79	92.83	0.3280	1.43	93.83
13	0.3694	1.61	94.44	0.2949	1.28	95.12
14	0.3065	1.33	95.77	0.2131	0.93	96.04
15	0.2183	0.95	96.72	0.1833	0.8	96.84
16	0.1837	0.8	97.52	0.1776	0.77	97.61
17	0.1485	0.65	98.6	0.1494	0.65	98.26
18	0.1244	0.54	98.71	0.1230	0.53	98.8
19	0.1027	0.45	99.15	0.0890	0.39	99.18
20	0.0678	0.29	99.45	0.0697	0.3	99.49
21	0.0574	0.25	99.7	0.0507	0.22	99.71
22	0.0388	0.17	99.87	0.0434	0.19	99.89
23	0.0309	0.13	100	0.0242	0.11	100

Table 5. Eigenvalues from principal components analysis (PCA) of 23 morphometric variables of metasoma and pedipalp segments (cf. Tabs. 6–7) measured from adult *Androctonus* from Oman, and adjacent Saudi Arabia and UAE. PCA was conducted separately for adult males (N = 55) and adult females (N = 54). Percentages and cumulative percentages of explained variance are listed in columns 3, 4, 6, and 7.

external and ventroexternal surfaces smooth. *Chela*: fixed finger with digital (D1), dorsal secondary (D3) and dorsal marginal (D4) carinae strong; manus with D1 and D3 weak or obsolete, D4 absent; ventroexternal, ventromedian and ventrointernal carinae present on movable finger; other carinae absent; internal surface of manus densely, finely granulate, other surfaces smooth, lustrous; 15 denticle subrows on dentate margin of movable finger, 13–14 on dentate margin of fixed finger, subrows usually flanked by internal and external accessory denticles, except for proximal subrow in some cases; proximal dentate margins of fingers weakly undulate or scalloped, leaving a gap with fingertips closed. *Trichobothriotaxy*: orthobothriotaxic, type Aβ (Vachon, 1974, 1975) (Figs. 137–145).

Legs (Figs. 116–119, 146–157, 163–167). *Femur*: I–III with inferior median carina denticulate-granulate; inferior prolateral and superior prolateral carinae granulate; superior median carina coarsely granulate, with irregular granulation proximally; femur IV with inferior median carina denticulate-granulate; inferior prolateral carina granulate, superior prolateral and superior median carinae weakly granulate; all prolateral surfaces sparsely granulate, with coarse granules on I, fine granules on II–IV; all retrolateral surfaces smooth except for sparse series of inferior retrolateral granules on I. *Patella*: I–IV with inferior median and inferior prolateral carinae weakly granulate or denticulate-granulate; prolateral median, superior prolateral and superior median carinae weakly granulate on II–III, weakly granulate or smooth on I and IV; all prolateral and retrolateral surfaces smooth. *Tibia*: I–III with regular series of long macrosetae on retrosuperior margin (bristle comb); III–IV with prominent tibial spurs. *Basitarsus*: I–III moderately compressed with flat retrolateral surfaces; regular series of long macrosetae on retrosuperior and retroinferior margins (bristle combs); leg III retrosuperior series 23–26 (mean± SD: 24.20 ± 1.30; median 24; N = 5); retrolateral spurs simple, prolateral spurs with non-bifurcate basal spiniform process, and numerous macrosetae, leg III spur macrosetal counts 28–66 (mean ± SD: 35.8 ± 14.9; median 29.5; N = 6). *Telotarsus*: I–IV relatively short, laterodistal apices truncate, superior distal median lobe prominent; heavily setose with long macrosetae arranged in prolateral, retrolateral and two ventral series; ungues long, curved and narrow.

Measurements. See Tables 3–4.

♂ Variable	PC1	PC2	PC3	PC4
Metasoma I L	-0.2170	**-0.6500**	-0.1091	0.0354
Metasoma I W	**-0.8683**	-0.0511	-0.1843	-0.1299
Metasoma I D	**-0.8592**	0.1099	-0.1633	-0.2138
Metasoma II L	-0.3651	**-0.5733**	-0.3611	0.1230
Metasoma II W	**-0.9303**	0.0544	-0.0572	-0.2123
Metasoma II D	**-0.9265**	0.1132	-0.0491	-0.0877
Metasoma III L	-0.4381	**-0.5104**	-0.3519	0.3324
Metasoma III W	**-0.9173**	0.1633	0.0608	-0.1997
Metasoma III D	**-0.9044**	0.1136	0.1073	0.0355
Metasoma IV L	-0.3351	**-0.6882**	-0.3684	0.1162
Metasoma IV W	**-0.9019**	0.1941	0.1523	-0.1360
Metasoma IV D	**-0.8040**	0.0556	0.4072	-0.0207
Metasoma V L	-0.4122	**-0.6466**	-0.1663	0.2440
Metasoma V W	**-0.6794**	0.1400	0.2313	0.2182
Metasoma V D	**-0.8271**	0.2842	0.0999	0.1696
Pedipalp chela L	0.2167	**-0.7882**	0.2779	-0.3530
Chela manus L	0.1116	**-0.5643**	0.4725	0.0195
Chela manus W	-0.1295	-0.2778	**0.7508**	0.2320
Chela movable finger L	0.0707	**-0.6008**	0.0486	**-0.5988**
Pedipalp femur L	0.0352	**-0.6229**	0.2509	0.2512
Pedipalp femur W	-0.5011	-0.4512	0.1135	0.2884
Pedipalp patella L	0.1367	**-0.6028**	0.0004	-0.3451
Pedipalp patella W	-0.3908	-0.1416	0.0369	-0.2307

Table 6. Loadings of 23 morphometric variables of metasoma and pedipalp segments on first four principal components from PCA of adult male *Androctonus* from Oman, and adjacent Saudi Arabia and UAE. Loadings of higher magnitude (> 0.5000) are indicated in bold, red font. Variables normalized to carapace L, log-transformed and standardized.

Distribution. Sand dunes of the Rub' al-Khali (Empty Quarter) in southeastern Saudi Arabia, United Arab Emirates, and northwestern parts of central Oman near the border of Saudi Arabia (Fig. 110, orange triangles).

Ecology. *A. ammophilus* **sp. n.** is arenicolous, inhabiting sand dunes in the Rub' al-Khali (Figs. 205–208). Adaptation to sandy substrates is indicated by the compressed basitarsi I–III, which bear linear series of long macrosetae (bristle combs). The much higher counts of macrosetae on the prolateral basitarsal spurs and the longer legs, compared to other species, may be specialized, ultrapsammophilous adaptations for locomotion on fine aeolian substrates.

Morphometric analysis. *A. ammophilus* **sp. n.** differed significantly from *A. omanensis* **sp. n.** in several morphometric ratios related to elongation of pedipalp, metasomal and leg segments (Figs. 168–170, Tab. 4). The ranges of individual ratios were overlapped, preventing their direct use as diagnostic characters for separating the species. However, the species could be separated by the joint distribution of several ratios in higher dimensions (Fig. 168), suggesting that a multivariate analysis would be informative. Indeed, application of PCA to 23 normalized morphometric variables describing the shapes of male pedipalp and metasomal segments enabled separation of *A. ammophilus* **sp. n.** from *A. omanensis* **sp. n.** in 2-dimensional morphospace of PC1 and PC2 (Fig. 111). Linear discriminant functions of the two putative taxa constructed from PC1–PC3 of males attained 100% correct classification of *A. ammophilus* **sp. n.** (geographic group III, Rub' al-Khali) vs. *A. omanensis* **sp. n.** (geographic groups I and II). A plot of canonical variate scores revealed separation of group III from groups I and II along the CV1 axis (F = 19.5, Wilks' lambda = 0.2125) (Fig. 112). CV1 had a large positive PC1 coefficient, and PC1 had large negative metasomal segment W and D loadings, indicating that the metasomal segments are narrower and not as deep in *A. ammophilus* **sp. n.** CV1 had a large negative PC2 coefficient, and PC2 had large negative metasomal segment L, and pedipalp segment L loadings, indicating that the metasomal and pedipalp segments are longer in *A. ammophilus* **sp. n.** (Figs. 111–112, Tabs. 5–8).

Effect of measurement errors. The multivariate scatter plots showing morphometric separation of *A. ammophilus* **sp. n.** from *A. omanensis* **sp. n.** (Figs. 111–112, 168) were based on single trial measurements taken from sclerites using a digital caliper with readout in units of mm, to 2 decimal places (0.01 mm) (see Materials & Methods). Specimens were manipulated by hand to align structural landmarks (Figs. 179–196) with

♀ Variable	PC1	PC2	PC3	PC4
Metasoma I L	**-0.6458**	0.2907	-0.0840	-0.3063
Metasoma I W	**-0.7991**	-0.2723	-0.1632	-0.1023
Metasoma I D	**-0.7308**	-0.1491	-0.3056	-0.3718
Metasoma II L	**-0.7090**	0.2316	-0.3712	0.0477
Metasoma II W	**-0.8675**	-0.3902	-0.0836	-0.0255
Metasoma II D	**-0.8325**	-0.2469	-0.2191	-0.0955
Metasoma III L	**-0.6852**	0.2970	-0.3600	0.2661
Metasoma III W	**-0.8582**	-0.3611	0.0579	0.0069
Metasoma III D	**-0.8509**	-0.3301	0.0777	-0.0986
Metasoma IV L	**-0.7491**	0.3188	-0.1274	0.2442
Metasoma IV W	**-0.8042**	-0.3997	0.1452	0.0569
Metasoma IV D	**-0.7450**	-0.2946	0.3344	-0.0887
Metasoma V L	**-0.5835**	**0.5047**	-0.2478	0.2897
Metasoma V W	**-0.7046**	-0.2911	0.2122	0.4026
Metasoma V D	**-0.7258**	-0.4685	0.1259	0.1456
Pedipalp chela L	-0.4859	**0.6915**	0.3639	-0.1166
Chela manus L	-0.4324	**0.5044**	0.4034	0.3875
Chela manus W	**-0.6639**	-0.0081	0.4706	0.0702
Chela movable finger L	-0.2341	**0.7859**	0.3333	-0.1744
Pedipalp femur L	-0.2909	**0.5346**	-0.1331	0.1284
Pedipalp femur W	**-0.5315**	0.3443	-0.2508	0.0153
Pedipalp patella L	-0.3535	**0.7552**	-0.1002	-0.1915
Pedipalp patella W	**-0.6130**	0.1966	0.2544	-0.4907

Table 7. Loadings of 23 morphometric variables of metasoma and pedipalp segments on first four principal components from PCA of adult female *Androctonus* from Oman, and adjacent Saudi Arabia and UAE. Loadings of higher magnitude (> 0.5000) are indicated in bold, red font. Variables normalized to carapace L, log-transformed and standardized.

	♂			♀		
	PC1	PC2	PC3	PC1	PC2	PC3
CV1	**1.6645**	-0.7814	0.0787	0.7216	**1.0755**	0.0650
CV2	-0.1718	-0.2560	**1.0923**	-0.0254	0.0797	**-1.0362**

Table 8. Coefficients of first three principal components PC1–PC3 (from PCA of Tabs. 5–7) used to construct canonical variates, CV1 and CV2, in a linear discriminant analyses of three geographic groups of adult male and female *Androctonus* from Oman, and adjacent Saudi Arabia and UAE. Analyses conducted separately for each sex. Coefficients of higher magnitude (> 1.000) are indicated in bold, red font.

the caliper jaws. How sensitive are the multivariate results to random errors that inevitably arise in the measurement process? Would separation of species be maintained if the data were reacquired in repeated measurement trials? To estimate the errors, 24 morphometric variables were measured repeatedly in 12 trials performed on one adult specimen, and standard deviations of measurements were computed as error estimates. The estimated errors ranged from 0.04 mm to 0.38 mm (Tab. 9). Larger errors were associated with pedipalp chela manus L, pedipalp chela L, metasoma I L and metasoma V L, indicating less reproducible positioning of caliper jaws in measuring the lengths of these structures. To evaluate the impact of these errors on the multivariate analysis, a perturbation method was applied (Hellton & Thoresen, 2014). Ten virtual measurement trials were conducted by adding computer-simulated errors to the raw data of the 55 specimens analyzed in Figs. 111–112. A pseudorandom number generator returned values from a normal distribution with zero mean and unit standard deviation, which were then multiplied by the error estimates of each variable to yield simulated errors. These virtual measurement trials were reanalyzed by PCA and LDA, and canonical scores were calculated. In all ten trials, the non-overlapping group separation between the two species was maintained in the resulting (PC1, PC2) and (CV1, CV2) scatter plots with similar F-values (range 14.8–17.0) and Wilks' lambda (range 0.240–0.275). This showed that the morphospecies separation was robust and resistant to noise from measurement errors.

Variable	Trial												Mean ± SD
	1	2	3	4	5	6	7	8	9	10	11	12	
Carapace L	12.5	12.44	12.68	12.12	12.4	12.59	12.69	12.47	12.57	12.64	12.6	12.6	12.52 ± 0.16
Metasoma I L	7.67	7.08	8.01	8.16	7.88	8.05	7.96	8	8.03	8.02	7.72	7.72	7.86 ± 0.29
Metasoma I W	8.61	8.43	8.6	8.67	8.39	8.6	8.58	8.58	8.53	8.59	8.59	8.59	8.56 ± 0.08
Metasoma I D	7.47	7.43	7.42	7.46	7.21	7.46	7.37	7.42	7.4	7.41	7.51	7.51	7.42 ± 0.08
Metasoma II L	9.28	9.21	9.28	9.46	9.45	9.19	9.2	9.3	9.23	9.09	9.11	9.36	9.26 ± 0.12
Metasoma II W	9.55	9.53	9.49	9.54	9.57	9.56	9.39	9.5	9.54	9.38	9.38	9.49	9.49 ± 0.07
Metasoma II D	8.1	8.04	8.14	8.06	8.04	8.12	8.08	8.05	8.12	8.18	7.89	8.09	8.08 ± 0.07
Metasoma III L	9.56	9.66	9.7	9.67	9.62	9.75	9.63	9.62	9.68	9.58	9.64	9.78	9.66 ± 0.06
Metasoma III W	10.68	10.88	10.66	10.62	10.58	10.67	10.55	10.64	10.69	10.66	10.59	10.53	10.65 ± 0.09
Metasoma III D	9.44	9.37	9.36	9.45	9.34	9.4	9.37	9.42	9.35	9.42	9.4	9.4	9.39 ± 0.04
Metasoma IV L	11.64	11.4	11.69	11.81	11.64	11.81	11.32	11.58	11.71	11.73	11.48	11.48	11.61 ± 0.16
Metasoma IV W	10.52	10.42	10.51	10.65	10.5	10.61	10.59	10.56	10.66	10.66	10.48	10.48	10.55 ± 0.08
Metasoma IV D	9.76	9.79	9.72	9.91	9.71	9.76	9.77	9.73	9.85	9.87	9.78	9.78	9.79 ± 0.06
Metasoma V L	12.05	12.24	12.08	12.72	12.24	12.53	12.28	12.26	12.19	11.76	12.41	12.41	12.26 ± 0.25
Metasoma V W	9.32	9.14	9.5	9.5	9.25	9.39	9.25	9.63	9.27	9.41	9.62	9.62	9.41 ± 0.17
Metasoma V D	7.67	7.64	7.44	7.7	7.67	7.63	7.67	7.71	7.73	7.46	7.69	7.69	7.64 ± 0.09
Pedipalp chela L	19.11	20.16	20.39	20.43	20.37	20.52	20.21	20.51	20.51	20.47	20.28	20.28	20.27 ± 0.38
Chela manus L	8.44	7.8	8.07	8.19	8.19	7.97	7.74	8.04	7.73	8.21	7.85	7.76	8.00 ± 0.23
Chela manus W	5.3	5.22	5.2	5.23	5.32	5.29	5.28	5.22	5.15	5.16	5.13	5.18	5.22 ± 0.06
Chela movable finger L	13.32	13.14	13.26	12.99	13.02	13.1	13.11	13.06	13.04	13.03	13.01	12.74	13.07 ± 0.14
Pedipalp femur L	9.67	9.6	9.55	9.64	9.68	9.98	9.62	9.86	9.6	9.56	9.54	9.2	9.63 ± 0.19
Pedipalp femur W	3.66	3.7	3.8	3.57	3.69	3.57	3.68	3.48	3.55	3.29	3.52	3.81	3.61 ± 0.15
Pedipalp patella L	11.76	11.66	11.88	11.65	11.76	11.51	11.56	11.68	11.64	11.44	11.73	11.34	11.63 ± 0.15
Pedipalp patella W	5.14	5.06	4.82	5.09	5.08	5.25	5.28	5.23	5.32	5.4	5.15	5.1	5.16 ± 0.15

Table 9. Measurement errors of morphometric variables. Digital caliper readings from 12 repeated manual measurement trials of morphometric variables of metasomal and pedipalp segments of a single adult *Androctonus omanensis* **sp**. **n**. (paratype female, 15 km W. of Barka, 13.X.1993). Resulting mean ± SD values for each variable listed in rightmost column.

Comparative morphometrics of other Arabian *Androctonus*. Morphometric variation of other populations of the *A.* '*crassicauda*' complex in the Arabian Peninsula was analyzed by Alqahtani et al. (2022a). They examined samples from several regions in Saudi Arabia, geographically grouped into four operational taxonomic units (OTUs): northern desert (OTU1), central deserts (OTU2), southwest highlands (OTU3), and the Tihama plain on the Red Sea coast (OTU4). They reported ANOVA results showing highly significant differences in morphometric ratios between OTUs, many with very low P-values ($P < 0.001$ in 11/18 male ratios) (Alqahtani et al., 2022: 10, tab. 7). Their multivariate analysis showed tight clustering of samples into three morphometric groups (OTU1+2, OTU3 & OTU4) cleanly separated by wide distances in canonical variate space ($F = 56.9$, Wilks' lambda = 0.00001) (op. cit.: 14, fig. 3). They concluded that "… *OTU3 and OTU4 populations showed significant speciation without overlapping* …", that "… *discrete populations can be readily distinguished based on a number of morphologic characters*, *particularly size of metasomal segment ratios*.", and that "… *morphological results indicate strong predictive* (sic) *of body proportion variation and suggest the existence of distinct taxa within* A. crassicauda *in Saudi Arabia*." Subsequently, they described OTU4 as a distinct species (*A. tihamicus* Alqahtani et al., 2023) with additional support from divergence of 16S mitochondrial DNA sequences.

The statistical results of Alqahtani et al. (2022a) stand in stark contrast to the results obtained in this study describing morphometric differences between *A. ammophilus* **sp**. **n**. and *A. omanensis* **sp**. **n**. Differences between morphometric ratios of the two species were much more modest, with higher P-values. Their separation by LDA was smaller, without tight clustering, with a lower F-value and a higher Wilks' lambda. This discrepancy casts doubt on the taxonomic

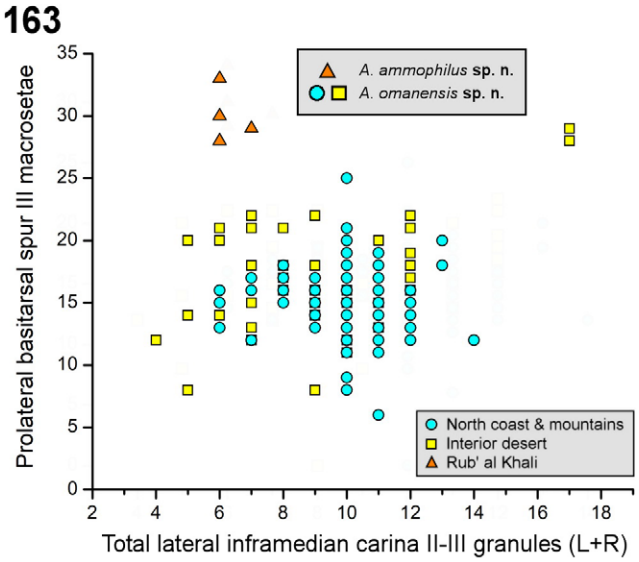

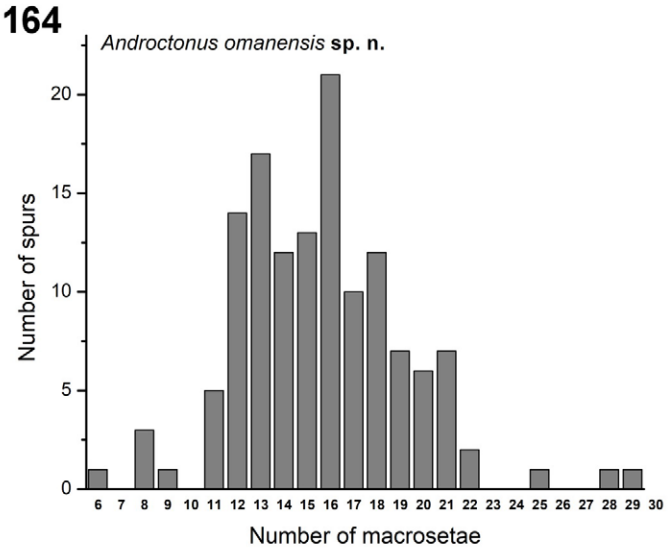

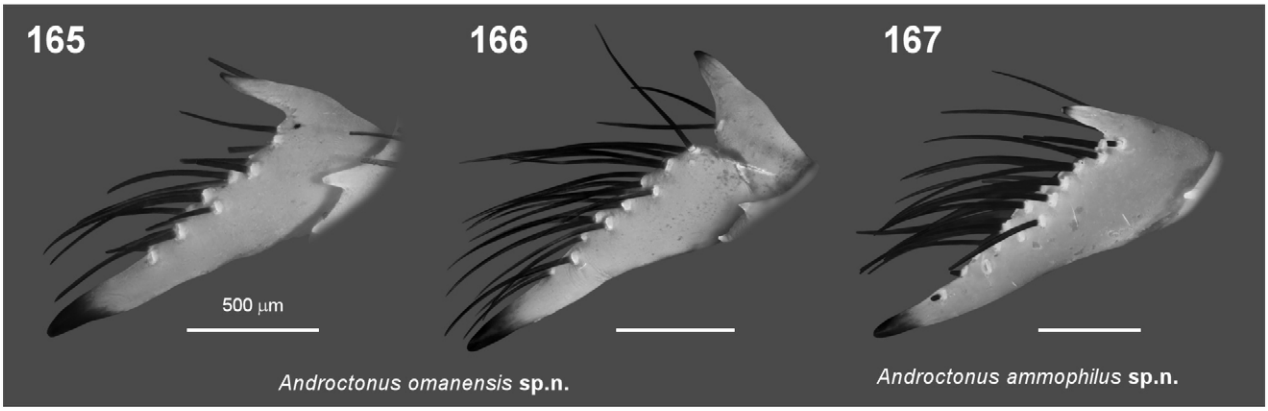

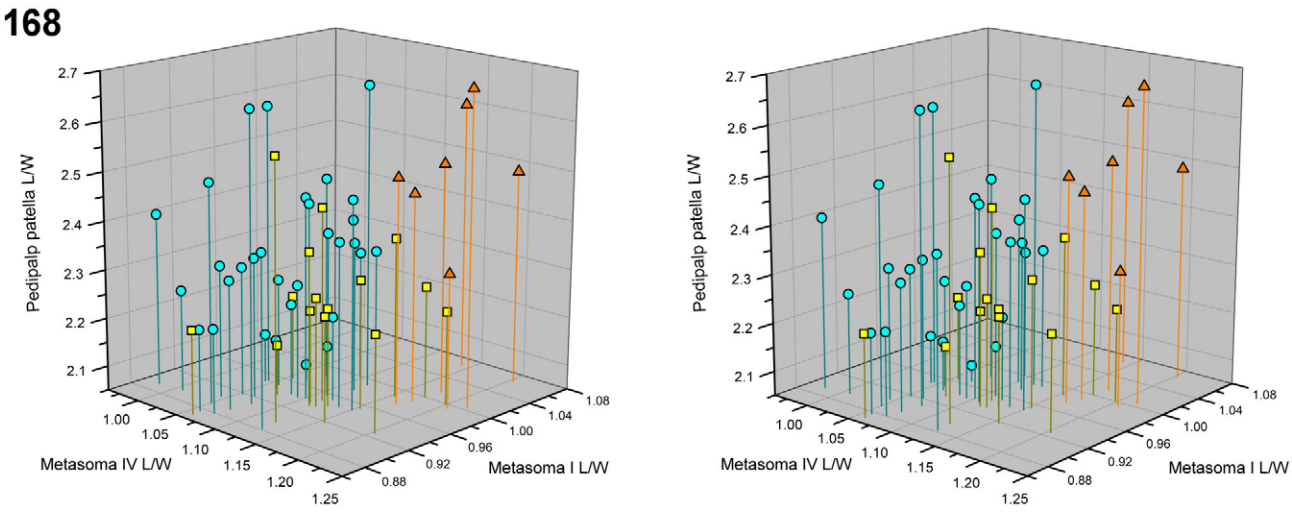

Figures 163–168. Meristic and morphometric differences of new species of *Androctonus*. **Figure 163**. Scatter plot of number of macrosetae on prolateral basitarsal spur of leg III (left or right) vs. total number of large granules on lateral inframedian carinae of metasomal segments II–III (summed left + right counts). *A*. *omanensis* **sp**. **n**.: cyan circles and yellow squares; *A*. *ammophilus* **sp**. **n**.: orange triangles. **Figure 164**. Histogram showing distribution of macrosetal count of prolateral basitarsal spur of leg III (left or right) in *A*. *omanensis* **sp**. **n**. (134 spurs, left and/or right in 32 ♂, 41 ♀). **Figures 165–167**. Right prolateral basitarsal spurs of leg III (prolateral views) from *A*. *omanensis* **sp**. **n**. (165–166) paratypes (165: Yitti ♂, 1.X.1995; 166: Yalooni ♀, 1989), and *A*. *ammophilus* **sp**. **n**. (167) holotype (Montasar ♂). UV fluorescence. Scale bars: 500 µm. **Figure 168**. 3D scatterplot of morphometric ratios (pedipalp patella L/W, metasoma IV L/W and metasoma I L/W) of males of *A*. *omanensis* **sp**. **n**. (cyan circles and yellow squares) and *A*. *ammophilus* sp. n. (orange triangles). Geographic distributions as indicated in Fig. 163 legend.

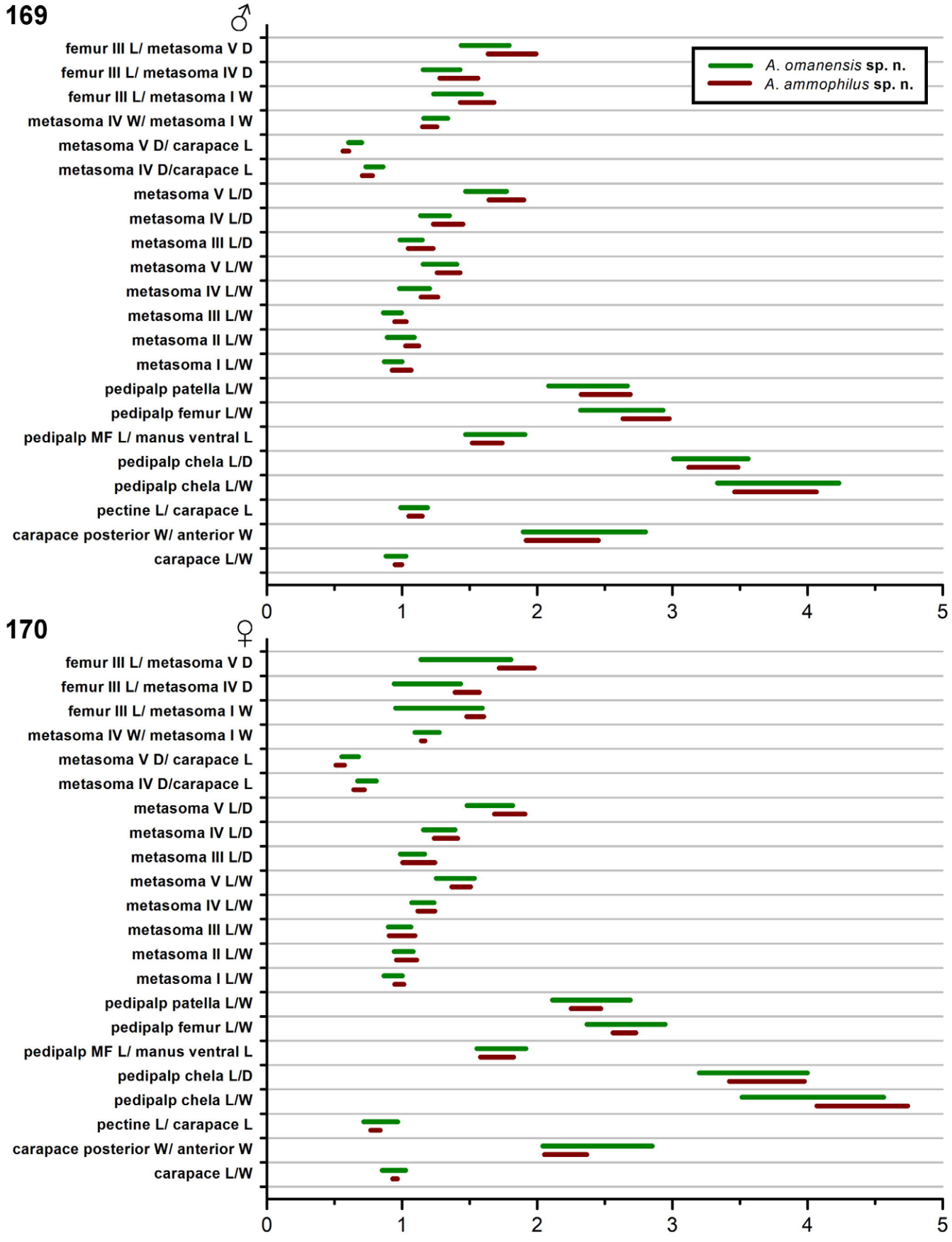

Figures 169–170. Ranges of selected morphometric ratios of males (169) and females (170) of *Androctonus omanensis* **sp. n.** (green bars: 48 ♂, 50 ♀) compared to *A. ammophilus* **sp. n.** (red-brown bars: 8 ♂, 4 ♀).

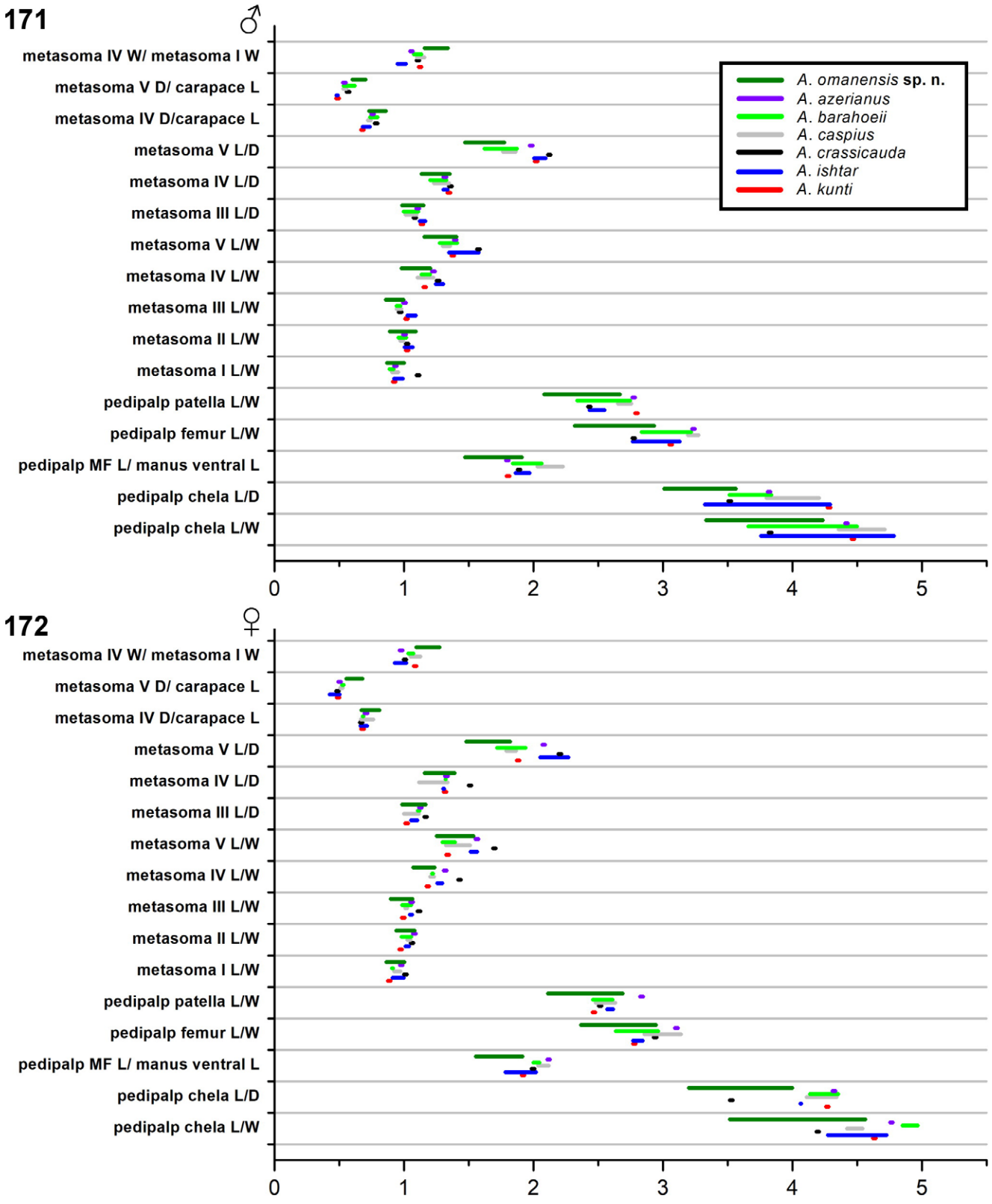

Figures 171–172. Ranges of selected morphometric ratios of males (171) and females (172) of *Androctonus omanensis* **sp. n.** (green bars: 48 ♂, 50 ♀) compared to corresponding ratios of: *A. azerianus* (violet bars: 1 ♂, 1♀), *A. barahoeii* (green bars: 4 ♂, 2 ♀), *A. caspius* (light gray bars: 3 ♂, 3♀), *A. crassicauda* (black bars: 1 ♂, 1 ♀), *A. ishtar* (blue bars: 2 ♂, 2 ♀) and *A. kunti* (red bars: 1 ♂, 1 ♀).

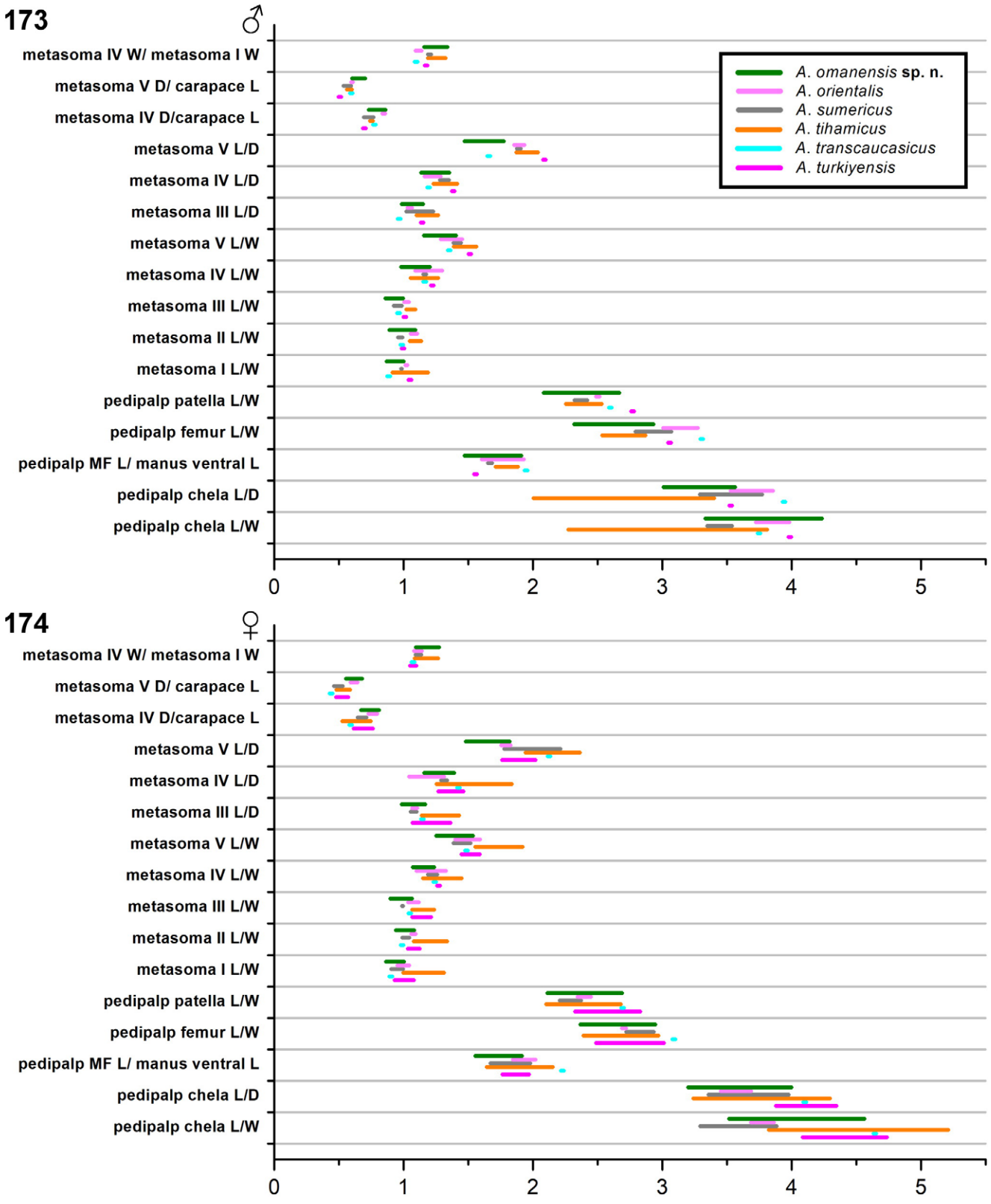

Figures 173–174. Ranges of selected morphometric ratios of males (173) and females (174) of *Androctonus omanensis* **sp. n.** (green bars: 48 ♂, 50 ♀) compared corresponding ratios of: *A. orientalis* (light magenta bars: 2 ♂, 3 ♀), *A. sumericus* (gray bars: 2 ♂, 3 ♀), *A. tihamicus* (orange bars: 5 ♂, 10 ♀), *A. transcaucasicus* (cyan bars: 1 ♂, 1 ♀) and *A. turkiyensis* (magenta bars: 1 ♂, 2 ♀).

relevance of the results presented here. It raises concerns about whether the recognition of the two species is justified by their morphometric differences which are considerably less than those reported for other populations of *A.* '*crassicauda*' complex in the Arabian Peninsula and claimed as evidence of "… *significant speciation* …" (Alqahtani et al., 2022a: 1, 5). To address this issue, it was necessary to review in detail the data and results of Alqahtani et al. (2022a). A reanalysis of the data, retrieved from the website of the journal *PeerJ*, exposed a multitude of errors that invalidated all of the results:

(i) *Numerous outliers in the data*. It appears that basic protocols for screening the raw data for errors were not followed. Using scatter plots to display static allometry, numerous prominent outliers in the data were detected in both sexes, in all four OTU groups: (i) males: OTU1, 1 sample, 2 variables; OTU2, 2 samples, 5 variables; OTU3, 1 sample, 2 variables; OTU4, 3 samples, 4 variables; (ii) females: OTU1, 1 sample, 1 variable; OTU2, 5 samples, 7 variables; OTU3, 2 samples, 3 variables; OTU4, 3 samples, 3 variables. Total numbers of variables affected were: 11 in males, and 11 in females (different from those in males).

(ii) *Random variation in sternite VII L*. This measurement was uncorrelated with carapace L in males, and only weakly so in females. The lack of static allometry, which was evident in all other sclerite measurements, suggests inaccurate measurement of sternite VII L. A likely cause is overlap and concealment of the anterior margin of the sternite by the posterior margin of sternite VI when the mesosoma is contracted.

(iii) *Extensive data duplication*. Almost half of the samples were duplicates, entered twice into spreadsheets as two identical rows. The authors claimed to have measured 38 males and 40 females, and these are indeed the numbers of rows in the respective spreadsheets. However, there were only 19 independent male samples, and 24 independent female samples. In males 19/38 samples, and in females 16/40 samples, were duplicates representing non-existent specimens. With nominal sample sizes almost twice the number of independent samples, results of statistical analyses were distorted and calculated significance values grossly exaggerated. Statistical errors resulting from artificially doubling the number of samples are worse for smaller sample sizes.

(iv) *Errors in morphometric ratios*. Multiple errors were identified in 18 morphometric ratios in the spreadsheet calculated from the raw data. Some were extreme outliers with absurd values, e.g., female carapace anterior W/ posterior W = 0.04; sternite VII L/ W = 0.007023256; female telson W/ metasoma V W = 0.96; female telson vesicle D/ L = 0.25; and male chela manus length/ movable finger length = 1.02. The first two ratios are unknown in any scorpion, and the other three unknown in any *Androctonus*. Some ratio errors were traced to outliers in the raw data (6 female and 7 male ratios). Outliers tainted all four OTUs, and the ratios of all four OTUs included errors. Other errors were traced to corruption of ratio columns in both male and female spreadsheets, by right-shifted data cells and substitution of text values for numeric values.

The presence of outliers, duplicates and errors is not the result of wrong supplemental data files being uploaded to *PeerJ*. Using these files, all statistical results in Alqahtani et al. (2022a) could be exactly replicated using the same software package. After removing outliers, deleting duplicates, and correcting corrupted data cells, tests on the remaining data yielded much higher P-values, and most of the significant differences between OTUs vanished. Reductions in numbers of variables with significant differences ($\alpha = 0.05$) were: morphometrics of males 30/39 to 3/39, of females 25/39 to 0/39; morphometric ratios of males 17/18 to 3/18, of females 7/18 to 2/18. Differences between OTUs were comparable to, or less than, those between *A*. *ammophilus* **sp**. **n**. and *A*. *omanensis* **sp**. **n**.

(v) *Questionable application of ANOVA*. The ANOVA test assumes continuous, normally distributed variables, and its application to discrete variables with small numbers of integer values may yield dubious results. Variables with large numbers of integer values might be approximated by continuous distributions. However, movable finger denticle subrow count, the only meristic variable for which highly significant OTU differences were reported in both sexes (P = ♂ 0.00047, ♀ 0.00674) had as few as 2 or 3 integer values. A more reliable test for differences between variables with small ranges of discrete values is the Likelihood Ratio test. Applying this to the data, with duplicate samples removed, the P-values increased to ♂ 0.0252, ♀ 0.3459, with much weaker or no significant differences.

(vi) *Under-sampling and overfitting of OTU groups*. Linear discriminant analysis (LDA) is a group-supervised dimensional reduction and classification method that maximizes the ratio of between-group variance to within-group variance. To obtain stable classifications, it is recommended that sample sizes of each group being fitted (the OTUs) be larger than the number of independent variables used to construct linear discriminant functions and canonical variates (Fletcher et al., 1978; NCSS, 2023; Williams & Titus, 1988; Williams et al., 1990). The number of variables used by Alqahtani et al. (2022a) were 15 for males, and 21 for females, but OTU sample sizes, after removing duplicates, were only 3–7 for males, and 4–9 for females. The small sample sizes suggest that the tight clustering and wide separation of OTUs is an artefact of overfitting, i.e. coefficients of large numbers of variables with statistical noise were easily adjusted to impose a desired classification on small numbers of samples. Most of the LDA coefficients were ca. 300–17,000, which is 2–3 orders of magnitude larger than the variables they are multiplying (sclerite measurements, ca. 2–10 mm), and the constant terms and pedipalp patella D (depth) coefficients were opposite in sign with much greater magnitudes ($\sim 5 \times 10^{15}$). These large numbers are symptomatic of an ill-conditioned within-group scatter matrix with determinant close to zero, that was inverted to solve the LDA problem. The model is unstable and arbitrary groupings can be fitted by selective choices of coefficients. Indeed, when group assignments of samples were randomly shuffled (Durstenfeld, 1964; Fisher & Yates, 1938) and the analyses repeated, LDA was still able to group the samples into three widely separated clusters by canonical

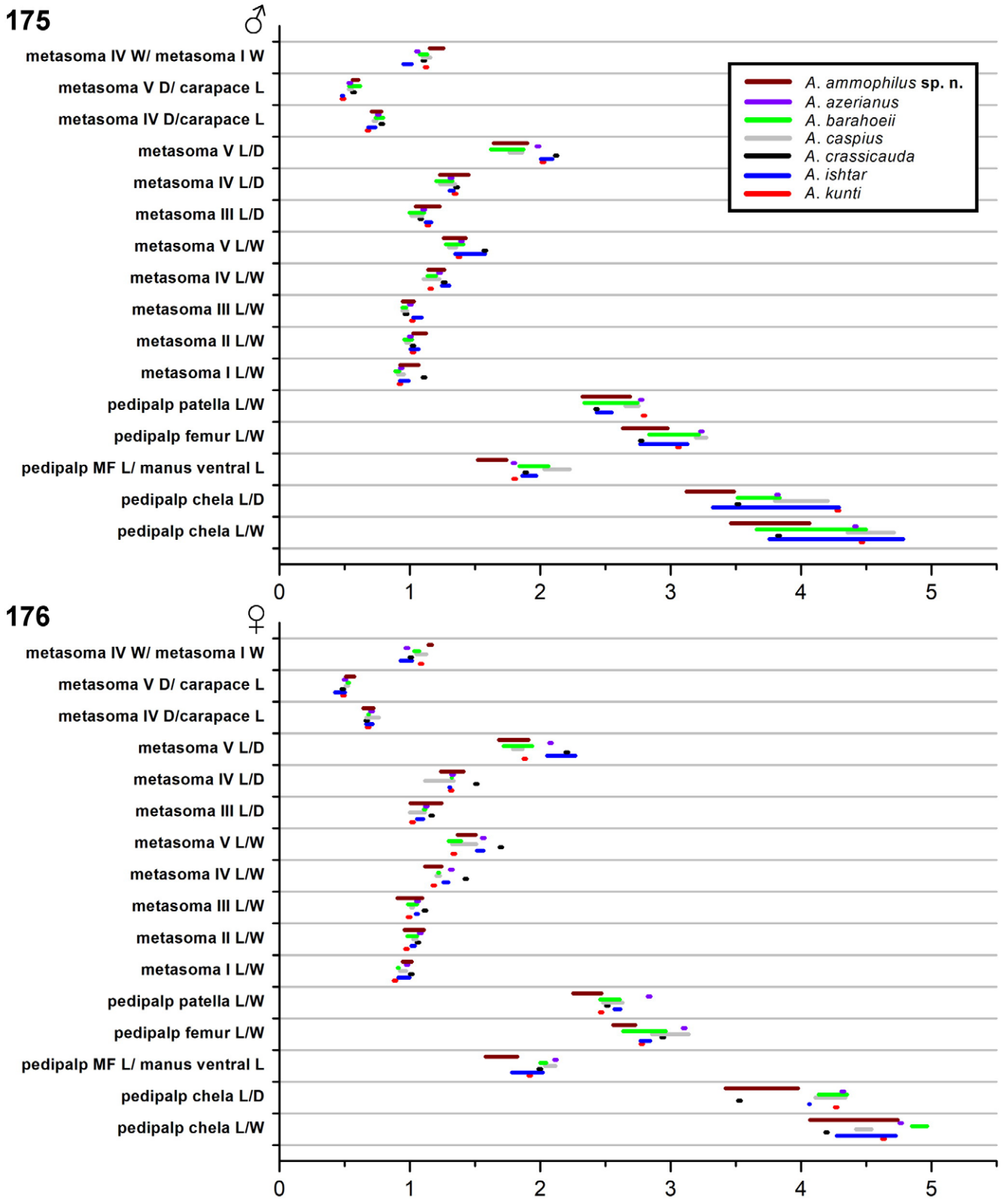

Figures 175–176. Ranges of selected morphometric ratios of males (175) and females (176) of *Androctonus ammophilus* **sp. n.** (red-brown bars: 8 ♂, 4 ♀) compared to corresponding ratios calculated from published measurements of: *A. azerianus* (violet bars: 1 ♂, 1♀), *A. barahoeii* (green bars: 4 ♂, 2 ♀), *A. caspius* (light gray bars: 3 ♂, 3♀), *A. crassicauda* (black bars: 1 ♂, 1 ♀), *A. ishtar* (blue bars: 2 ♂, 2 ♀) and *A. kunti* (red bars: 1 ♂, 1 ♀).

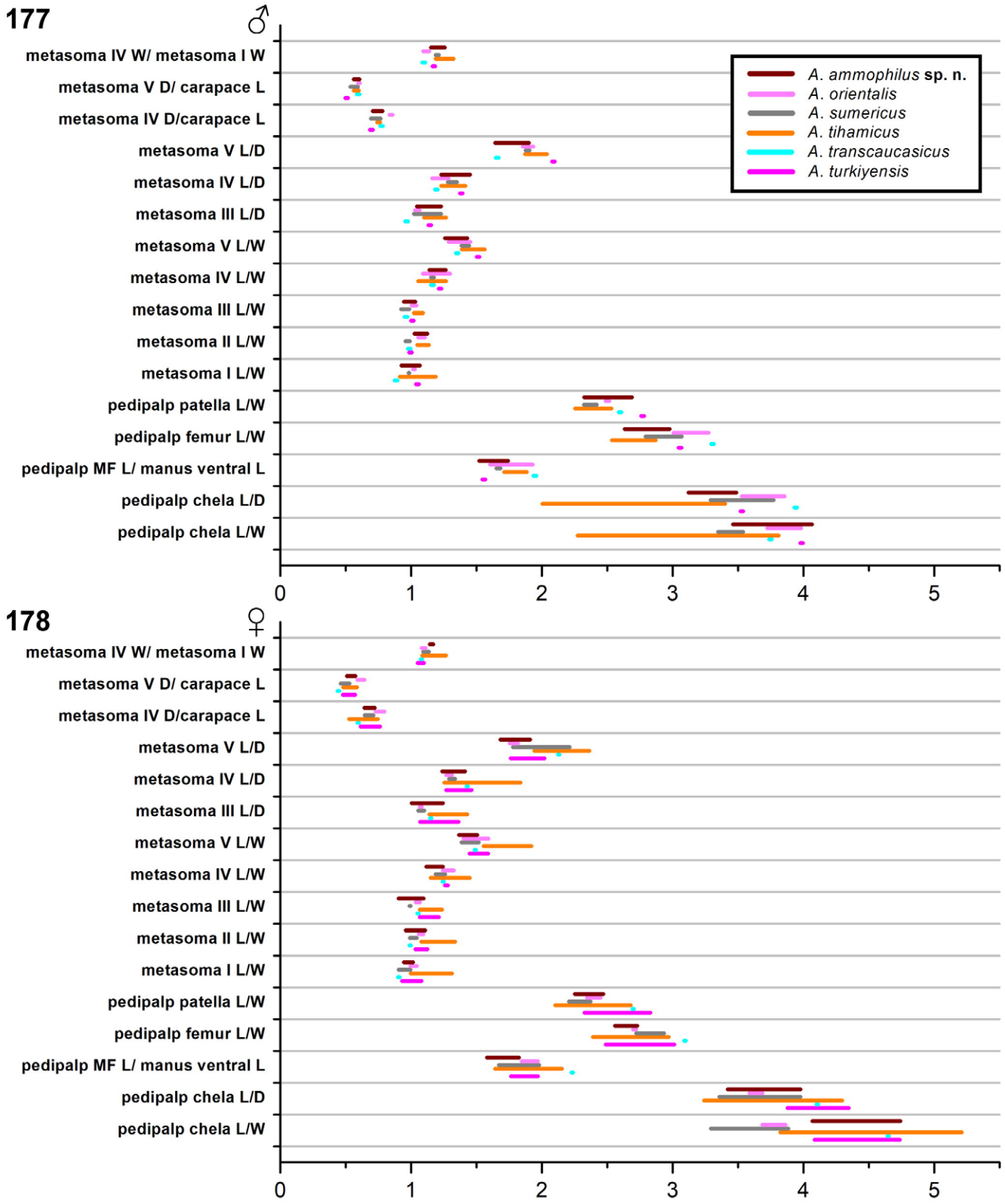

Figures 177–178. Ranges of selected morphometric ratios of males (177) and females (178) of *Androctonus ammophilus* **sp**. **n**. (red-brown bars: 8 ♂, 4 ♀) compared corresponding ratios calculated from published measurements of: *A*. *orientalis* (light magenta bars: 2 ♂, 3 ♀), *A*. *sumericus* (gray bars: 2 ♂, 3 ♀), *A*. *tihamicus* (orange bars: 5 ♂, 10 ♀), *A*. *transcaucasicus* (cyan bars: 1 ♂, 1 ♀) and *A*. *turkiyensis* (magenta bars: 1 ♂, 2 ♀).

scores, fragmenting the original groups. Similar findings were obtained after two additional random permutations of group membership. Moreover, when one sample of each sex (arbitrarily selected from OTU2) was set aside as a test sample, and LDA was applied to the remaining samples as training data, the test samples could not be classified as belonging to any of the three groups, i.e., the classification was not robust and could be not be generalized. The overfitting problems were further compounded by numerous outliers. Outliers have large deviations from the mean and thus add quadratically magnified errors to between-group and within-group scatter matrices. After removing duplicates and outliers, and restricting input variables to the three with smallest Wilk's lambda, group clustering disappeared and canonical scores overlapped. Clustering was also absent when the data were analyzed by the unsupervised dimensional reduction method of PCA, and when LDA was applied to the first three principal components (explaining 79.52% of the variance in males, and 81.79% in females after varimax rotation). The results of the corrected analyses again stand in contrast to the results presented here showing separation of *A*. *ammophilus* **sp**. **n**. from *A*. *omanensis* **sp**. **n**., not because they show much greater separation of OTUs, but because they show no separation at all. In conclusion, the clustering and group separation of samples of Arabian *A.* '*crassicauda*' complex reported by Alqahtani et al. (2022a) are the result of errors in data compilation and analysis. As such, they cannot serve as a benchmark for evaluating the taxonomic significance of the morphometric separation between *A*. *ammophilus* **sp**. **n**. and *A*. *omanensis* **sp**. **n**.

Meristic characters.

Adult males of *A*. *ammophilus* **sp**. **n**. from sites in the Rub' al-Khali (Al Hafrah, Montesar, Qitbit) differed significantly from *A*. *omanensis* **sp**. **n**. samples obtained from the rest of Oman in two meristic characters: (i) higher numbers of macrosetae on leg III prolateral basitarsal spurs (28–33 vs. 6–29; $P = 5 \times 10^{-15}$), and (ii) lower total numbers of enlarged granules composing the lateral inframedian carinae confined to the posterior ends of metasoma segments II and III (6–7 vs. 4–17; P = 0.007) (one-tailed t-tests). The species were separable by spur macrosetal counts except for overlapping high counts (28–29) in one outlier female from Thumrait out of a total of 73 specimens of *A*. *omanensis* **sp**. **n**. (Fig. 164). They overlapped in summed granule counts of lateral inframedian carinae, although *A*. *ammophilus* **sp**. **n**. had on average fewer granules, typically two per carina on segment II, and one per carina on segment III (e.g., Fig. 121). Fig. 163 shows that *A*. *ammophilus* **sp**. **n**. was separable and disjunct from *A*. *omanensis* **sp**. **n**. in the joint distribution of the two meristic variables. An additional male from Mihrad, Saudi Arabia (Rub' al-Khali) had much higher spur macrosetal counts: right leg II 41, right leg III 66. These meristic variables were not recorded at the time when female samples from the UAE were loaned and examined. They are provisionally listed under the species diagnosis, and should be further tested by larger samples of both sexes of *A*. *ammophilus* **sp**. **n**.

Discussion

Analysis of morphological variation of *Androctonus* samples from Oman, and adjacent Saudi Arabia and UAE, revealed that populations in the region can be divided into two allopatric forms. These are proposed to represent a pair of sister species: (i) *A*. *omanensis* **sp**. **n**., distributed over coastal and inland desert plains of Oman, and (ii) *A*. *ammophilus* **sp**. **n**., distributed over dunes of the Rub' al-Khali (Empty Quarter) in northwestern Oman, adjacent Saudi Arabia and the UAE. Although the two are quite similar with overlapping variation in characters, they can be differentiated by multivariate morphometric analysis and a combination of meristic characters. *A*. *ammophilus* **sp**. **n**. differs from *A*. *omanensis* **sp**. **n**. in having less robust pedipalps and metasoma, longer legs, and a combination of denser setation on prolateral basitarsal spurs and fewer granules on lateral inframedian carinae of metasoma II–III. These differences may be indicative of diffferential substrate adaptation. Both species are psammophilous, exhibiting typical adaptations for locomotion in sandy habitats, such as compressed basitarsi with broad macrosetal combs and telotarsi with long, curved ungues (Fet et al., 1998, Prendini, 2001). However, their preferred substrates have different physical properties. In Oman, *A*. *omanensis* **sp**. **n**. is found on nabkha dunes formed around shrubs, and on sedimentary plains with firmer, more stable sand substrates for burrowing and surface activities (Figs. 201–204). Conversely, *A*. *ammophilus* **sp**. **n**. is found among aeolian dunes of the Rub' al-Khali (Figs. 205–208), where loose, fine sand driven by Shamal winds offers a less stable substrate (Nelli et al., 2024). These dunes would host a more specialized endemic fauna, categorized as ultrapsammophiles (Newlands, 1972). The more elongate pedipalps, legs, and metasomal segments of *A*. *ammophilus* **sp**. **n**. are features associated with greater psammophilous adaptation. They may improve streamlining and reduce frictional drag when moving through loose sand (Prendini, 2001; Williams, 1969). Denser setation on the basitarsal spurs may assist locomotion on unconsolidated sand, expanding areas of tarsal contact (Fet et al., 1998) and increasing the penetration forces of legs intruding into dry granular media (Ding et al., 2010). A similar geographic/ ecomorphic divergence is seen in the buthid genus *Vachoniolus* in Oman (Lowe, 2010): the pedipalps, legs and metasoma of the semi-psammophilous/ psammophilous *V. gallagheri* Lowe, 2010, distributed over alluvial fans and wadis in north-central Oman, are shorter and more robust; those of the ultrapsammophilous *V. globimanus* Levy et al., 1973, distributed over dunes of the Rub' al-Khali, are more elongate.

A. *omanensis* **sp**. **n**. and *A*. *ammophilus* **sp**. **n**. are hypothesized to be allopatric sister taxa that diverged through a process of ecological speciation, mediated by macrospatial habitat isolation (Butlin & Faria, 2024; Coyne & Orr, 2004; Rundle & Nosil, 2005; Schluter, 2001; Shafer et al., 2013). Genetic exchange between their populations is presumed to have been reduced by differential substrate preferences that evolved in concert with differential adaptations to the more stable sand deposits on desert plains in Oman, vs. the less stable

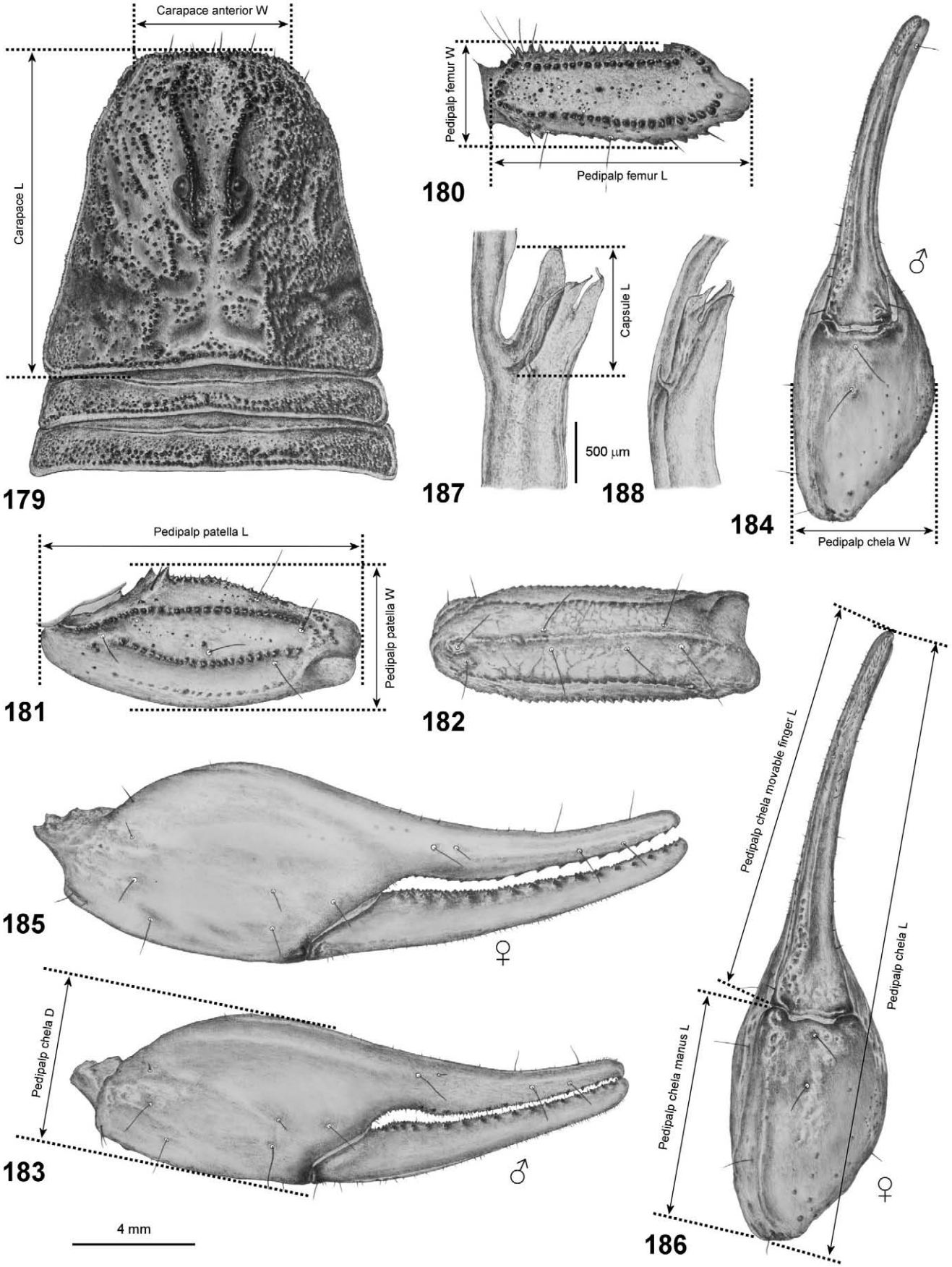

Figures 179–**188**. *Androctonus omanensis* **sp**. **n**. Structures and measurements. **Figure 179**. Carapace and tergites I–II of male. **Figures 180**–**184**. Pedipalp segments of male. Femur in dorsal view (180), patella in dorsal (181) and external (182) views, and chela in external (183) and ventral (184) views. **Figures 185**–**186**. Pedipalp chela of female in external (185) and ventral (186) views. **Figures 187**–**188**. Hemispermatophore capsule region in convex (187) and anterior (188) views. Scale bars: 4 mm (179–186), 500 μm (187–188). Paratype male, Dhuai, 21.X.1997 (179–184, 187–188), and paratype female, 15 km W. of Barka, 13.X.1993 (185–186).

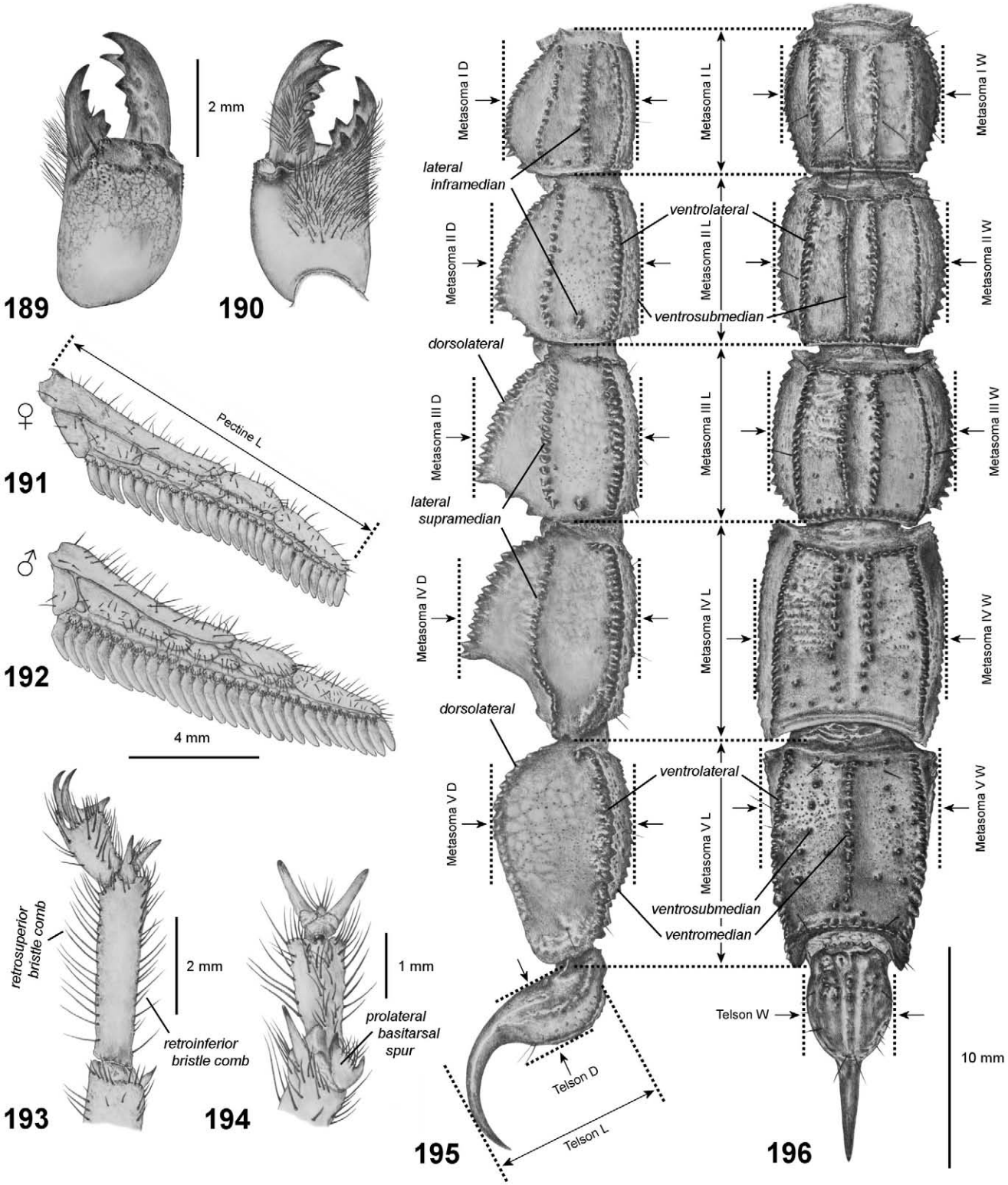

Figures 189–**196**. *Androctonus omanensis* **sp**. **n**. Structures, measurements and terminology. **Figures 189**–**190**. Right chelicera of male, in dorsal (189) and ventral (190) views. **Figures 191**–**192**. Left combs of pectines in ventral view of female (191) and male (192). **Fig**. **193**. Distal tibia, basitarsus and telotarsus of right leg III in retrolateral view. Macrosetal (bristle comb) terminology indicated. **Fig**. **194**. Distal basitarsus and telotarsus of right leg III of male in ventral view. Prolateral basitarsal spur indicated. **Figs**. **195**–**196**. Metasoma and telson of male in right lateral (195) and ventral (196) views. Carinal terminology indicated. Scale bars: 10 mm (195–196), 4 mm (191–192), 2 mm (189–190, 193), 1 mm (194). Paratype male, Dhuai, 21.X.1997 (189–190, 192, 195–196), paratype male (193–194) and female (191), 15 km W. of Barka, 13.X.1993.

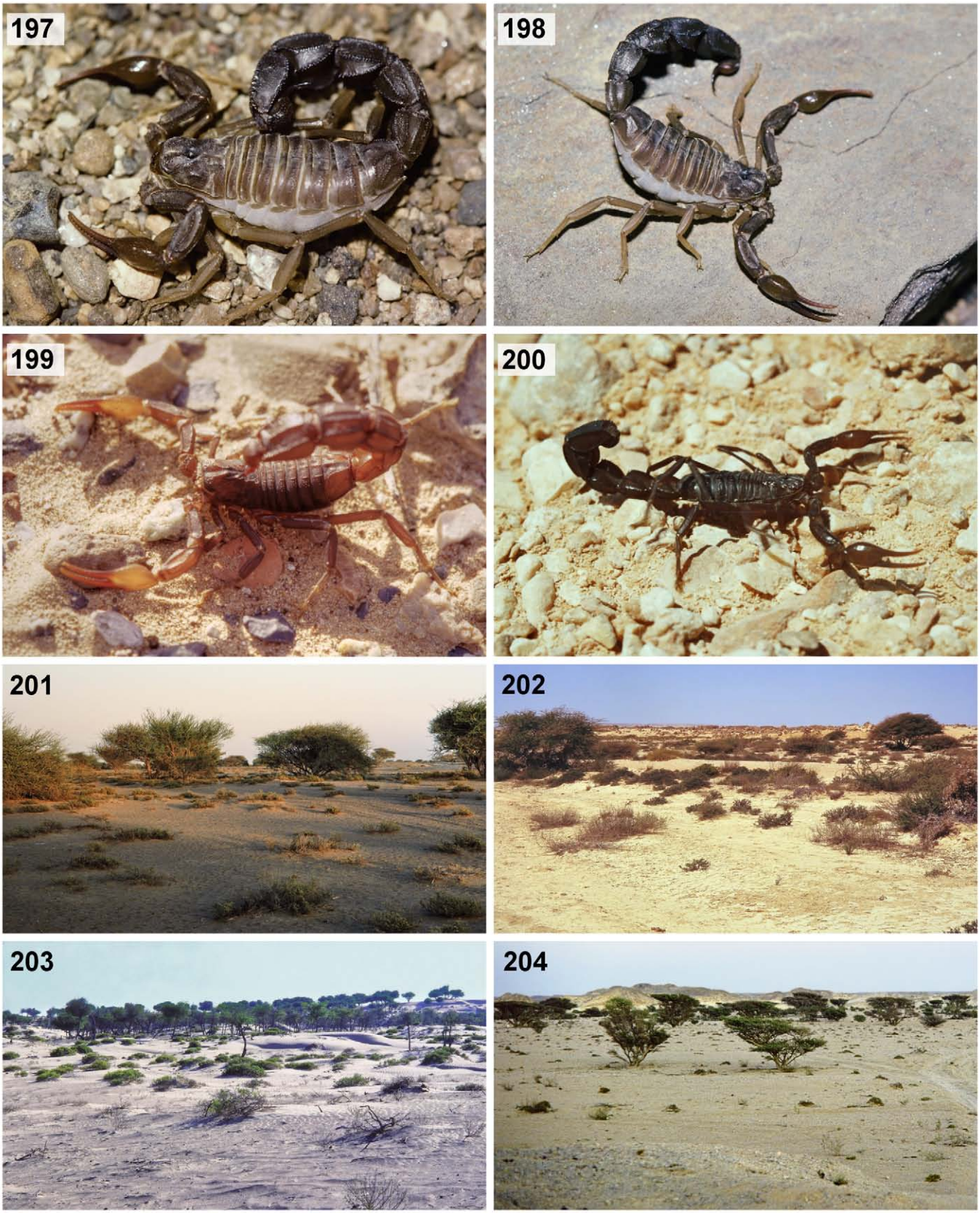

Figures 197–204. *Androctonus omanensis* **sp. n**. In vivo habitus (197–200) and dune habitats (201–204). **Figures 197–198**. Adult female, Muscat. **Figure 199**. Adult male, Wadi Matam, W. of Wahiba (Sharqiyah) Sands. **Figure 200**. Adult male, Thumrait, Dhofar Province (photograph by J. N. Barnes). **Figure 201**. Al Abyad dune field, W. of Barka, Batinah coast, near the type locality. **Figure 202**. Ad Duqm, central coast. **Figure 203**. *Prosopis* woodlands, E. edge of Wahiba (Sharqiyah) Sands. **Figure 204**. Thumrait, Dhofar Province.

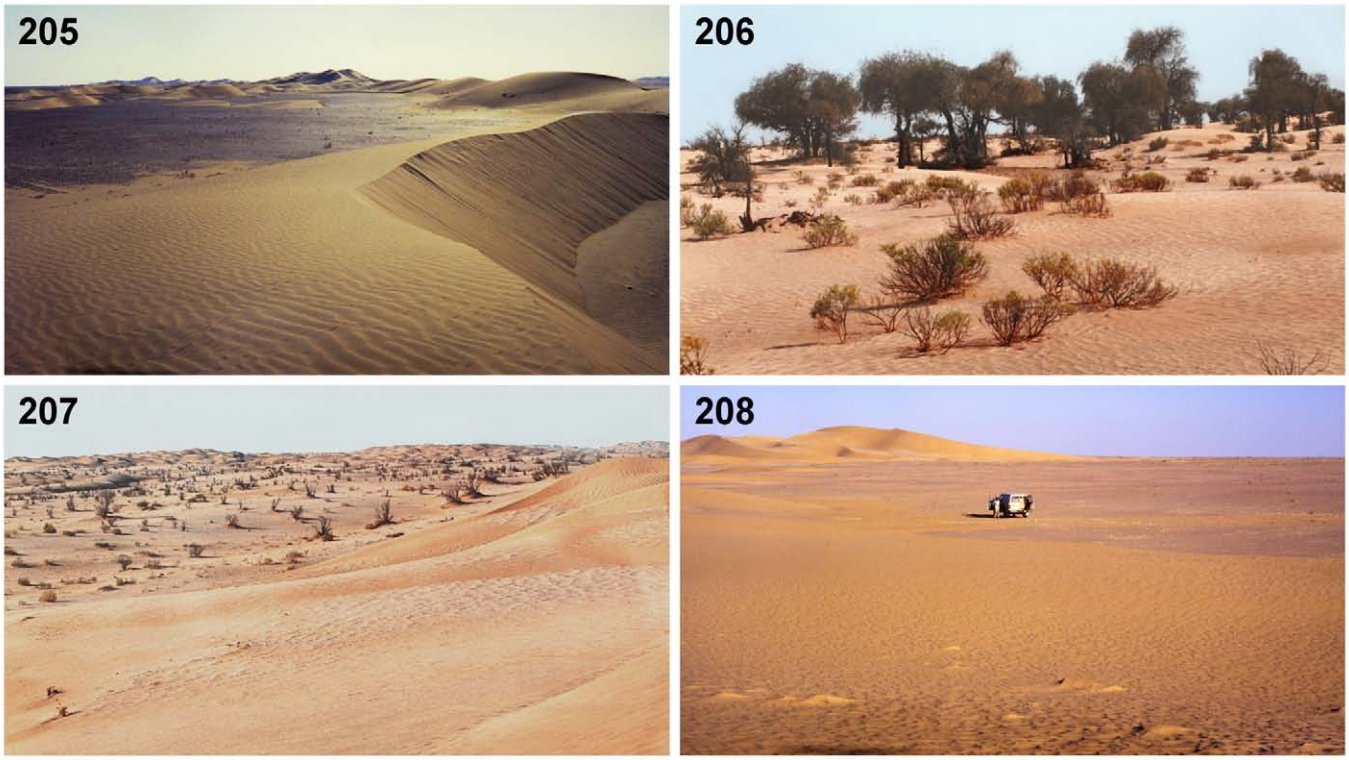

Figures 205–**208**. Habitats of *Androctonus ammophilus* **sp**. **n**. in Oman, at edge of Rub' al-Khali (Empty Quarter). **Figure 205**. Ramlat as Sahmah. **Figures 206**–**208**. Ramlat Muqshin

sands of aeolian dunes in the Rub' al-Khali. Biogeographic evidence supports an important role for substrate specialization in scorpion speciation (Prendini, 2001). Genetic differences accumulate when rates of selection favoring local substrate adaptation outpace rates of gene flow between populations. Gene flow is predicted to be low because burrowing scorpions are philopatric, sedentary, sit-and-wait predators with limited dispersal ability (Polis, 1990). In arid environments, they spend much of their lives within their burrows, sheltering from adverse surface conditions (Adams et al., 2016; Warburg & Polis, 1990). Adverse conditions currently prevail in the zone between the Rub' al-Khali and the central plains and coast of Oman that divides the two species. The climate there is hyper-arid with less than 50 mm of annual rainfall, relative humidity below 20%, and high temperatures exceeding 50°C (mean annual temperature 26°C) (Ghazanfar, 2004; Glennie, 2001).

In the Miocene, the climate of the Arabian Peninsula was warm and temperate, and the Rub' al-Khali was a lush, sedimentary basin with swamps, savannah grasslands and woodlands (Kingston & Hill, 1999). In the Pliocene, conditions shifted from subtropical to semi-arid (Salzmann et al., 2011). Subsequently, dunes of the Rub' al-Khali were formed during Pleistocene glaciations when dry periods lowered sea levels and exposed sediments in the Gulf to deflation and transport by intensified Shamal winds (Almutlaq et al., 2022; Glennie, 2001; Glennie & Singhvi, 2002). Analysis of data from luminescence and radioisotope dating of sediments indicated prominent phases of aeolian deposition in the penultimate glacial period, 186–130 ka and 115–106 ka (Preusser, 2009). Ecological speciation of *A*. *ammophilus* **sp**. **n**. by ultrapsammophilous adaptation could have commenced in this timeframe. Selection rates would have been variable because this epoch was punctuated by several wet interludes of ~10 ky. During these interglacial periods (MIS 3, 5a, 5c and 5e) strong SW monsoon winds carried moisture inland from the Indian Ocean, and shallow lakes were spread over the Rub' al-Khali (Jennings et al., 2015; Matter et al., 2014). In these humid episodes, the dunes would have been less mobile and stabilized by denser vegetation.

In facilitating speciation of *A*. *ammophilus* **sp**. **n**., the Rub' al-Khali would also have played the role of an environmental barrier, isolating ancestral populations of *A*. *omanensis* **sp**. **n**. from *Androctonus* in more northern parts of the Arabian Peninsula. The distribution of *A*. *omanensis* **sp**. **n**. along coastal regions of Oman aligns with local centers of endemism considered to represent Pleistocene refugia: the Al Hajar mountains in the north; areas of the central coast, including Huqf, Jiddat al Harasis and Jiddat Al Arkad; and the Dhofar mountains in the south (Borrell et al., 2019; Feulner, 2024; Gazanfar, 1992; Lowe, 2000; Mateiciucová et al., 2023; Rose et al., 2019). These areas currently experience a less extreme climate than the Rub' al-Khali, with lower temperatures and greater availability of water from precipitation or condensation of fog during the summer monsoon (Borrell et al., 2019). The hyper-aridity and high temperatures of the Rub' al-Khali act as agents of vicariance, blocking northward dispersal of fauna poorly adapted to survive the more adverse conditions. Such isolation was also suggested to restrict the range of another buthid scorpion in Oman, *Leiurus macroctenus* Lowe et al., 2014. This species extends along the southeast coast, overlapping the range of *A*. *omanensis* **sp**. **n**. (Lowe et al., 2014:

119, 121, fig 99). However, the exclusion of *Leiurus* from the northern coast and Al Hajar ranges indicates that these two genera experienced different biogeographic histories in Oman.

The main uplift of the Al Hajar mountain ranges occurred in the Eocene (40–30 Ma), with further uplift in the Miocene (20–15 Ma) (Hansman et al., 2017). With elevations reaching 3,000 m a. s. l., these ranges have profoundly influenced the biogeography of much of the fauna of northern Oman (e.g., Burriel-Carranza et al., 2025; SimÓ-Riudalbas et al., 2017). The graded differences in morphometrics and coloration of *A. omanensis* **sp. n.** populations of the northern Batinah coast, relative to those of interior desert plains and southeast coast, suggest that the Al Hajar ranges have had some effect in curtailing gene flow between these populations. The species appears to be restricted to lower elevations, as none of the collection records were above 600 m a. s. l. This barrier may not have been sufficient to bring about speciation because no specific characters were found to separate north coastal from interior populations, and their morphometrics were overlapped. The Al Hajar ranges are split by the Semail Gap, a low elevation, linear channel running along an ancient fault line dating back to the Eocene (Scharf et al., 2019). This opening could be a conduit for genetic interchange. Indeed, there are several collection records of *A. omanensis* **sp. n.** from sites within the Semail Gap (Fig. 110). Future molecular studies can address the question of whether north coastal and interior populations comprise two or more cryptic species.

Acknowledgments

The author gratefully acknowledges the curators who provided loans of *Androctonus* material for this study: Ambros Hänggi (NHMB), L. Bartolozzi and Sarah Whitman (MZUF), Frantisek Kovařík (FKCP), Jacqueline Heurtault (MNHN), H. W. Levi and Laura Leibensperger (MCZ), and Scott F. Larcher (USNM); and the many collectors who assisted in the field and contributed specimens or data, including: J. Neil Barnes, Jim Dundon, S. M. Farook, Martin Fisher, Michael D. Gallagher, Andrew S. Gardner, Ian Harrison, Anitha Saji (EAD), and Mark Stockmann. This work is a continuation of studies on the scorpion fauna of Oman originally sponsored by H. H. The Minister of National Heritage and Culture, Sultanate of Oman, with support from Khair Bin Antar Salim, Director of Museums, Said Ali Said Al-Farsi, Saddiqa Ramdhan, Ministry of National Heritage and Culture, and Michael D. Gallagher, ex curator, Oman Natural History Museum (ONHM). Two anonymous reviewers provided comments and suggested corrections.

References

ADAMS, A. M., E. MARAIS, J. S. TURNER, L. PRENDINI & B. PINSHOW. 2016. Similar burrow architecture of three arid-zone scorpion species implies similar ecological function. *The Science of Nature*, 103, 56: 1–11.

AL-KHAZALI, A. H. & E. A. YAĞMUR. 2023. *Androctonus sumericus* sp. nov., a new scorpion from Dhi Qar Province, Iraq (Scorpiones: Buthidae). *Zoology in the Middle East*, 69 (4): 1–10.

ALMUTLAQ, F., F. NAHAS & K. MULLIGAN, 2022. Calculation of the Rub' al-Khali sand dune volume for estimating potential sand sources. *Remote Sensing*, 14, 1216: 1–14. https://doi.org/10.3390/rs14051216.

ALQAHTANI, A. R., A. BADRY, F. M. ABD AL GALIL & Z. S. AMR. 2022a. Morphometric and meristic diversity of the species *Androctonus crassicauda* (Olivier, 1807) (Scorpiones: Buthidae) in Saudi Arabia. *PeerJ*, 10:e14198. http://doi.org/10.7717/peerj.14198 (https://peerj.com/articles/14198/

ALQAHTANI, A. R., A. BADRY, H. ALY, S. A. M. AMER, F. M. ABD AL GALIL, M.A. AHMED, S. KADASAH & Z.S. AMR. 2022b. Genetic diversity and population structure of *Androctonus crassicauda* (Scorpiones: Buthidae) in different ecogeographical regions of Saudi Arabia and Iran. *Zoology in the Middle East*, 68: 171–179. doi: 10.1080/09397140.2022.2051915.

ALQAHTANI, A. R., A. BADRY, S. A. M. AMER, , F. M. A. A. AL GALIL, M. A. AHMED & Z. S. AMR. 2022c. Intraspecific molecular variation among *Androctonus crassicauda* (Olivier, 1807) populations collected from different regions in Saudi Arabia. *Journal of King Saud University – Science*, 34 (4): 1–7 101998.

ALQAHTANI, A. R., E. A. YAĞMUR & A. BADRY. 2023. *Androctonus tihamicus* sp. nov. from the Mecca Province, Saudi Arabia (Scorpiones, Buthidae). *ZooKeys*, 1152: 9–34.

AL-SAFADI, M. M. 1992. Additions to the scorpion fauna of Yemen. *Zoology of the Middle East*, 6: 95–99.

AMR, Z., M. A. ABU BAKER, M. AL-SARAIREH & D. A. WARRELL. 2021. Scorpions and scorpion sting envenoming (scorpionism) in the Arab Countries of the Middle East. *Toxicon*, 191: 83–103.

AMR, Z. S., M. S. ROBB, J. M. G. NUNES, M. A. ABU BAKER & A. WALSH. 2016. Diet of the Omani owl, *Strix butleri*, near Nakhal, Oman. *Zoology in the Middle East*, 62: (1): 17–20.

BARAHOEI, H., O. MIRSHAMSI, M. AMIRI, A. MOEINADINI & E. RAKHSHANI. 2025. Integrative taxonomy reveals the existence of a new species of fat-tailed scorpion *Androctonus* (Buthidae) in Iran. *Turkish Journal of Zoology*, 49:

BARAHOEI, H., O. MIRSHAMSI, N. SANCHOULI, M. G. MOGHADDAM, C. LEHMANN-GRABER & L. MONOD. 2022. Review of *Androctonus baluchicus* (Pocock, 1900) with description of new species from Iran (Scorpiones: Buthidae). *Arthropoda Selecta*, 31 (2): 197–212.

BARAHOEI, H., S. NAVIDPOUR, M. ALIABADIAN, R. SIAHSARVIE. & O. MIRSHAMSI. 2020. Scorpions of Iran (Arachnida: Scorpiones): Annotated checklist, DELTA database and identification key. *Journal of Insect Biodiversity and Systematics*, 6 (4): 375–474.

BIRULA, A. A. 1900. Beitrlige zur Kenntniss der Scorpionenfauna Ost-Persiens. (1. Beitrag). *Bulletin de I' Academie Imperiale des Sciences de St.-Petersbourg*, 12(4): 355–375.

BORRELL, J. S., G. AL ISSAEY, D. A. LUPTON, T. STARNES, A. AL HINAI, S. AL HATMI, R. A. SENIOR, T. WILKINSON, J. L. H. MILBORROW, A. STOKES-REES & A. PATZELT. 2019. Islands in the desert: environmental distribution modelling of endemic flora reveals the extent of Pleistocene tropical relict vegetation in southern Arabia. *Annals of Botany*, 124: 411–422.

BURRIEL-CARRANZA, B., H. TEJERO-CICUÉNDEZ, A. CARNÉ, G. MOCHALES-RIAÑO, A. TALAVERA, S. AL SAADI, J. ELS, J. ŠMÍD, K. TAMAR, P. TARROSO & S. CARRANZA. 2025. Integrating genomics and biogeography to unravel the origin of a mountain biota: the case of a reptile endemicity hotspot in Arabia. *Systematic Biology*, 74 (2): 230–249.

BUTLIN, R. R. & R. FARIA. 2024. Local adaptation and reproductive isolation: when does speciation start? *Evolutionary Journal of the Linnean Society*, 3, kzae003: 1–7. https://doi.org/10.1093/evolinnean/kzae003.

COYNE, J. A. & H. A. ORR. 2004. *Speciation*. Sinauer Associates, Inc., Massachusetts, U.S.A.

DEHGHANI, R. & B. FATHI. 2012. Scorpion sting in Iran: a review. *Toxicon*, 60: 919–933.

DESOUKY, M. M. A. & A. M. ALSHAMMARI. 2011. Scorpions of the Ha'il Region, northern Saudi Arabia, and molecular phylogenetics of two common species, *Androctonus crassicauda* and *Scorpio maurus kruglovi*. *Bulletin of the British Arachnological Society*, 15(6): 193–200.

DING, Y., N. GRAVISH, C. LI, R. D. MALADEN, N. MAZOUCHOVA, S. S. SHARPE, P. B. UMBANHOWAR & D. I. GOLDMAN. 2012. Comparative studies reveal principles of movement on and within granular media. Pp. 281–292 *in* CHILDRESS, S., A. HOSOI, W. W. SCHULTZ & J. WANG (eds.) *Natural Locomotion in Fluids and on Surfaces*. *Swimming*, *Flying*, *and Sliding*. The IMA Volumes in Mathematics and its Applications, IMA, Vol. 155. Springer Nature.

DURSTENFELD, R. 1964. Algorithm 235: Random permutation. *Communications of the Association for Computing Machinery*, 7 (7): 420. doi:10.1145/364520.364540. S2CID 494994.

EL-HENNAWY, H.K. 1992. A catalogue of the scorpions described from the Arab Countries (1758-1990) (Arachnida: Scorpionida). *Serket*, 2 (4): 95–153.

FET, V. & G. LOWE. 2000. Family Buthidae. Pp. 54–286 *in* Fet, V., W. D. Sissom, G. Lowe & M. E. Braunwalder. *Catalog of the Scorpions of the World* (*1758-1998*). The New York Entomological Society.

FET, V., G. A. POLIS & W. D. SISSOM. 1998. Life in sandy deserts: the scorpion model. *Journal of Arid Environments*, 39: 609–622.

FET, V., M. E. SOLEGLAD & G. LOWE. 2005. A new trichobothrial character for the high-level systematics of Buthoidea (Scorpiones: Buthida). *Euscorpius*, 23: 1–40.

FEULNER, G. 2024. The Mountain Regions of the United Arab Emirates: An Ecosystem Perspective. Pp. 161–216 *in* Burt, J. A. (ed.), *A Natural History of the Emirates*. Springer Nature.

FINNEGAN, S. 1932. Report on the scorpions collected by Mr. Bertram Thomas in Arabia. *Journal of the Linnaean Society* (*Zoology*), *London*, 38: 91–98.

FISHER, R. A. & F. YATES. 1938. *Statistical tables for biological*, *agricultural and medical research*. London: Oliver & Boyd.

FLETCHER, J. M., W. J. RICE & R. M. RAY. 1978. Linear discriminant function analysis in neuropsychological research: some uses and abuses. *Cortex*, 14: 564–577.

FRANCKE, O. F. 1977. Scorpions of the genus *Diplocentrus* from Oaxaca, Mexico (Scorpionida, Diplocentridae). *Journal of Arachnology*, 4: 145–200.

GHAZANFAR, S. A. 1992. Quantitative and biogeographic analysis of the flora of the Sultanate of Oman. *Global Ecology and Biogeography Letters*, 2 (6): 189–195.

GHAZANFAR, S. A. 2004. Biology of the central desert of Oman, *Turkish Journal of Botany*, 28 (1): 65–71.

GLENNIE, K. W. 2001. Evolution of the Emirates' land surface: an introduction. Pp. 9–27 *in* Al Abed, I & P. Hellyer (eds.) *United Arab Emirates: a new perspective.* Trident Press, London.

GLENNIE, K. W. & A. K. SINGHVI. 2002. Event stratigraphy, paleoenvironment and chronology of SE Arabian deserts. *Quaternary Science Reviews*, 21: 853–869.

HANSMAN, R. J., U. RING. S. N. THOMSON, B. DEN BROK & K. STÜBNER. 2017. Late Eocene uplift of the Al Hajar mountains, Oman, supported by stratigraphy and low-temperature thermochronology. *Tectonics*, 36: 3081–3109.

HARADON, R. M. 1984. New and redefined species belonging to the *Paruroctonus baergi* group (Scorpiones, Vaejovidae). *Journal of Arachnology*, 12: 205–221.

HELLTON, K. H. & M. THORESEN. 2014. The impact of measurement error on principal component analysis. *Scandinavian Journal of Statistics*, 41: 1051–1063.

HEMPRICH, F. W. & EHRENBERG, C. G. 1828. Zoologica II. Arachnoidea. In: *Symbolae Physicae seu Icones et Descriptiones Animalium Evertebratorum Sepositis Insectis quae ex Itinere per Africam Borealem et Asiam Occidentalem. Friderici Guilelmi Hemprich et Christiani Godofredi Ehrenberg*, *Medicinae et Chirurgiae Doctorum*, *Studio Novae aut Illustratae Redierunt*. Percensuit et Regis Iussu et Impensis Edidit Dr. C. G. Ehrenberg. Decas Prima. *Berolini ex Officina Academica*, Venditur a Mittlero: plate II: *Androctonus*.

HENDRIXSON, B. E. 2006. Buthid scorpions of Saudi Arabia, with notes on other families (Scorpiones: Buthidae, Liochelidae, Scorpionidae). *Fauna of Arabia*, 21: 33–120.

ISMAIL, M., M. A. ABD-ELSALAM & M. S. AL-AHAIDIB. 1994. *Androctonus crassicauda* (Olivier), a dangerous and unduly neglected scorpion – I. pharmacological and clinical studies. *Toxicon*, 32 (12): 1599–1618.

JENNINGS, R. P., J. SINGARAYER, E. J. STONE, U. KREBS-KANZOW, V. KHON, K. H. NISANCIOGLU, M. PFEIFFER, X. ZHANG, A. PARKER, A. PARTON, H. S. GROUCUTT, T. S. WHITE, N. A. DRAKE & M. D. PETRAGLIA. 2015 The greening of Arabia: multiple opportunities for human occupation of the Arabian Peninsula during the Late Pleistocene inferred from an ensemble of climate model simulations. *Quaternary International*, 382: 181–199.

KINGSTON, J. D. & A. HILL. 1999. Late Miocene palaeoenvironments in Arabia: a synthesis. Pp. 389–407 (Ch. 27) *in* WHYBROW, P. J. & A. HILL (eds.) *Fossil vertebrates of Arabia*: *with emphasis on the late Miocene faunas*, *geology*, *and palaeoenvironments of the Emirate of Abu Dhabi*, *United Arab Emirates*. Yale University Press.

KOVAŘÍK, F. 2009. *Illustrated catalog of scorpions*. *Part I*. Jakub Rolćík – Clairon Production, Prague, 170 pp.

KOVAŘÍK, F. & Z. AHMED. 2013. A review of *Androctonus finitimus* (Pocock, 1897), with description of two new species from Pakistan and India (Scorpiones, Buthidae). *Euscorpius*, 168: 1–10.

KOVAŘÍK, F., G. LOWE, P. JUST, A. I. AWALE, A. S. A. ELMI & F. ŠŤÁHLAVSKÝ. 2018. Scorpions of the Horn of Africa (Arachnida: Scorpiones). Part XV. Review of the genus *Gint* Kovařík et al., 2013, with description of three new species from Somaliland (Scorpiones, Buthidae). *Euscorpius*, 259: 1–41.

KOVAŘÍK, F., G. LOWE, J. PLÍŠKOVÁ & F. ŠŤÁHLAVSKÝ. 2016. Scorpions of the Horn of Africa (Arachnida: Scorpiones). Part VII. *Parabuthus* Pocock, 1890 (Buthidae), with description of *P. hamar* sp. n. and *P. kajibu* sp. n. from Ethiopia. *Euscorpius*, 228: 1–58.

KOVAŘÍK, F., G. LOWE & F. ŠŤÁHLAVSKÝ. 2025. Three new species of *Androctonus* from Morocco (Arachnida: Scorpiones: Buthidae). *Euscorpius*, 420: 1–29.

LEVY, G. & AMITAI, P. 1980. *Scorpiones*. *Fauna Palaestina. Arachnida I*. Jerusalem: The Israel Academy of Sciences and Humanities..

LOURENÇO, W. R. 2005. Nouvelles considérations taxonomiques sur les espèces du genre *Androctonus* Ehrenberg, 1828 et description de deux nouvelles espèces (Scorpiones, Buthidae). *Revue Suisse de Zoologie*, 112 (1): 145–171.

LORIA, S. F. & L. PRENDINI. 2014. Homology of the lateral eyes of Scorpiones: a six-ocellus model. *PLoS ONE*, 9 (12): e112913. doi:10.1371/journal.pone.0112913.

LOWE, G. 1993. Tales of tails: scorpions in Oman. *Newsletter of the Historical Association of Oman*, 2: 1–3.

LOWE, G. 2000. A new species of *Babycurus* (Scorpiones: Buthidae) from northern Oman. *Entomological News*, 111 (3): 185–192.

LOWE, G. 2010a. New picobuthoid scorpions (Scorpiones: Buthidae) from Oman. *Euscorpius*, 93: 1–53.

LOWE, G. 2010b. The genus *Vachoniolus* (Scorpiones: Buthidae) in Oman. *Euscorpius*, 100: 1–37.

LOWE, G. 2010c. Two new species of *Hottentotta* Birula, 1908 (Scorpiones: Buthidae) from northern Oman. *Euscorpius*, 103: 1–23.

LOWE, G. & V. FET. 2024. A survey of proximal sensilla associated with denticle subrows on scorpion pedipalp fingers (Arachnida: Scorpiones), with observations on scorpion fluorescence. *Euscorpius*, 382: 1–109.

LOWE, G. & V. TANG. 2024. Clustered setation on the pedipalps of buthid scorpions (Scorpiones: Buthidae). *Euscorpius*, 398: 1–109.

LOWE, G., E. A. YAĞMUR & F. KOVAŘÍK. 2014. A review of the genus *Leiurus* Ehrenberg, 1828 (Scorpiones: Buthidae) with description of four new species from the Arabian Peninsula. *Euscorpius*, 191: 1–129.

MATEICIUCOVÁ, I., M. WILDING A, J. OTAVA & J. ŠINDELÁŘ. 2023. The Al-Hajar Mts as a prehistoric refugium? On the habitability of karst mountain places in Oman during arid climate periods. *Journal of Arid Environments*, 212, 104951: 1–27.

MATTER, A., E. NEUBERT, F. PREUSSER, T. ROSENBERG & K. AL-WAGDANI. 2014. Palaeo-environmental implications derived from lake and sabkha deposits of the southern Rub‘ al-Khali, Saudi Arabia and Oman. *Quaternary International*, 382: 120–131.

NCSS. 2023. NCSS Documentation. Multivariate Analysis. Discriminant Analysis. https://www.ncss.com/wp-content/themes/ncss/pdf/Procedures/NCSS/Discriminant_Analysis.pdf

NELLI, N., D. FRANCIS, M. SOW, R. FONSECA, A. ALKATHEERI, E. BOSC & G. BERGAMETTI. 2024. The wind-blown sand experiment in the Empty Quarter desert: roughness length and saltation characteristics. *Earth and Space Science*, 11, e2024EA003512. https://doi.org/10.1029/2024EA003512: 1–25.

NEWLANDS, G. 1972. Notes on psammophilic scorpions and a description of a new species (Arachnida: Scorpionides). *Annals of the Transvaal Museum*, 27: 241–253.

OLIVIER, G. A. 1807. *Voyage dans l‘Empire Othoman, l‘Egypte et la Perse, fait par ordre du gouvernement, pendant les six premières années de la République. Tome troisième*. VIII + 566 pp; atlas: 8 pp., pl. 34-50. Paris; Henri Agasse.

OZKAN, O., S ADIGÜZEL, S. YAKIŞTIRAN, Y. CESARETLİ, M. ORMAN & K. Z. KARAER. 2006. *Androctonus crassicauda* (Olivier 1807) scorpionism in the Sanliurfa provinces of Turkey. *Acta Parasitologica Turcica*, 30 (3): 239–245.

POCOCK, R. I. 1895. On the Arachnida and Myriopoda obtained by Dr. Anderson‘s collector during Mr T. Brent‘s expedition to the Hadramaut, South Arabia, with a supplement upon the scorpions obtained by Dr. Anderson in Egypt and the Eastern Soudan. *Journal of the Linnean Society*, 25: 292–316.

POCOCK, R. I. 1897. Descriptions of some new species of scorpions from India. *Journal of the Bombay Natural History Society*, 11: 102–117.

POLIS, G. A. 1990. Ecology. Pp. 247–293 *in* POLIS, G. A. (ed.). *The Biology of Scorpions*. Stanford University Press, Stanford, CA.

PRENDINI, L. 2001. Substratum specialization and speciation in southern African scorpions: the effect hypothesis revisited. Pp. 113–138 *in* FET, V & P. A. SELDEN (eds.). *Scorpions 2001. In Memoriam Gary A. Polis*. Burnham Beeches, Bucks. British Arachnological Society.

PREUSSER, F. 2009. Chronology of the impact of Quaternary climate change on continental environments in the Arabian Peninsula. *Comptes Rendus Geoscience*, 341: 621–632.

ROSE, J. I., Y. H. HILBERT, V. I. USIK, A. E. MARKS, M. M. ALI JABOOB, V. ČERNÝ, R. CRASSARD & F. PREUSSER. 2019. 30,000-year-old geometric microliths reveal glacial refugium in Dhofar, southern Oman. *Journal of Paleolithic Archaeology*, 2: 338–357.

RUNDLE, H. D. & P. NOSIL. 2005. Ecological speciation. *Ecology Letters*, 8: 336–352.

SAJI, A., Z. S. AL RASHDI, S. AHMED, P. S. SOORAE & S. AL DHAHERI. 2021. Diversity and composition of epigeal arthropods using pitfall trapping method in different habitat types of Abu Dhabi Emirate, UAE. *Saudi Journal of Biological Sciences*, 28: 3751–3758.

SALZMANN, U., M. WILLIAMS, A. M. HAYWOOD, A. L. A. JOHNSON, S. KENDER & J. ZALASIEWICZ. 2011. Climate and environment of a Pliocene warm world. *Palaeogeography, Palaeoclimatology, Palaeoecology*, 309: 1–8.

SCHARF, A., F. MATTERN, D. MORAETIS, I. CALLEGARI & C. WEIDLE. 2019. Postobductional kinematic evolution and geomorphology of a major regional structure - the Semail Gap fault zone (Oman Mountains). *Tectonics*, 38: 2756–2778.

SCHLUTER, D. 2001. Ecology and the origin of species. *Trends in Ecology and Evolution*, 16 (7): 372–380.

SCHNEIDER, C. A., W. S. RASBAND & K. W. ELICEIRI. 2012. NIH Image to ImageJ: 25 years of image analysis. *Nature Methods*, 9 (7): 671–675. doi:10.1038/nmeth.2089

SHAFER, A. B. A. & J. B. W. WOLF. 2013. Widespread evidence for incipient ecological speciation: a meta-analysis of isolation-by-ecology. *Ecology Letters*, 16: 940–950.

SIMÓ-RIUDALBAS, M., P. TARROSO, T. PAPENFUSS, T. AL-SARIRI & S. CARRANZA. 2017. Systematics, biogeography and evolution of *Asaccus gallagheri* (Squamata, Phyllodactylidae) with the description of a new endemic species from Oman. *Systematics and Biodiversity*, doi: 10.1080/14772000.2017.1403496: 1–17.

SISSOM, W. D. 1990. Systematics, biogeography and paleontology. Pp. 64–160 *in* POLIS, G. A. (ed.) *The Biology of Scorpions*. Stanford University Press, Stanford, California.

SISSOM, W. D., G. A. POLIS & D. D. WATT. 1990. Field and laboratory methods. Pp. 445–461 *in* POLIS, G. A. (ed.). *The Biology of Scorpions*. Stanford University Press, Stanford, CA.

STAHNKE, H. L. 1971. Scorpion nomenclature and mensuration. *Entomological News*, 81: 297–316.

STAHNKE, H. L. 1972. A key to the genera of Buthidae (Scorpionida). *Entomological News*, 83 (5): 121–133.

TIGAR, B. J. & P. E. OSBORNE. 1999. The influence of the lunar cycle on ground-dwelling invertebrates in an Arabian desert. *Journal of Arid Environments*, 43: 171–182.

TIKADER B. K. & BASTAWADE D. B., 1983. The fauna of India: Scorpions. Scorpionida, Arachnida. Vol III. *Zoological Survey of India*, Calcutta, 668pp.

VACHON, M. 1952. *Études sur les scorpions*. Institut Pasteur d'Algérie. Alger.

VACHON, M. 1963. De l'utilité, en systématique, d'une nomenclature des dents de chélicères chez les scorpions. *Bulletin du Musèum National d'Histoire Naturelle*, *Paris*, (2), 35 (2): 161–166.

VACHON, M. 1966. Liste des scorpions connus en Egypte, Arabie, Israël, Liban, Syrie, Jordanie, Turquie, Irak, Iran. *Toxicon*, 4: 209–218.

VACHON, M. 1974. Étude des caractères utilisés pour classe les familles et les genre de Scorpiones (Arachnides). 1. La trichobothriotaxie en Arachnologie. Sigles trichobothriaux et types de trichobothriotaxie chez les scorpions. *Bulletin du Muséum National d'Histoire Naturalle Paris*, *Zoologie*, (3) 104 (140): 857–958.

VACHON, M. 1975. Sur l'utilisation de la trichobothriotaxie du bras des pedipalps des Scorpions (Arachnides) dans le classement des genres de famille des Buthidae Simon. *Compte rendus hebdomadaires des séances de l'Academie des Sciences*, *Paris Ser.D Sciences Naturelles*, 281 (21): 1597–1599.

VACHON, M. 1979. Arachnids of Saudi Arabia. Scorpiones. *Fauna of Saudi Arabia*, 1: 30–66.

VACHON, M. & R. KINZELBACH. 1987. On the taxonomy and distribution of the scorpions of the Middle East. Pp. 91-103 *in* KRUPP, F., SCHNEIDER, W & KINZELBACH, R. (eds.). *Proceedings of the Symposium on the Fauna and Zoogeography of the Middle East*, *Mainz*, 1985. Beihefte zum Tübinger Atlas des Vorderen Orients, Reihe A (Naturwissenschaften), 28.

WARBURG, M. R. & G. A. POLIS. 1990. Behavioral responses, rhythms, and activity Patterns. Pp. 224–246 *in* POLIS, G. A. (ed.). *The Biology of Scorpions*. Stanford University Press, Stanford, CA.

WILLIAMS, B. K. & K. TITUS. 1988. Assessment of sampling stability in ecological applications of discriminant analysis. *Ecology*, 69 (4): 1275–1285.

WILLIAMS, B. K., K. TITUS & J. E. HINES. 1990. Stability and bias of classification rates in biological applications of discriminant analysis. *Journal of Wildlife Management*, 54 (2): 331–341.

WILLIAMS, S. C. 1969. A new species of *Syntropis* from Baja California Sur, Mexico with notes on its biology. *Pan-Pacific Entomologist*, 45: 285–291.

WOOD, N. 1993. Scorpion search. *Petroleum Development Oman News*, 4: 12–17.

YAĞMUR, E. A. 2021. *Androctonus turkiyensis* sp. n. from the Şanlıurfa Province, Turkey (Scorpiones: Buthidae). *Euscorpius*, 341: 1–18.

YAĞMUR, E. A. 2023. *Androctonus kunti* sp. n. from Iğdır Province, Turkey (Scorpiones: Buthidae). *Euscorpius*, 371: 1–23.

YAĞMUR, E. A., F. KOVAŘÍK, V. FET, G. LOWE, M. MORADI & F. KALAMI. 2025a. Review of *Androctonus* Ehrenberg, 1828 in Iran, with redescription of *A. crassicauda* (Olivier, 1807) and *A. orientalis* (Birula, 1900) stat. n., and descriptions of four new species (Scorpiones: Buthidae). *Euscorpius*, 422: 1–69.

YAĞMUR, E. A., K. H. SAEID, A-K. A. MOHAMMED, A-J. M. A. KARIM & F. R. ALI. 2025b. *Androctonus ishtar* sp. n. from Dohuk and Nineveh provinces, Iraq (Scorpiones: Buthidae). *Journal of Natural History*. 59: 1757–1773.

YTHIER, E. 2021. A new species of *Androctonus* Ehrenberg, 1828 from the Sahelian wooded steppes of Burkina Faso (Scorpiones: Buthidae). *Faunitaxys*, 9 (31): 1–7.

YTHIER, E. & LOURENÇO, W. R. 2022. A new species of *Androctonus* Ehrenberg, 1828 from Western Sahara (Scorpiones: Buthidae). *Serket*, 18 (3): 239–251.